NASA CONTRACTOR REPORT

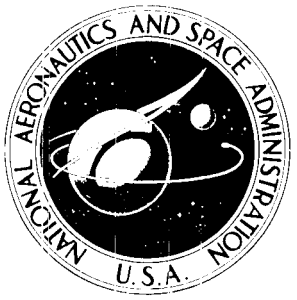

NASA CR-1908

NASA CR-1908

A STUDY OF BOUNDARY LAYER TRANSITION ON OUTGASSING CONES IN HYPERSONIC FLOW

by C. J. Stalmach, Jr., J. J. Bertin, T. C. Pope, and M. H. McCloskey

Prepared by
VOUGHT AERONAUTICS COMPANY
Dallas, Texas
for Langley Research Center

NATIONAL AERONAUTICS AND SPACE ADMINISTRATION • WASHINGTON, D. C. • DECEMBER 1971

1. Report No.	2. Government Accession No.	3. Recipient's Catalog No.
NASA CR-1908		

4. Title and Subtitle	5. Report Date
A STUDY OF BOUNDARY LAYER TRANSITION ON OUTGASSING CONES IN HYPERSONIC FLOW	December 1971
	6. Performing Organization Code
7. Author(s)	8. Performing Organization Report No.
C. J. Stalmach, Jr., J. J. Bertin, T. C. Pope and M. H. McCloskey	
	10. Work Unit No.
9. Performing Organization Name and Address	
Vought Aeronautics Company Dallas, Texas	11. Contract or Grant No. NAS1-9524
	13. Type of Report and Period Covered
12. Sponsoring Agency Name and Address	Contractor Report
National Aeronautics and Space Administration Washington, D. C. 20546	14. Sponsoring Agency Code

15. Supplementary Notes

16. Abstract

Surface heat-transfer rates and pressures were measured at hypersonic speeds on sharp cones at zero angle of attack with and without gas injection. Using the non-injection results for reference data the effects on heating and transition location of surface roughness and injectant rate, distribution and composition were determined. The transition location was sensitive to the injectant distribution. The transition Reynolds numbers were significantly greater when the injectant distribution was constant than with a variable distribution. The measured heat-transfer distributions were also strongly dependent upon the injectant distribution. Transition Reynolds number results obtained during this program with a variable injectant distribution were correlated with a limited amount of data available for a degrading model tested in a different facility. Transitional data with constant injectant distribution were correlated with earlier results. An empirical correlation of heat-transfer reduction due to gas injection in turbulent flow was developed for both distributions tested. Several effects of mass addition on heating and transition, which have been earlier reported, were observed. The simulation employed for the study of surface roughness requires further refinement since the heating data and the measured surface pressures were significantly affected by the cavity effect of the roughness elements.

17. Key Words (Suggested by Author(s))	18. Distribution Statement
Boundary layer transition Gas injection Heat transfer Sharp conic bodies	Unclassified - Unlimited

19. Security Classif. (of this report)	20. Security Classif. (of this page)	21. No. of Pages	22. Price*
Unclassified	Unclassified	77	$3.00

*For sale by the National Technical Information Service, Springfield, Virginia 22151

FOREWORD

This report covers the program conducted under Contract No. NAS1-9524, Control No. 132-221 from October 1969 to May 1971 under the technical direction of Mr. R. L. Wright. The experimental program was conducted in the Hypervelocity Wind Tunnel of the Vought Aeronautics Company, Dallas, Texas and the analysis was performed at the Department of Aerospace Engineering and Engineering Mechanics of the University of Texas at Austin. The authors wish to express their appreciation to Mr. J. L. Lindsey of Vought Aeronautics Company for his design and direction of the fabrication of the test models, and to Mr. J. L. Zickler of the University of Texas at Austin for his contribution to the analysis effort.

TABLE OF CONTENTS

LIST OF SYMBOLS

A	area
$A_{b,tr}$	circular area of cone at point of transition
A_w	wetted area of cone
C	constant in linear viscosity-temperature relation
C_i	dimensionless, total flow rate through the porous skin $\int \rho_w v_w dA/\rho_\infty u_\infty \pi r_b^2$
C_p	pressure coefficient
$C_{p,inj}$	specific heat of the injectant gas
$C_{p,str}$	specific heat of the stream gas
d_{orig}	coefficient in expression for rate of change of displacement thickness
D	diameter
f	transformed stream function
F	injection correlation parameter $\int_{x_o}^{x_{tr}} \rho_w v_w dA/\rho_\infty u_\infty (A_{b,tr})$
J_{ci}	inviscid flow function in weak interaction over a right circular cone
M	Mach number
MW_{inj}	molecular weight of the injectant gas
MW_{str}	molecular weight of the stream gas
P	local, static pressure
P_∞	free-stream static pressure
$\dot{q}$	local heat transfer rate
r	radius
Re_x	Reynolds number integrated over the wetted distance from the apex
Re_c/ft	local unit Reynolds number

$Re_{x,tr}$	Reynolds number integrated over the wetted distance to the transition location
$Re_{x,tr,0}$	no-injection value of Reynolds number integrated over the wetted distance from the apex to the transition location (used for reference in correlations of the effect of mass-injection)
$Re_{\delta^*,tr}$	transition Reynolds number based on inviscid flow properties and displacement thickness at the transition location
$Re_{\theta,tr}$	transition Reynolds number based on inviscid flow properties and momentum thickness at the transition location
Re_{∞}/ft	free-stream unit Reynolds number
$Re_{x,tr,f}$	transition Reynolds number based on transition point located using shadowgraph (end of transition)
$Re_{x,tr,i}$	transition Reynolds number based on transition point located using heat transfer method (beginning of transitional zone)
s	transformed x-coordinate $\int_o^x \rho_e \mu_e u_e r^{2k} dx$
St	Stanton number
St_o	no-injection, or reference, value of Stanton number
T	temperature
u	velocity parallel to cone surface
v	velocity normal to cone surface
x	distance from apex measured along conical generator
x_o	length of non-porous tip
x_L	total length of cone
x_{tr}	distance from apex to transition location
z	distance from apex measured along cone centerline
γ	ratio of specific heats
λ	instrumentation ray

ρ	density
θ_c	semi-vertex angle of cone
μ	viscosity

Subscripts

b	base
e	value at edge of boundary layer
orig	value of inviscid flow quantities if there were no viscous effects
r	recovery
t or te	stagnation value
w	wall value
∞	free-stream value

Superscripts

k	indicates planar (k = 0) or axisymmetric (k = 1) flow
$\overline{\quad}$	average value

A STUDY OF BOUNDARY LAYER TRANSITION ON OUTGASSING CONES IN HYPERSONIC FLOW

By C. J. Stalmach, Jr., J. J. Bertin*,
T. C. Pope and M. H. McCloskey**
Vought Aeronautics Company
Dallas, Texas

SUMMARY

Surface heat-transfer rates and pressures were measured at hypersonic speeds on sharp cones at zero angle of attack with and without gas injection. The non-injection results were employed as reference data for the definition of the effects of surface roughness and injectant rate, distribution and composition on heating and transition location. For a given mass injection rate the transition location was sensitive to the injection distribution. The transition Reynolds numbers were significantly greater when the injection distribution was constant than when the distribution decreased rapidly with distance from the apex. Similarly the measured heat-transfer distributions were strongly dependent upon the injectant distribution. Transition Reynolds number results obtained during this program with a variable injection distribution compared favorably with the limited amount of data available for a degrading model tested in a different facility. The transition measurements for a constant injection distribution were correlated with earlier wind tunnel results. An empirical correlation of heat transfer reduction due to gas injection in turbulent flow served well for both distributions tested. Several effects of mass addition on heating and transition, which have been earlier reported, were observed. The simulation employed for the study of surface roughness requires further refinement since the heating data and the measured surface pressures were significantly affected by the cavity effect of the roughness elements used in the present program.

INTRODUCTION

Boundary layer transition at supersonic and hypersonic speeds has become of increased interest because of its importance in the design of space vehicles and hypersonic inlets. The design of heat shields for space vehicles has been necessarily conservative and highly speculative because the location of transition is difficult to define and the heat transfer is strongly dependent upon the state of the boundary layer. Thus, it is necessary to continue to seek methods to better predict the location of transition.

*Consultant, Assistant Professor, Dept. of Aerospace Engineering and Engineering Mechanics, The University of Texas at Austin.

**Consultant, Research Assistant, Dept. of Aerospace Engineering and Engineering Mechanics, The University of Texas at Austin.

A theoretical prediction of transition is almost impossible because of the complexity of the transition process and the large number of important parameters. Therefore, correlations of available experimental data have been sought to predict values of the transition Reynolds number. In obtaining the experimental data, it would be desirable to simulate in a single facility all of the pertinent parameters experiences in flight, but this is not possible because of the limitations of ground facilities. Thus, the effect of an individual parameter is studied by carefully varying the parameter of interest while attempting to hold the other parameters constant. The large number of parameters and their interdependence has caused an experimental investigation of a single parameter to be difficult. Multiple parameter variation has led to many of the contradictory conclusions which appear in the literature. The problem is further complicated since boundary-layer transition has been related by some investigations to noise radiated from the tunnel boundary layer.

Factors which affect the transition Reynolds number on cones in supersonic and hypersonic flow include (but are not limited to):

(1) local Mach number,
(2) local unit Reynolds number,
(3) wall-to-recovery temperature ratio,
(4) distributed surface roughness (such as a charred surface),
(5) gaseous injection into the boundary layer (including rate and molecular weight of the injected gases).

A brief review of these transition-related parameters and their expected effect on the transition location follows to suggest possible correlation parameters.

(1) Local unit Reynolds number - Stability theory indicates that the transition Reynolds number may depend upon the local unit Reynolds number, if a physical wavelength spectrum of disturbances remains fairly constant over a range of operating conditions (ref. 1). Numerous investigators (e.g., Stainback, ref. 2 and Everhart and Hamilton, ref. 3) have observed an increase in the transition Reynolds number with local unit Reynolds number. The unit Reynolds number effect observed in wind tunnels has often been associated with aerodynamic noise radiated from the tunnel-wall boundary layer (refs. 4 and 5). However, transition data obtained by Potter (ref. 6) in a ballistic range where significant free-stream disturbances were absent exhibited a unit Reynolds number effect comparable to that observed in conventional wind tunnels.

(2) Local Mach number - Although there are exceptions (e.g., ref. 2), ground test data indicate a marked increase of transition Reynolds number with local Mach number at moderate supersonic to hypersonic Mach numbers.

(3) Surface temperature - The stability of a laminar boundary layer has been found to be significantly affected by heating or by cooling (usually indicated parametrically by a temperature ratio, or enthalpy

ratio, such as T_w/T_r or T_w/T_e). Lees (ref. 7) found that heat-transfer from the fluid to the wall stabilized a laminar boundary layer for two-dimensional disturbances and that, if there is a sufficient amount of cooling, the boundary layer could be completely stabilized. Reshotko (ref. 8) presents data supporting the trend toward complete stabilization. Using the flight data of Rumsey and Lee (ref. 9), Reshotko observed that, for conditions outside the predicted region of complete stabilization, transition did occur (as expected), but at relatively high Reynolds numbers.

However, the unqualified prediction that cooling stabilizes the boundary layer must be considerably modified because of the existence of unstable higher modes, which are not stabilized by cooling the wall (Mack, ref. 10). Another factor which could contribute to the transition reversal that has been observed by numerous workers as the model is "cooled" (e.g., ref. 11 and ref. 12) is the relative increase due to cooling in the magnitude of disturbances from fixed roughness (ref. 13). Since both effects could be present, problems in the identification of trends due to wall temperature variations contribute to the confusion in the literature.

A further complication is associated with wind tunnel data. Since a low value of T_w/T_r may be obtained either by cooling the wall or by heating the test gas, alternative effects may arise. Wagner, et al (ref. 4), noted that reducing T_w/T_r by heating the flow significantly decreased $Re_{x,tr}$, possibly because of nonuniform mixing of the supply gas in the stagnation chamber. The decrease in $Re_{x,tr}$ noted by Wagner occurred in the range $1.0 \leq T_w/T_r \leq 1.2$, which is a special case with heat transfer from the model to the fluid. The data reported by Maddalon (ref. 14) later showed that temperature spotiness in moderately heated hypersonic tunnels (helium) apparently does not effect transition location.

(4) Vehicle surface finish - The effects of surface roughness for a particular vehicle are difficult to assess. Certainly, roughness represents a disturbance to the flow and roughness elements have often been used to fix the point of transition on models in the wind tunnel. The effectiveness of roughness in promoting premature transition has been found to depend on the Mach number (ref. 15) as well as the size, the shape, and the distribution of roughness elements. Van Driest and Blumer (ref. 16) derived an empirical relation, which was very sensitive to the temperature ratio, to define the effective roughness height.

However, many flight vehicles of interest have relatively "smooth" finishes. The measured surface roughness depends radically on the measurement technique (ref. 17). Inadvertant blemishes (particularly those unrecorded) which could occur during handling and/or during the flight present problems in data analysis. Degrading ablative thermal protection systems result in an ill-defined, time-dependent roughness. Wilkins and Tauber (ref. 18) observed well-defined surface patterns (similar to turbulence wedges) downstream of small

irregularities premachined into plastic models. Analyzing data from blunt vehicles, Hearne, et al, (ref. 19) concluded, "There is a general trend for a reduced Re_θ at transition with increase in surface roughness, but the influence is not strong".

(5) Gaseous injection into the boundary layer - It is obvious that the injection of ablation products into the boundary layer introduces a destabilizing disturbance. However, an increase in injection rate normally results in a lower surface temperature which tends to stabilize a laminar boundary layer. The injection of heavy molecules should produce an effect similar to cooling, i.e., an increase in the density of the gas near the surface. The counterbalancing of such stabilizing and destabilizing effects associated with injection has been observed experimentally by Scott and Anderson (ref. 20). Using a porous cone with a sharp, solid tip, the transition Reynolds number was found to decrease with increased injection (initially more for helium than for air per unit change of injection rate). However, for a fixed injection rate, it was found that precooling the injectant muted the destabilizing effect of gas injection to the point that injection of relatively cool helium resulted in a transition Reynolds number greater than the no-blowing value. Additional studies of transition have been conducted with a uniform gaseous injection distribution for porous cones with sharp, solid tips (refs. 21 and 22). The sharp-cone transition Reynolds number decreased significantly with increasing injection rate and with decreasing molecular weight of the injectant.

In a study of the combined film and transpiration cooling effects on a slightly blunted cone (ref. 23), premature transition due to injectants was observed. By relating the data of ref. 23 to transition locations observed previously in the Vought Aeronautics Company Hypervelocity Wind Tunnel using different models, the effect of the injectants could be estimated. For a given mass of injectant the reduction in transition Reynolds number observed with a nonuniform injection distribution was greater than had been observed by others with uniform injection. The data underlined the desirability of obtaining transition measurements which reflect the injection distribution without varying model geometries.

Other studies of the effect of mass addition on boundary layer transition have used models made of low-temperature melting/subliming materials, such as paradichlorobenzene (refs. 24 and 25) or camphor (ref. 26). Although the authors of refs. 24 and 25 found that the transition Reynolds numbers were lower for the ablating cones, the high molecular weight injectant of ref. 26 gave "no significant effects of ablation for these test conditions".

During the current study heat-transfer-rate and surface-pressure distributions were measured in the Vought Aeronautics Company Hypervelocity Wind Tunnel using both nonporous and porous conical models. The quantitative data supplemented by shadowgraphs were used to determine the effects of injection

(including injectant properties, mass-injection rate, and mass-injection distribution) on the surface pressures, the heat-transfer rates and the transition locations at a nominal freestream Mach number of 12.

More detailed discussions of the data analysis performed at the University of Texas are given in references 27, 28, and 29.

EXPERIMENTAL APPARATUS, TEST PROCEDURE, AND DATA REDUCTION

The experimental apparatus consisted of the wind tunnel, the models, the injectant supply system, and the calibration devices.

Wind Tunnel

The test program was conducted in the Vought Aeronautics Company Hypervelocity Wind Tunnel (HVWT) which is a modified arc-heated facility. The tunnel provides constant flow properties for relatively long run times by means of a variable-volume arc chamber. An on-site digital computer was used for data acquisition and reduction. A double-pass flow visualization system was employed to record shadowgraphs of the model boundary layer and shock wave pattern. A detailed description of the facility is given in refs. 30 and 31.

Models

Three basic sharp-nose conic configurations were tested during this program. Two of the models had 0.004-inch thick nickel skin, half angles of 5 and 12 degrees, and were used to obtain no-injection measurements. The third model was a 12° half-angle cone with an injectant supply system to allow the passage of gas through the 0.008-inch porous, sintered nickel skin.

The thin skins were prepared for each of the models in a similar manner. The skin was cut from sheet stock and chromel-constantan thermocouple junctions were spot welded to the inner surface. For the solid models the skin was rolled into a cone and the butt joint on the 12° cone was secured with an electron beam weld and with solder on the 5° cone. These thin skin shells were overlayed on cones which had insulating surfaces (nylon for the 12° cone and epoxy for the 5° cone). The thermocouple junctions were centered over 0.125-inch diameter holes in the body which resulted in negligible heat loss to the body at the junctions. The porous skin was rolled into a cone and joined by electron beam welding. This skin was fitted over a conic inner body machined from aluminum with provisions for supplying an injectant gas to a plenum under the porous cone. The single porous skin provided a blowing distribution which varied inversely with the distance from the apex. The model was subsequently modified by adding a second instrumented porous skin, separated from the original skin by a second plenum, to provide a uniform injectant distribution.

Each model was fitted with a sharp, nonporous nose section nominally 4% of the model length. These tip sections were fabricated from stainless steel so that a sharp apex would be maintained during the course of the tests.

The models had one instrumentation ray consisting of closely spaced thermocouple junctions to provide a detailed heat transfer rate distribution. A second ray was used to obtain pressure data and for secondary heating measurements. The comparison of heat transfer data from the two rays provided a means for evaluating the flow symmetry. The surface pressures were measured with transducers mounted within the models.

Model dimensional data are given in Table I and an illustration of the transducer locations on a model is shown in Fig. 1. A drawing showing the internal passageways for the injectant and a photograph of the porous model prior to final assembly are presented in Fig. 2. Views of two configurations mounted in the tunnel may be seen in Fig. 3. Fig. 3a shows the basic porous model while Fig. 3b is a photograph of the porous model with a screen overlay which was used during the tests related to roughness effects. The experimental study of the effects of roughness was performed with two screen overlays and the double-skin porous model. The geometry of the roughness elements is defined in Table IB.

Injectant Supply System

The injectant supply system for the porous model configurations consisted of the injectant reservoir, a regulator system to control the mass flow rate, a calibrated metering system to measure the flow rate, the model internal passageway and associated plumbing, and solenoid valves to initiate and terminate the supply of injectant to the model.

Calibrations

Calibrations were conducted to obtain the injectant mass flow rate and the velocity distribution along the model. The flow rate was determined by measuring the injectant total pressure and temperature upstream of a sonic orifice of calibrated effective area. This area was calibrated as a function of both supply pressure and gas used as injectant. The velocity distribution of the injected gas was measured with a compensating hot wire system which was developed by Vought Aeronautics Company to provide good resolution of the injectant velocity at low static pressure levels. Samples of the measured injectant distributions are presented in Fig. 4 for a nominal injectant rate of 0.35%. The sharp "dips" for the $\lambda = 135^{\circ}$ survey are located at the pressure orifices.

Test Procedure

Once the calibrations described above and the calibrations of the model and flow diagnostic transducers were completed, the test procedure was as follows. The injection supply system was set at the proper pressure to pro-

vide the desired injection rate. The tunnel was prepared for operation at the desired flow condition and, after the energy bank was charged and the data channel zeros were recorded on magnetic tape, an automatic run sequence was engaged. This sequence activated the injectant supply system, initiated the data acquisition program, fired the tunnel, and triggered the spark source for the flow visualization system. After the termination of the run, the sequence shutdown all of the tunnel systems and associated equipment.

Data Reduction

The data from the flow diagnostic transducers and the model pressure and heat transfer sensors were acquired by means of a digital computer and were stored on magnetic tape. Following a run, the data were retrieved and processed by a data reduction computer program. The flow conditions were obtained using the methods described in ref. 32. The heat transfer rates were determined from computer curve fits of the model temperature time histories and the thermal mass of the particular skin.

Run Schedule

A summary of the pertinent parameters for each run condition is given in Table II.

DISCUSSION OF RESULTS

Pressure Correlations

The pressure measurements for the 12° cones at a nominal freestream Mach number of 12 and a freestream Reynolds number of 6×10^{6} per foot are presented in Fig. 5. Included in the figure are surface pressure measurements which were obtained using the solid model, the porous model without injection, and the porous model with injection. Examination of the pressure distributions indicates that mass-injection had little or no discernable effect on the pressure. This is consistent with the fact that the displacement thickness of the computed viscous flow did not vary significantly over the range of mass-injection rates. There were some exceptions, such as the low pressure recorded at the forward station for a high injection rate.

The theoretical value for the pressure coefficient at the apex is that for inviscid flow of a perfect gas past a sharp cone (ref. 33). To approximate the effect of the expanding flow in the conical nozzle, the pressure was assumed to decrease linearly from the value computed for the apex of the model in accordance with the ratio of freestream values at the apex and at the base (solid line of Fig. 5). For the conditions of this test the freestream static pressure at the base was approximately 0.8 of the freestream static pressure at the apex. The pressure perturbations due to viscous interaction have been

calculated using the relations of Hayes and Probstein (ref. 34):

$$\frac{P}{P_{orig}} = 1 + \gamma J_{ci} \frac{M}{M_{orig}} \frac{d_{orig}}{\sqrt{3}} \frac{M_{orig}^3 \sqrt{C_{orig}}}{\sqrt{Re_{x,orig}}} \qquad (1)$$

As would be expected at the high Reynolds numbers of this program, the effect of viscous interaction is relatively small.

An experimental fairing of the pressure data was also constructed as shown in Fig. 5. The experimental fairing of Fig. 5 was used to compute the boundary conditions in a numerical solution of the viscous layer.

Heat-Transfer Correlations

No-injection, or reference, results.- The experimental heat-transfer-rate distributions for six of the "no-injection" flow conditions are presented in Fig. 6. Using heat-transfer distributions as a guide, boundary layer transition occurred for all four non-injection test conditions at the higher Reynolds number, i.e., conditions 1, 4, 7, and 13, but did not occur for any non-injection runs at the lower Reynolds number.

For the laminar portion of the model the agreement between the heat-transfer measurements along the two instrumented rays was considered excellent, and thus, the flow was clearly symmetric. However, within the transitional flow, significant differences often existed between the heating-rates measured at a particular body location on the two rays. Furthermore, although the number of thermocouples on the $\lambda = 135^{\circ}$ ray was limited, even the transition "location" may differ somewhat from one ray to the other, viz, Fig. 6b. This was not believed to represent an asymmetry in the flow, but rather is a manifestation of the fact that the transition process takes place over a distance and is a nonlinear amplification of disturbances.

The theoretical laminar heating distributions, which are included in Fig. 6, were calculated using three different methods:

(1) Eckert's reference temperature method (ref. 35) with the inviscid flow properties assumed constant along the cone and computed using the sharp cone value of the pressure (ref. 33), designated ERT, TP,

(2) Eckert's reference temperature method with the inviscid flow properties computed assuming an isentropic expansion in accordance with the experimental pressure distribution (e.g., Fig. 5), designated ERT, EP, and

(3) a numerical routine developed at the University of Texas to solve the laminar boundary layer equations accounting for nonsimilar effects which are present (ref. 36) with the inviscid flow proper-

ties computed assuming an isentropic expansion in accordance with the experimental pressure distribution (Fig. 5), designated NONSIMBL, EP, and

(4) the NONSIMBL, TP nomenclature denotes the use of the numerical routine with the inviscid flow properties assumed constant and computed using the sharp cone value of the pressure (ref. 33).

For the solid cones, i.e., conditions 1 through 6, the agreement between the calculated heat-transfer rates and the measured values in the laminar region was considered very good. The use of the experimental pressures slightly improved the correlation between the calculated and the measured heating rates.

The two theoretical distributions based on the experimental pressures, i.e., ERT, EP, and NONSIMBL, EP, are almost identical, e.g., Fig. 6b. Such close agreement for these "no-injection" computations was not surprising, since the boundary layer for supersonic flow past a sharp cone is usually assumed to be "similar".

For the porous cones the agreement between the calculated and the measured heat-transfer rates was not considered good except for condition 30, i.e., the lower Reynolds number condition. The experimental distribution which closely follows the theoretical distribution indicates that the flow was laminar at all points. The agreement between the calculated and the measured heat-transfer rates was considered satisfactory for conditions 7 and 13, i.e., the higher Reynolds number condition using a model with a single, porous skin and with a double, porous skin, respectively. Some deviation between the calculated and the measured distributions was noted and might be attributed to model "breathing". It was possible that the character of the boundary layer might have been altered by localized suction or blowing (which were balanced so that the net mass transfer was zero, since the injectant supply passage just beneath the skin was not vented). However, the effect of breathing per se is believed to be small. This conclusion is based on the following reasoning:

(1) The pressure differential between the surface pressure (open symbols of Fig. 7) and the pressures measured using orifices located in the injection passage (solid symbols of Fig. 7) is greater near the apex. Thus, one would conclude that inward flow, or suction, (and, therefore, relatively higher local heating rates) should be greater near the apex. However, a comparison of the distributions (or trends) for the measured and the theoretical heat-transfer rates indicates the opposite, i.e., the increases in local heating are greatest at downstream locations, viz, Fig. 6d.

(2) Additional evidence that this deviation is related to transition may be seen by comparing the locations of transition for the porous model as determined using the heat-transfer-rate distribution with that determined using the shadowgraphs. If the shadowgraph location of transition was defined to be that point downstream of which there were no traces of a laminar boundary layer,

then x_{tr} varied from 0.58 ft. to 0.61 ft. for condition 13 as shown in Fig. 8. Assuming that the heat-transfer data indicate the transition location to be that point at which the heat-transfer data begin to deviate from a "laminar" distribution, x_{tr} was 0.52 ft. This corresponds to $x_{tr} = 0.66\ x_L$ in Fig. 6e. However, a turbulent burst was clearly evident in the shadowgraph at x = 0.40 ft., indicating the transition process was fairly well developed at this point on the $\lambda = 180^o$ ray. Thus, at least for the no-injection conditions, it is believed that the "sharp" change in the heat transfer distribution does not necessarily provide a realistic transition location on the porous models. Instead, modest deviations of the measurements from laminar theory (which occur upstream of the "sharp" change and which might otherwise be attributed to experimental error) indicate the existence of the transition process as modified by slight breathing.

Therefore, the differences between the measured and theoretical heating-rates which might otherwise be attributed to experimental error for conditions 7 and 13 are believed to be the result of a transition process, which may be modified by slight "breathing" through the porous skin.

The fact that the transition "location" determined from the shadowgraph is downstream of the transition "location" determined from the heat transfer distribution is typical since the shadowgraph represents the end of transition whereas the heat transfer data were used to locate the beginning of transition. However, Fig. 8 does illustrate an interesting feature: the existence of a turbulent burst upstream of the apparent heat-transfer-determined transition "location". Since turbulent bursts characterize the third phase of the transition process as described by Morkovin (ref. 37), the photograph indicates that the transition process is well underway at the point where the slope of the heat-transfer-rate distribution changes rapidly. As discussed previously, this anomaly in the heat-transfer results is believed to reflect a peculiarity in the transition process (which produced subtle changes in the heat-transfer data) for the "no-injection" conditions of flow over porous models.

Fig. 8 is representative of the quality of the shadowgraphs obtained during the current program. The shock wave angle was measured to be 14.5^o, which compares closely with the theoretical value of 14.3^o given in ref. 33 for a 12^o cone. No correction was made to account for the boundary layer displacement thickness, since it was small.

The effect of gas injection on laminar heat transfer. - Gas injected into the boundary layer can significantly affect the shear stress at the wall and the local heat transfer for both laminar and turbulent viscous flows. Even the character of the boundary layer may change, since injection may promote early transition. Changes may also occur in the inviscid flow if the rate of gas injection is very high, often termed massive blowing. However, since the blowing rates of the present program were not sufficient to alter the inviscid flow, attention will be given only to the effects of injection on the viscous flow. Correlation parameters, which indicate the effect of mass-injection, depend upon the properties of the injectant, the injection rate, and the in-

jection distribution. The latter is usually characterized as being in one of two broad classes: (1) film cooling or (2) transpiration cooling.

Film cooling involves injecting a gas or liquid over a limited portion of the total surface, either tangentially or perpendicularly to that surface, and allowing the injectant to be spread by the freestream gas into a thin film over the remainder of the surface. Several distinct trends have been observed in relation to film cooling:

(1) By increasing the mass flow rate in the injection region, downstream heating rates can be decreased, providing boundary layer transition does not occur.

(2) Lighter gases are more effective than heavier gases in reducing the heat transfer rates (ref. 38).

(3) The effectiveness of film cooling in reducing the heat transfer decreases with distance from the injection region (ref. 23 and ref. 39).

Transpiration cooling results when injection occurs perpendicular to the surface over the entire surface that is to be cooled. Since the injectant is introduced through a porous surface, the rate of fluid injection can be adjusted by mechanical means. Therefore, the heating rates can be controlled by varying the injection rate and the temperature of the injectant.

Several of the same trends associated with film cooling have been noted for transpiration cooling. More specifically:

(1) In the laminar region, the higher the injection rate the lower the heating rate. That is, for a given injectant, at a given location, the heating rate decreases as the injection rate increases if flow remains laminar (ref. 40).

(2) The lower the molecular weight the more effective the gas is as a coolant (ref. 40). At a given location, at a given injection rate, the lighter the gas the more reduction in heat transfer, providing the flow remains laminar. This effect is present because the effectiveness of an injectant in reducing the heating rate depends on its ability to move away from the wall. The lighter gases are able to move more quickly into these regions (ref. 40 and ref.19).

(3) Lighter gases are more destabilizing to the boundary layer (ref.39). As a result, premature transition may occur due to injection and turbulent heating rates might exist in a region that, without injection, would have had lower laminar heating rates. A heavier molecular weight gas will give a result similar to cooling the wall (i.e., increasing the density near the surface), and thus, have less of an effect on the transition of the boundary layer (ref. 40).

Three injectant gases were used in the present program: nitrogen (MW=28), methane (MW=16), and freon (monochlorodiflouromethane-$CHClF_2$, MW=86). The

heat-transfer-rate distributions which are representative of the data of the present program are presented in Fig. 9 for several conditions. Tests were conducted at a freestream Reynolds number per foot of about 6×10^6 for all three gases injected uniformly over the entire surface, i.e., the local injection rate was essentially independent of location. In addition, data were obtained using nitrogen injected with a variable mass-injection distribution at a freestream Reynolds number of 6×10^6 per foot. This variable distribution only roughly approximated a "similar" distribution. Methane was also injected in a "constant" distribution with a freestream Reynolds number per foot of approximately 3×10^6. The rate of mass injection was another variable of the test program. The rate of the mass injection (integrated over the entire cone) ranged from 0.20% to 2.1% of the freestream mass flux across an area equal to that of the cone base.

The data are compared with theoretical heat transfer distributions computed using the NONSIMBL numerical routine (ref. 36). This routine provides numerical solutions of a laminar boundary layer for the following conditions:

(1) either compressible or incompressible flow
(2) possible pressure gradient in the external flow
(3) two-dimensional or axisymmetric configuration
(4) arbitrary freestream gas
(5) arbitrary injectant, injection rate, and injection-rate distribution
(6) arbitrary wall temperature

The solution is limited to nonreacting flows. The input for NONSIMBL includes the molecular weights of the stream and of the injectant gases, the gas constant for the stream gas, the stagnation temperature and the stagnation pressure of the inviscid flow (both of which are assumed constant), the static pressure distribution (from which the edge properties are calculated assuming isentropic expansion or compression), the mass-injection distribution, and the wall-temperature distribution. Also input are the specific heat, the viscosity, and the thermal conductivity for both the stream and the injectant gases. Since these properties were calculated using temperature-dependent polynomial approximations, it was possible to utilize real gas values for the specific heat, the viscosity, and the thermal conductivity.

As can be seen in Fig. 9, there is relatively good agreement in the laminar region between the data and the theoretical values predicted by NONSIMBL for all but one run condition. The exception is for the highest freon injection, Fig. 9e, which will be discussed later. In Fig. 9a the agreement may not seem acceptable until one realizes that except for the first thermocouple the measurements are either in the transitional or in the turbulent region.

The effect on the heat transfer of increasing the injection rate is shown for a uniform injection in Fig. 10 and for variable injection in Fig. 11. Only data for those thermocouples in the laminar region are presented. The data for runs with methane, nitrogen, and freon with a "constant" mass injection distribution at a freestream Reynolds number per foot of approximately 6×10^6 are presented in Fig. 10. The Reynolds number is also 6×10^6 for the data of Fig.11, but with nitrogen injected with a "similar" (variable) mass injection distribution.

For each of these conditions NONSIMBL indicates that, had the boundary layer remained laminar, "blow-off" would have occurred at the highest injection rate, as evidenced by the fact that the Stanton number went to zero. Note that the agreement between theory and experiment in the laminar region is extremely good for the no-injection and for the highest injection cases, e.g., Fig. 10b. However, the agreement is not as good for the lower injection rates. A possible source of this discrepancy at the lower injection rates may be due to possible differences between the calibrated injection distribution, which was used as input for NONSIMBL, and the actual injection distribution which existed during the test. Although the total flow rate (as indicated by C_i) was measured during each test and was therefore known, it was not possible to measure the actual injection distribution. The differences are believed to be small, since the measured heating rates do not differ radically from the computed values.

It might be noted that for "similar" injection of nitrogen, no heat-transfer measurement appears in Fig. 11 for the maximum injection rate, i.e., condition 10 for which $C_i = 2.1\%$. For this condition the experimental heat-transfer-rate distribution indicated that the first thermocouple was in the transitional zone. The theoretical heat-transfer-rate distribution indicated that "blow-off" would have occurred prior to the first thermocouple had the boundary layer remained laminar.

These figures concur with two findings often appearing in the literature, namely that as injection rate is increased the laminar heating rate (represented by the Stanton number) decreases and the onset of transition moves forward.

The effect of the molecular weight of the injectant on the laminar heating rates is indicated in Fig. 12 where the Stanton number distribution is presented for no-injection, freon, nitrogen, and methane injected with a "constant" distribution at a Reynolds number per foot of approximately 6×10^6. It can be seen that at a particular laminar station the lighter gas is more effective in reducing the heat transfer. It might also be noted that the lighter the gas, the more quickly the flow transits.

Finally, the effect of different mass-injection distributions is seen by comparing Fig. 10b with Fig. 11. These figures indicate that near the apex where the injection is at a peak for the "similar" distribution (Fig. 11) the heating rates are less than the heating at the same locations for the "constant" distribution (Fig. 10b). However, the "constant" distribution causes the greater reduction in the heat transfer rates further downstream, because for a given total mass-injection rate the local injection rate over the last four-fifths of the model will be greater for the "constant" than for the "similar" mass injection distribution.

Although the theory, as represented by NONSIMBL, was considered to be a reasonable representation of the data on an individual basis, more general correlations were sought. Since it has been widely utilized in the literature, e.g., ref. 19 and ref. 41, the term $(\rho_w v_w / \rho_e u_e)\sqrt{Re_x}$ was a component of the initial correlating parameter. This parameter also included a factor to account

for the difference between the molecular weight of the injectant and that of the stream gas, $(MW_{str}/MW_{inj})^{0.25}$, and a factor to account for the non-porous region near the apex, $((x-x_o)/x)^{0.50}$. As can be seen in Fig. 13, the ratio of Stanton number with injection to Stanton number without injection decreased as the injection parameter increased. An increase in $(\rho_w v_w/\rho_e u_e)$ indicates directly that the local injection is increased and the terms $(Re_x)^{0.50}$ and $((x-x_o)/x)^{0.50}$ increase as one proceeds downstream, i.e., as the boundary layer thickens for a particular test condition. This figure includes laminar data from all conditions that had a "constant" mass-injection distribution. The shaded band was obtained using theoretical values of the Stanton numbers generated by NONSIMBL using the calibrated mass-injection distribution for the test condition. Part of the breadth of the theoretical band is attributed to the variations in flow conditions from one run to another and to the fact that the injection distributions were not truly constant. The results where the Stanton number ratio is greater than one are those from thermocouple number one (with the exception of condition 22, which was obtained using thermocouple number two). Thermocouple number one was nearest the apex and frequently indicated heating rates which differed significantly from theory (refer to Fig. 9). Also, it should be noted that condition 16 (the highest injection rate using freon) exhibits the greatest disagreement with the theoretical band. As previously mentioned, the only run in which the experimental heat-transfer rate distribution disagreed radically with the theoretical distribution was the highest freon injection. In this case the theory underpredicts the data considerably. However, in Fig. 9c the theoretical values for the highest nitrogen injection rate (condition 19) agree with the measurements. By comparing condition 16 in Fig. 9e with condition 19 in Fig. 9c, it can be seen that the theoretical heating rate distributions appear qualitatively correct in that for a given injection rate and freestream condition, the heavier molecular-weight injectant (in this case freon) is less effective in reducing the heating rate. Thus, the theoretical distribution for the highest freon injection run appears to be correct. The lack of correlation of the high injection freon data in Fig. 13 reflects the disagreement between theory and data with high freon injection in Fig. 9e. It is considered that the differences between other experimental and theoretical values in Fig. 13 result primarily from the possible deviation between the mass injection distribution input for the numerical solution and that which occurred during the test.

The correlation parameter used in Fig. 13 was also employed with the heat transfer reduction data for the "similar" mass injection distribution. However, it was apparent that a different parameter was required to obtain an acceptable correlation. It was found that these data could be correlated more satisfactorily with a parameter that included the total mass injected, C_i, the Reynolds number, the distance to the particular station, and the ratio of the product of the velocity and density at the edge of the boundary layer to the product of the velocity and density in the freestream. Fig. 14 indicates that as this parameter increases, the ratio of Stanton numbers decreases. This parameter is similar to those used to correlate data from film cooling investigations (ref. 23). The success of this parameter in correlating the present data was attributed to the peculiar injection distribution. The relatively large local injection rate near the apex for the "similar" injection distribution appeared

as film cooling to the thermocouples of the laminar region, all of which were located just downstream of the high injection-rate region.

The effect of gas injection on turbulent heat transfer. - Heating rates indicative of fully turbulent flow were obtained at two thermocouples for the no-injection run at the high Reynolds number condition, $Re_\infty/ft = 6 \times 10^6$. Since gaseous injection induced early transition, the boundary layer at these two thermocouples would be turbulent for tests with injection also. Therefore, one could analyze the heating-rate measurements at these two thermocouples to establish the effect of mass-injection on turbulent heat transfer.

The reduction in heat-transfer due to mass-injection (in the form of the ratio of the Stanton number in the presence of mass-injection to the Stanton number measured at the same thermocouple without injection) is presented in Fig. 15. The injection-rate parameter used is that used by Baronti, et al, (ref. 42), i.e.,

$$\frac{\rho_w v_w}{\rho_e u_e St} \quad .$$

Included for comparison with the present data is a band representing the experimental results from a variety of reports as summarized in ref. 42. Although the injection-rate parameter does not include a factor to reflect the use of different injectants, Baronti, et al, note "as is expected, significant Mach number and molecular weight effects are obtained". The data from the present program clearly indicate the need to consider the properties of the injectant.

The reduction in heat transfer is presented in Fig. 16 as a function of an injection rate parameter which includes the injectant,

$$\frac{\rho_w v_w}{\rho_e u_e St} \left(\frac{C_{p,inj}}{C_{p,str}} \right) \quad .$$

The use of the specific-heat ratio as the pertinent correlation property for turbulent flow has been suggested by Hearne, et al, (ref. 19), among others. As can be seen, the correlation is significantly improved by the inclusion of a specific-heat ratio in the injection-rate parameter.

As noted, only the last couple of thermocouples for the noninjection run were in turbulent flow. Using these heating rates as a reference may produce misleading results, since the noninjection data may be in the local "peak" heating zone typical of the end of transition. Therefore, caution is advised in using the results of Figs. 15 and 16.

Boundary Layer Transition Correlations

Three methods were used to determine the "location" of transition of the boundary layer. They were:

(1) the point at which the heat-transfer data first deviated from the laminar distribution,
(2) the point at which the heat transfer data indicated the flow was completely turbulent, and
(3) the point on the shadowgraph downstream of which the boundary layer appeared to be completely turbulent.

The transition locations determined by the second and third methods usually agreed within the ability to define the location. Thus, the location determined by these two methods was assumed to be the end of the transitional zone. The location of transition determined by the first and the third methods are presented in Table III. The individual values appearing in this table were obtained by averaging the transition data whenever there was more than one value of the transition location available. For example, the shadowgraph locations in Table III are the average of the values obtained for two rays ($\lambda = 0^{o}$ and $\lambda = 180^{o}$) in each of the shadowgraphs and the heat transfer determined locations were obtained from the two instrumented rays. Also, if a particular condition had repeat runs, the data obtained from all of the runs were averaged.

The flow field as indicated by the shadowgraph and the heat transfer distribution are compared in Fig. 17. The results, which are typical, are for constant nitrogen injection $C_i = 0.32\%$. The transition locations determined by the three methods may be seen. The onset of transition as determined by the deviation from the laminar heating distribution is upstream of the transition locations determined using the other two criteria. Furthermore, it is difficult to confidently distinguish between the transition locations of these two criteria.

In Fig. 17 it should be noted that between the transition location determined by heat transfer data and the location determined by the shadowgraphs are two turbulent bursts. Numerous turbulent bursts were observed in the transitional boundary layer for those tests with mass injection. For the injection runs the bursts always occurred between the heat-transfer-determined beginning-of-transition location and the end-of-transition location determined from the shadowgraph.

In addition, Table III includes values of other transition related parameters. These are the freestream Mach number, the freestream unit Reynolds number, the local Mach number, the local unit Reynolds number, the ratio of the wall-to-stagnation-temperature, the integrated transition Reynolds number based on wetted length to transition, the transition value of the displacement thickness Reynolds number, and the momentum thickness Reynolds number. The displacement thickness and the momentum thickness at the transition location were computed using the numerical code. Values are presented for the transition locations as determined using the heat-transfer-rate distributions for the porous models (conditions 7 and 13), but the previous discussion concerning the in-

fluence of the porous surface should be considered.

No-injection, or reference, results. - Determining the effect of the injectant properties, the mass-injection rate, and the injection distribution on boundary layer transition was one of the primary objectives of the contractual effort. To establish the effect of gas injection on a particular transition parameter, it is first necessary to determine the "no-injection" value of that parameter at the same flow conditions. To establish the "validity" of these reference values of the transition Reynolds number, comparisons were made with the results available in the literature for comparable conditions. The word validity is in quotes because of the controversy concerning the relation of tunnel noise to transition measurements made in wind tunnels. No attempt was made to establish the validity of the transition measurements in the absolute sense, but it was shown that the transition Reynolds numbers from the present program are consistent with previous results and, therefore, serve as a satisfactory reference to establish the effect of gas injection.

The transition Reynolds number based on local flow properties at the edge of the boundary layer and the displacement thickness is presented in Fig. 18 as a function of the local, inviscid Mach number. The shadowgraph-determined locations compare favorably with the values obtained previously in the HVWT (ref. 43). The data also compare favorably with the correlation from a summary of wind tunnel data which appeared in ref. 44. Satisfaction with this favorable comparison is tempered when one considers that the summary correlation represents a broad range of acceptable values.

Of the numerous transition investigations reported in the open literature it was to be expected that several would include flow parameters comparable to those of the present program which were nominally a local Mach number of 7 or 10, a local unit Reynolds number of 10×10^6/ft, and a temperature ratio of 0.16. The limited non-injection data are seen to agree favorably with the literature as shown in ref. 27.

Effects of gas injection on transition. - Using the departure of the heat transfer data from the laminar distribution to indicate the beginning of transition and the shadowgraph locations to indicate the end of transition, the ratio $Re_{x,tr,f}/Re_{x,tr,i}$ (an indication of the length of the transitional zone) was calculated. Fig. 19 presents this ratio for the various injectant gases at the different injection rates. In addition to the data from the present test, the correlation for no-injection data of ref. 45 is also presented in this figure. The transition length ratio for the no-injection test of the present program agrees with the no-injection correlation of ref. 45. The data of Fig. 19 indicate that, for a particular injectant, as the injection rate increases, the length of the transitional zone decreases. As would be expected, the similar mass-injection distribution gave results that did not correlate well with the data from the "constant" mass-injection distribution, but did indicate the same general trend of decreased transitional zone length with increased injection for a given onset-of-transition Reynolds number.

Table III permits a careful examination of the effect on transition of mass injection rate, injectant, and mass-injection distribution, since it

presents transition locations for all the conditions tested. Also presented in the table are values of two other transition parameters, $Re_{\delta^*,tr}$ and $Re_{\theta,tr}$. The values of the displacement thickness and the momentum thickness used to calculate these transition Reynolds numbers were computed using NONSIMBL.

As can be seen in Table III, as the injection rate increases, using a particular injectant the transition Reynolds number decreases for all three gases tested. This effect is present even for freon (MW = 86), the heaviest gas used in this program. It is noted that Mateer and Lawson (ref. 26) reported "no significant effect of ablation for these test conditions", but these data were for a very high molecular weight gas (camphor, MW = 152). Also, it can be seen by comparing the results for the two types of nitrogen mass-injection distribution that the "similar" distribution induces transition earlier than the "constant" distribution for a given total amount of injection. Because the "similar" injection distribution caused transition to occur so early, the procedures used to define the transition locations had to be modified for conditions 9 and 10. As previously mentioned, the first thermocouple was in the transitional zone for the maximum injection case (condition 10). Therefore, the intersection of the fairing of the measured heating rates in the transitional zone with the theoretical laminar distribution was assumed to be the transition location for the "heat-transfer method". Because transition occurred upstream of the shadowgraph field of view for conditions 9 and 10, the "point" at which the experimental heat-transfer distribution indicated the boundary layer was turbulent was assumed to represent the shadowgraph value of the transition location for Table III. Finally, Table III allows some insight into the effect of the type of injectant on the transition point. The results for "constant" mass-injection distribution of nitrogen and methane at a given injection rate, indicate that the lighter gas causes earlier transition, as often noted in the literature.

As with the heat-transfer-rate distribution data, an effort was made to correlate the transition Reynolds number data. The reduction in the transition Reynolds number for the tests with constant injection is presented in Fig. 20 as a function of F, where

$$F = \frac{\int_{x_o}^{x_{tr}} \rho_w v_w \, dA}{\rho_\infty u_\infty A_{b,tr}} \tag{2}$$

a parameter suggested by Marvin and Akin (ref. 22). Also included in Fig. 20 are the correlation line

$$\frac{Re_{x,tr}}{Re_{x,tr,0}} = 1 - 0.25\left(\frac{MW_{str}}{MW_{inj}}\right)^{0.25} F \tag{3}$$

and the data of ref. 22, which also were for a "constant" injection distribution. The transition location for the data presented from ref. 22 were determined using the beginning of transitional-zone heat-transfer methods. The shadowgraph value of the transition Reynolds numbers for the tests with injection were referenced to the transition Reynolds number with no injection obtained by using the shadowgraphs from condition 13. The heat-transfer-rate determined transition Reynolds numbers for injection tests were referenced to the transition Reynolds number with no injection from condition 4. The philosophy of these choices is based on the results briefly described earlier and in detail in ref. 28.

For tests at the lower Reynolds number, i.e., $Re_\infty/ft = 3 \times 10^6$, transition occurred only for the higher injection rates of methane. Therefore, correlations of the effect of injection on the transition criteria could not be made, since the "no-injection" reference values were not available.

The data of Fig. 20 indicate that the length of laminar flow decreases as the parameter F, modified by the usual molecular weight ratio, increases. These "constant" injection data are considered to be in relatively good agreement with the correlation of Marvin and Akin for the three injectants.

Data for the "similar" mass-injection distributions are shown in Fig. 21. It should be noted that a significantly greater reduction in the transition Reynolds number resulted for a given amount of mass injection (integrated to the transition location), because of the relatively large amount of injection near the apex for the "similar" mass injection distribution. It seems logical that relatively large local injection into the thin viscous layer near the apex would accentuate the destabilizing effect of injection. It is felt that the same parameter would not adequately correlate data obtained with the two different mass injection distributions. The inadequacy of a single correlation parameter was also noted in the discussion of the heat-transfer-rate distributions.

Data from ref. 25 are also presented in Fig. 21. Since these data are from an ablating cone of paradichlorobenzene, the amount of gas injected into the boundary layer is dependent on the local heat transfer rate, i.e., is a function of x, and the mass injection rate is greatest near the apex. Thus, the distribution of ref. 25 is of a somewhat similar nature to the variable injection distribution of the present program. However, the non-degrading region near the apex represented 23% of the ablating models of ref. 25, but only about 4% of the models of the present program were nonporous. The agreement between the data of ref. 25 and those of the present program is considered to be relatively good (Fig. 21), considering the differences between the two tests.

The transition data for the "similar" mass injection runs of the present program are presented in Fig. 22 as a function of $C_i/A_{w,tr}$, where $A_{w,tr}$ is the wetted area up to transition. The correlation provides little insight into the behavior of the viscous flow. As can be seen in Fig. 22, the distance to transition in the presence of the two high injection rates, i.e. C_i of 0.70% and 2.1%, does not change appreciably, although the injection parameter $C_i/A_{w,tr}$ does. Due to

the locally high injection rates near the apex in the "similar" mass injection distributions, the boundary layer tends to be "blown-off". Because of this it is considered that premature transition is due to a "tripping action" of the injection, as opposed to a multi-stage breakdown of the laminar flow.

Fig. 23 presents $Re_{\theta,tr}$ as a function of the correlation parameter F. Also presented in Fig. 23, as solid symbols, are data from ref. 22. All the data were obtained with a "constant" mass injection distribution. The methane data from the present program suggest that there is a reduction in $Re_{\theta,tr}$ as F increases. However, the transition Reynolds number for the data from the nitrogen runs appeared to be independent of F. The freon data indicated an increase by $Re_{\theta,tr}$ as F increased. The variations are such, however, that one could assume that the transition Reynolds number based on momentum thickness was essentially independent of F.

Surface Roughness

The surface roughness of a particular vehicle is a difficult parameter to assess. Certainly, roughness represents a disturbance to the flow and roughness elements have often been used to fix the point of transition on models in the wind tunnel. The effectiveness of roughness in promoting premature transition has been found to depend on the Mach number (ref.15) as well as the size, the shape, and the distribution of roughness elements. Van Driest and Blumer (ref. 16) derived an empirical relation, which is very sensitive to the temperature ratio, to define the effective roughness height.

For a degrading ablative thermal protection system, the surface roughness poses an ill-defined, time-dependent problem. In an attempt to simultaneously simulate both the roughened surface of the degrading ablator and the gaseous injection of the ablation process, a fine mesh screen was overlayed on the porous skin of the 12° cone with constant injectant distribution. The characteristics of the two screens which were used are given in Table I. Surface-pressure and heat-transfer-rate distributions and shadowgraphs were obtained for the test conditions of Table II.

The surface pressure distributions for the tests at the low Reynolds number are presented in Fig. 24. For the K_2-screen the experimental values of the pressure coefficient were consistently lower than the results obtained with the smooth model. With the exception of the measurements from the middle orifice (where later examination revealed a scorch pattern) the pressure coefficients for the model with the K_1-screen were likewise lower than the values for the smooth models. These pressure measurements (together with the heat-transfer data) suggest that the flow over a screen element behaved much like the flow over a cavity.

Because the screen elements created continuous disruptions which prohibited the establishment of a well-behaved boundary layer, it was difficult to assess the effect of the upstream boundary layer on the flow field in the "cavity". The diameter of the screen wire was approximately equal to the computed value of the displacement thickness at the first thermocouple for the smooth model

and was approximately one-fourth the computed displacement thickness for the last thermocouple of the smooth model.

Measurements are available (ref. 46) for the pressure distribution in an isolated rectangular cavity with a relative geometry approximately that of a single screen element. The length-to-depth ratios for the elements of the K_1 and K_2 screens were 6.1 and 6.9, respectively. The static pressure in the center of a cavity with a length-to-depth ratio of 5 is approximately 0.95 of the static pressure at the separation step while the pressure at the base of the recompression step of the cavity is approximately 1.1 times the static pressure at the separation step. Thus, the relatively high pressure measured at the middle orifice of the screen covered model and the accompanying scorch pattern noted on the model surface are probably associated with the recompression step of the cavity formed by a screen element. The remaining pressure data are typical of measurements along the floor of a cavity.

Because the flow field exhibited characteristics of flow over open cavities the significance of the effect of the combined mass injection and surface roughness on the heat-transfer-rate distributions was somewhat obscured. The test conditions of the run schedule (Table II) were selected to provide data for:

(1) two surface roughnesses at the same nominal stream conditions with no injection, i.e., conditions 25 and 29 and

(2) the effect of mass-injection for a given surface roughness with the same nominal stream conditions, i.e., conditions 20 and 21, conditions 25 and 26 (Fig. 25), and conditions 29 and 32.

Examination of the data presented in Fig. 26 indicates that the heat-transfer-rate distributions were approximately the same with no injection for both roughness elements although the wire diameters and mesh were substantially different for the two element configurations. However, the similarity of results is not unexpected if the flow views the screen elements as a series of cavities, since the length-to-depth ratio for the elements of the two screens are approximately equal.

Although the "cavity effect" apparently dominated the heat-transfer data (so that the heat-transfer rates on the screen-covered model were less than the laminar heat-transfer rates on the smooth model at the same stream conditions), it was established that:

(1) roughness elements greatly reduced the transition Reynolds number,
(2) gaseous injection through the porous, screen-covered surface further reduced the transition Reynolds number, and
(3) gaseous injection slightly reduced the heat-transfer to the screen-roughened models at all thermocouples.

The two methods used to determine the "location" for transition of the boundary layer for this portion of the program were:

(1) the point at which the heat-transfer data first deviated from the

"laminar" distribution* and

(2) the point on the shadowgraph downstream of which the boundary layer appeared to be completely turbulent.

The transition locations and the corresponding transition Reynolds numbers are presented in Table III. As was the case for the smooth models, the transition Reynolds number determined using the "heat-transfer" method was less than that determined using the "shadowgraph" method. Because the surface roughness radically altered the viscous flow field, values of the properties at the edge of the boundary layer and the transition Reynolds numbers based on displacement thickness and on momentum thickness were not computed.

A further discussion of the analysis of the results obtained during this phase of the program is given in ref. 29.

*Since the screen overlay caused the measured heat-transfer-rate distribution to deviate so radically from the computed laminar distribution, the applicability of these transition results to other roughness situations is questionable.

CONCLUSIONS

Based on the data and analyses presented herein the following conclusions are made for the configurations and test conditions of this program.

1. Gaseous injection had little effect on the surface pressure measurements.

2. The agreement between the theoretical and the experimental heat-transfer rate in the laminar region was acceptable, with the exceptions of the heat-transfer data for the higher rates of freon injection and for screen overlayed roughness models.

3. For a given mass injection rate in a given distribution the laminar region heat transfer decreases as the molecular weight of the injectant decreases.

4. For a given injectant in a given distribution the laminar region heat transfer decreases as the injection rate increases.

5. A satisfactory empirical correlation of heat transfer reduction in turbulent flow with gas injection was obtained by including the specific-heat ratio in the injection-rate parameter.

6. For a given mass injection rate in a given distribution the transition Reynolds number decreases as the molecular weight of the injectant decreases.

7. For a given injectant in a given distribution the transition Reynolds number decreases as the injection rate increases.

8. The heating rate distributions confirmed that the shadowgraphs reliably locate the end of transition and that turbulent bursts were normally located in the transition zone.

9. The momentum thickness transition Reynolds number for the methane injection runs indicate that there is a slight reduction in $Re_{\theta,tr}$ as F increases. However, the momentum thickness Reynolds number for the data from the nitrogen runs appeared to be independent of F.

10. For a given mass injection rate (integrated over the surface of the entire cone), the transition location and heat transfer rates are sensitive to the mass injection distribution. The transition Reynolds numbers were significantly greater when the local injection rate was constant over the surface of the cone, i.e., $\rho_w v_w = C$, than when the local injection rate decreased rapidly with distance from the apex.

11. Transition Reynolds number results obtained with a constant injection distribution correlated well with previously published results for other gases in a different facility.

12. Transition Reynolds number results obtained with a variable injectant distribution were ocrrelated with a limited amount of data available for a degrading model tested in a different facility.

13. For a particular injectant the length of the transitional zone decreases as the injection rate increases.

REFERENCES

1. Reshotko, E.: Stability Theory as a Guide to the Evaluation of Transition Data. AIAA Paper 68-669, presented at the AIAA Fluid and Plasma Dynamics Conference, Los Angeles, June 1968.

2. Stainback, P. C.: Some Effects of Roughness and Variable Entropy on Transition at a Mach No. of 8. AIAA Paper 67-132, presented at the 5th Aerospace Sciences Meeting, New York, January 1967.

3. Everhart, P. E.; and Hamilton, H. H.: Experimental Investigation of Boundary Layer Transition on a Cooled 7.5 Total Angle Cone at Mach 10. NASA TND-4188, October 1967.

4. Wagner, R. D.; Maddalon, D. V.; Weinstein, L. M.; and Henderson, A., Jr.: Influence of Measured Freestream Disturbances on Hypersonic Boundary Layer Transition. AIAA Paper 69-704, presented at 2nd Fluid and Plasma Dynamics Conference, San Francisco, June 1969.

5. Pate, S. R.; and Schueler, C. J.: An Investigation of Radiated Aerodynamic Noise Effects on Boundary Layer Transition in Supersonic and Hypersonic Wind Tunnels. AIAA Journal, Vol. 7, No. 3, March 1969, pp. 450-457.

6. Potter, J. L.: Observations on the Influence of Ambient Pressure on Boundary Layer Transition. AEDC-TR-68-36, March 1968.

7. Lees, L.: The Stability of the Laminar Boundary Layer in a Compressible Fluid. NASA Report No. 876, 1947.

8. Reshotko, E.: Transition Reversal and Tollmien-Schlichting Instability. Physics of Fluids, Vol. 6, No. 3, March 1963, pp. 335-342.

9. Rumsey, C. B.; and Lee, D. B.: Measurements of Aerodynamic Heat Transfer and Boundary Layer Transition on a 10° Cone in Free Flight at Supersonic Mach Numbers up to 5.9. NASA TND-745, May 1961.

10. Mack, L. M.: Boundary Layer Stability Theory. JPL Report 900-277, May 1969.

11. Diaconis, N. S.; Jack, J. R.; and Wisniewski, R. J.: Boundary Layer Transition at Mach 3.12 as Affected by Cooling and Nose Blunting. NACA TN 3928, January 1957.

12. Richards, B. E.; and Stollery, J. L.: Further Experiments on Transition Reversal at Hypersonic Speeds. AIAA Journal, Vol. 4, No. 12, December 1966, pp. 2224-2226.

13. Potter, J. L.; and Whitfield, J. D.: The Relation Between Temperature and the Effect of Roughness on Boundary Layer Transition. Journal of the Aerospace Sciences, Vol. 28, No. 8, August 1961, pp. 663-664.

14. Maddalon, D. V.: Effect of Varying Wall Temperature and Total Temperature on Transition Reynolds Number at Mach 6.8. AIAA Journal, Vol. 7, No. 12, December 1969, pp. 2355-2357.

15. Whitfield, J. D.; and Ianuzzi, F. A.: Experiments on Roughness Effects on Cone Boundary Layer Transition Up to Mach 16. AIAA Journal, Vol. 7, No. 3, March 1969, pp. 465-470 (was AIAA Paper 68-377).

16. van Driest, E. R.; and Blumer, C. B.: Boundary Layer Transition on Cones and Spheres at Supersonic Speeds - Effects of Roughness and Cooling. AFOSR Scientific Report 67-2048, July 1967.

17. Merlet, C. F.; and Rumsey, C. B.: Supersonic Free-Flight Measurement of Heat Transfer and Transition on a 10° Cone Having a Low Temperature Ratio. NASA TND-951, August 1961.

18. Wilkins, M. E.; and Tauber, M. E.: Boundary Layer Transition on Ablating Cones at Speeds up to 7 km/sec. AIAA Journal, Vol. 4, No. 8, August 1966, pp. 1344-1348.

19. Hearne, L. F.; Chin, J. H.; and Woodruff, L. W.: Study of Aerothermodynamic Phenomena Associated with Reentry of Manned Spacecraft. Lockheed Missiles and Space Company Report Y-78-66-1, May 1966.

20. Scott, C. J.; and Anderson, G. E.: Boundary Layer Transition with Gas Injection. University of Minnesota, Rosemount Aeronautical Laboratories, Research Report No. 151, July 1958. (Condensed version in Journal of the Aeronautical Sciences, Vol. 25, No. 12, December 1958, p. 791.)

21. Scott, C. J.: Experimental Investigations of Laminar Heat Transfer and Transition with Foreign Gas Injection - A 16° Porous Cone at M = 5. University of Minnesota, Rosemount Aeronautical Laboratories, Research Report No. 174, October 1960.

22. Marvin, J. G.; and Akin, C. M.: Combined Effects of Mass Addition and Nose Bluntness on Boundary-Layer Transition. AIAA Journal, Vol. 8, No. 5, May 1970, pp. 857-863.

23. Wimberly, C. R.; McGinnis, F. K.; and Bertin, J. J.: Transpiration and Film Cooling Effects on the Aerodynamic Forces and Heat Transfer for a Slightly Blunted Slender Cone at Mach 12 and 17. AIAA Journal, Vol. 8, No. 6, June 1970, pp. 1032-1038.

24. DiCristina, V.: Three-Dimensional Laminar Boundary Layer Transition on a Sharp 8° Cone at Mach 10. AIAA Journal, Vol. 8, No. 5, May 1970.

25. Fischer, M. C.: An Experimental Investigation of Boundary Layer Transition on a 10° Half-Angle Cone at Mach 6.9. NASA TN-5766, April 1970.

26. Mateer, G. G.; and Larson, H. K.: Unusual Boundary Layer Transition Results on Cones in Hypersonic Flow. AIAA Journal, Vol. 7, No. 4, April 1969, pp. 660-664.

27. Bertin, J. J.; McCloskey, M. H.; Tamburello, N.; and Hull, D. J.: A Study of Boundary Layer Transition on Outgassing Cones in Hypersonic Flow, Part I - The No Injection or Reference, Measurements. Aerospace Engineering Report 71001, The University of Texas at Austin, January 1971.

28. McCloskey, M. H.; Bertin, J. J.; and Zickler, J. L.: A Study of Boundary Layer Transition on Outgassing Cones in Hypersonic Flow, Part II, The Effect of Mass-Injection on Laminar Heating and Boundary Layer Transition. Aerospace Engineering Report 71002, The University of Texas at Austin, February 1971.

29. Bertin, J. J.; Zickler, J. L; and McCloskey, M. H.: A Study of Boundary Layer Transition on Outgassing Cones in Hypersonic Flow, Part III, Surface Roughness and the Effect of Gas Injection on Turbulent Heat Transfer. Aerospace Engineering Report 71004, The University of Texas at Austin, February 1971.

30. Stalmach, C. J., Jr.: Design and Operation of a Variable Volume Arc Chamber in a Hypervelocity Wind Tunnel. Proceedings of the 4th Hypervelocity Techniques Symposium, November 1965.

31. Stalmach, C. J., Jr.: Application of LTV's Unique Long Run Time Hypervelocity Wind Tunnel to Reentry Problem Areas. Proceedings of the 7th Navy Symposium on Aeroballistics, June 1966.

32. Pope, T. C.: Equations for the Reduction of Flow Property Data in the LTV Hypervelocity Wind Tunnel. LTV Report No. 2-59740/6R-2310, May 1966.

33. Ames Research Staff: Equations, Tables, and Charts for Compressible Flow. NACA Report 1135, 1953.

34. Hayes, W. D.; and Probstein, R. F.: Hypersonic Flow Theory. Academic Press, New York, 1959.

35. Eckert, E. R. G.: Engineering Relations for Friction and Heat Transfer to Surfaces in High Velocity Flow. Journal of the Aeronautical Sciences, Vol. 22, No. 8, August 1955, pp. 585-587.

36. Bertin, J. J.; and Byrd, O. E., Jr.: The Analysis of a Nonsimilar Boundary Layer - A Computer Code (NONSIMBL). University of Texas at Austin, Aerospace Engineering Report 70002, August 1970.

37. Morkovin, M. V.: Transition from Laminar to Turbulent Shear Flow a Review of Some Recent Advances in Its Understanding. Transactions of the ASME, Vol. 80, July 1958, pp. 1121-1128.

38. Hillsamer, M. E.; and Mallard, S. R.: The Effects of Active Cooling on the Aerothermodynamic Characteristics of Slender Bodies of Revolution. AEDC-TR-65-22, February 1965.

39. Goldstein, R. J.; and Jabbari, M. Y.: Film Cooling Effectiveness with Helium and Refrigerant 12 Injection Into a Supersonic Flow. AIAA Journal, Vol. 8, No. 12, December 1970, pp. 2273-2274.

40. Gross, J. F.; Hartnett, J. P.; Masson, D. J.; and Gasley, C., Jr.: A Review of Binary Boundary Layer Characteristics. Project Rand RM-2516, June 1959.

41. Leadon, B. M.; Scott, C. J.; and Anderson, G. E.: Mass-Transfer Cooling of a 20° Porous Cone at M = 5. University of Minnesota, Rosemount Aeronautical Laboratories, Research Report No. 143, July 1957.

42. Baronti, P.; Fox, H.; and Soll, D.: A Survey of the Compressible Turbulent Boundary Layer with Mass Transfer. Astronautica Acta, May - June 1967, Vol. 13, No. 3, pp. 239-249.

43. Stalmach, C. J., Jr.; and Bertin, J. J.: A Proposed Study of Boundary Layer Transition of Outgassing Cones In Hypersonic Flow. LTV Aerospace Report 2-59740/8R-2514, July 1968.

44. Sullivan, E. M.; Ericson, W. D.; Smith, G. L.; and Sutles, J. T.: Some Aspects of Interplanetary Earth Entry Simulation. Presented at the 15th Institute of Environmental Sciences, Anaheim, California, April 1969.

45. Kipp, H. W.; and Masek, R. V.: Aerodynamic Heating Constraints on Space Shuttle Vehicle Design. ASME Paper 70-HT/Apt-45, April 1970.

46. Voorhees, C. G.; and Bertin, J. J.: Effect of Upstream Mass-Injection as the Pressure Field in a Cavity. AIAA Journal, Vol. 7, No. 4, April 1969, pp. 747-749.

TABLE I. - MODEL SUMMARY DATA

A. Basic Models

Skin Material	Skin Thickness In.	θ_c deg.	Base Diameter In.	No. of Sensors on Primary Heat Transfer Ray	Injectant Distribution
Solid Nickel	0.004	5.0	2.615	15	-
Solid Nickel	0.004	12.0	3.950	15	-
Sintered Nickel (Porous, Single Skin)	0.008	12.0	3.950	20	Variable
Sintered Nickel (Double, Porous Skin)	0.008	12.0	4.028	20	Constant

Primary heat transfer ray was $\lambda = 0^\circ$ for all models
Primary pressure ray (secondary heat transfer ray) was $\lambda = 135^\circ$ for all models except the last which was $\lambda = 225^\circ$

B. Screen Overlays

Overlay	Wires/inch	Wire Diameter in.
K_1	28	0.005
K_2	14	0.009

TABLE II. - TEST CONDITION SUMMARY

Condition No.	Run No.	M_∞	$Re_\infty/ft. \times 10^{-6}$	T_{t_e} °K	C_i %	Injectant	θ_c Deg.	Distribution	Skin
1	22, 23	11.6	6.70	1870	-	-	5	-	Solid
2	21	11.6	3.17	1970	-	-	|	-	|
3	19, 20	13.8	3.51	1520	-	-	|	-	|
4	10, 11	11.5	5.30	1920	-	-	12	-	|
5	12, 13	11.7	2.76	1990	-	-	|	-	|
6	14,15,18	14.0	3.64	1480	-	-	|	-	|
7	4	11.9	6.13	1790	0.00	-	|	Variable	Single,Porous
8	6,3	11.9	5.34	1847	0.35	N_2	|	|	|
9	2,7	12.0	5.69	1872	0.70	|	|	|	|
10	5	12.0	6.34	1740	2.10	|	|	|	|
11	41	11.7	6.19	1902	0.33	CH_4	|	Constant	Double,Porous
12	42	11.8	6.24	1863	0.67	|	|	|	|
13	29, 35	11.8	6.35	1851	0.00	-	|	-	|
14	40	12.2	7.91	1602	0.32	$CHClF_2$	|	Constant	|
15	38	11.9	6.33	1857	0.66	|	|	|	|
16	39	11.9	6.63	1811	2.03	|	|	|	|
17	31	11.9	6.77	1803	0.32	N_2	|	|	|
18	34	11.8	6.72	1832	0.63	|	|	|	|
18a	30	11.7	6.36	1881	0.80	|	|	|	|
19	36, 37	11.8	6.52	1832	1.95	|	|	|	|
20	50	11.9	7.50	1709	0.00	-	|	-	Double,porous +K_1
21	49	11.9	7.30	1729	0.31	CH_4	|	Constant	Double,porous +K_1
22	52, 53	11.7	6.33	1873	0.33	$CHClF_2$	|	|	Double,porous
23	54, 55	11.8	6.67	1836	0.17	CH_4	|	|	|
24	56	11.7	6.11	1898	1.32	|	|	|	|
25	58	11.8	3.21	1921	0.00	-	|	-	Double,porous +K_2
26	59	11.8	3.35	1876	0.25	CH_4	|	Constant	|
27	45	11.8	3.40	1813	0.52	|	|	|	Double,Porous
28	57	11.8	3.26	1872	1.04	|	|	|	|
29	48	11.9	3.58	1784	0.00	-	|	-	Double,porous +K_1
30	43	12.0	3.34	1831	|	-	|	-	Double,Porous
31	44	12.0	3.56	1768	0.26	CH_4	|	Constant	|
32	46, 47	11.8	3.40	1848	|	|	|	|	Double,porous +K_1

TABLE III. - TRANSITION RELATED PARAMETERS

Note: The first set of data for each condition is based on heat transfer data (start of transition), the second set is based on shadowgraph (end of transition).

Condition No.	M_e	$Re_c/ft \times 10^{-6}$	T_w/T_{t_e}	x_{tr} ft	$Re_{x,tr} \times 10^{-6}$	$Re_{\delta^*,tr} \times 10^{-3}$	$Re_{\theta,tr} \times 10^{-2}$
1	10.13	9.69	.161	.625	6.31	20.92	7.85
	10.25	9.32		.891	8.82	25.87	9.26
2	Totally Laminar						
3	Totally Laminar						
4	7.01	9.87	.152	.346	3.55	7.77	6.21
	7.04	9.77		.384	3.93	8.19	6.53
5	Totally Laminar						
6	Totally Laminar						
7	7.22	10.29	.167	.511	5.25	10.51	7.77
	7.28	9.99		.608	6.61	11.51	8.37
8	7.09	9.63	.162	.292	2.91	8.63	6.37
	7.15	9.36		.406	3.99	10.32	7.53
9	7.01	10.61	.160	.125	1.33	6.73	4.91
	7.08	10.34		.250*	2.65	9.62	6.76
10	6.99	11.36	.172	.113	1.28	9.47	5.14
	7.05	11.14		.218*	2.49	"blow-off"	
11	7.13	11.52	.158	.281	3.31	8.92	6.22
	7.22	11.07		.480	5.18	12.34	8.25

*x_{tr} upstream of shadowgraph field of view, location based on end of heat transfer data

(Continued)

TABLE III. - (continued)

Condition No.	M_e	$Re_c/ft \times 10^{-6}$	T_w/T_{t_e}	x_{tr} ft	$Re_{x,tr} \times 10^{-6}$	$Re_{\delta^*,tr} \times 10^{-3}$	$Re_{\theta,tr} \times 10^{-2}$
12	7.09 7.18	11.53 11.08	.161	.227 .435	2.67 5.02	8.83 14.65	5.87 8.74
13	7.22 7.28	11.05 10.79	.162	.508 .597	5.89 6.86	10.82 11.77	7.97 8.57
14	7.05 7.19	12.42 11.74	.188	.282 .545	3.58 6.78	9.13 13.25	7.35 8.83
15	7.11 7.22	11.46 10.92	.162	.292 .526	3.43 6.05	9.04 12.96	8.17 12.09
16	7.09 7.17	11.64 11.26	.165	.268 .440	3.19 5.16	"blow-off"	
17	7.11 7.28	11.81 10.64	.167	.313 .616	3.81 7.27	10.01 14.69	7.23 10.21
18	7.09 7.26	12.30 11.46	.164	.226 .555	2.83 6.75	8.43 18.27	6.07 11.99
18a	7.11 7.17	13.20 12.85	.171	.236 .378	3.17 5.03	10.61 15.89	7.37 10.32
19	7.06 7.11	11.93 11.67	.164	.179 .299	2.16 3.57	9.85 "blow-off"	6.86
20	Screen Overlay K_1		-	.072 **	0.93 **	- -	- -
21	Screen Overlay K_1		-	.072 **	0.93 **	- -	- -

**x_{tr} upstream of shadowgraph field of view

(Continued)

TABLE III. - (concluded)

Condition No.	M_e	$Re_c/ft \times 10^{-6}$	T_w/T_{t_e}	x_{tr} ft	$Re_{x,tr} \times 10^{-6}$	$Re_{\delta^*,tr} \times 10^{-3}$	$Re_{\theta,tr} \times 10^{-2}$
22	7.12	11.77	.160	.261	3.14	8.06	6.71
	7.25	11.13		.531	6.24	11.98	10.10
23	7.13	12.08	.163	.302	3.73	9.07	6.45
	7.24	11.52		.529	6.43	12.30	8.50
24	7.08	11.84	.158	.165	1.99	8.16	5.35
	7.16	11.45		.348	4.10	"blow-off"	
25	Screen Overlay K_2		-	.233	1.37	-	-
				.415	2.32	-	-
26	Screen Overlay K_2		-	.171	0.99	-	-
				.368	2.10	-	-
27	7.36	5.43	.165	.640	3.71	11.40	6.96
	Totally Laminar						
28	7.23	5.67	.160	.368	2.16	9.74	5.73
	7.31	5.49		.529	3.06	13.71	7.26
29	Screen Overlay K_1		-	.358	2.04	-	-
				.439	2.48	-	-
30	Totally Laminar						
31	Totally Laminar						
32	Screen Overlay K_1		-	.264	1.52	-	-
				.360	2.05	-	-

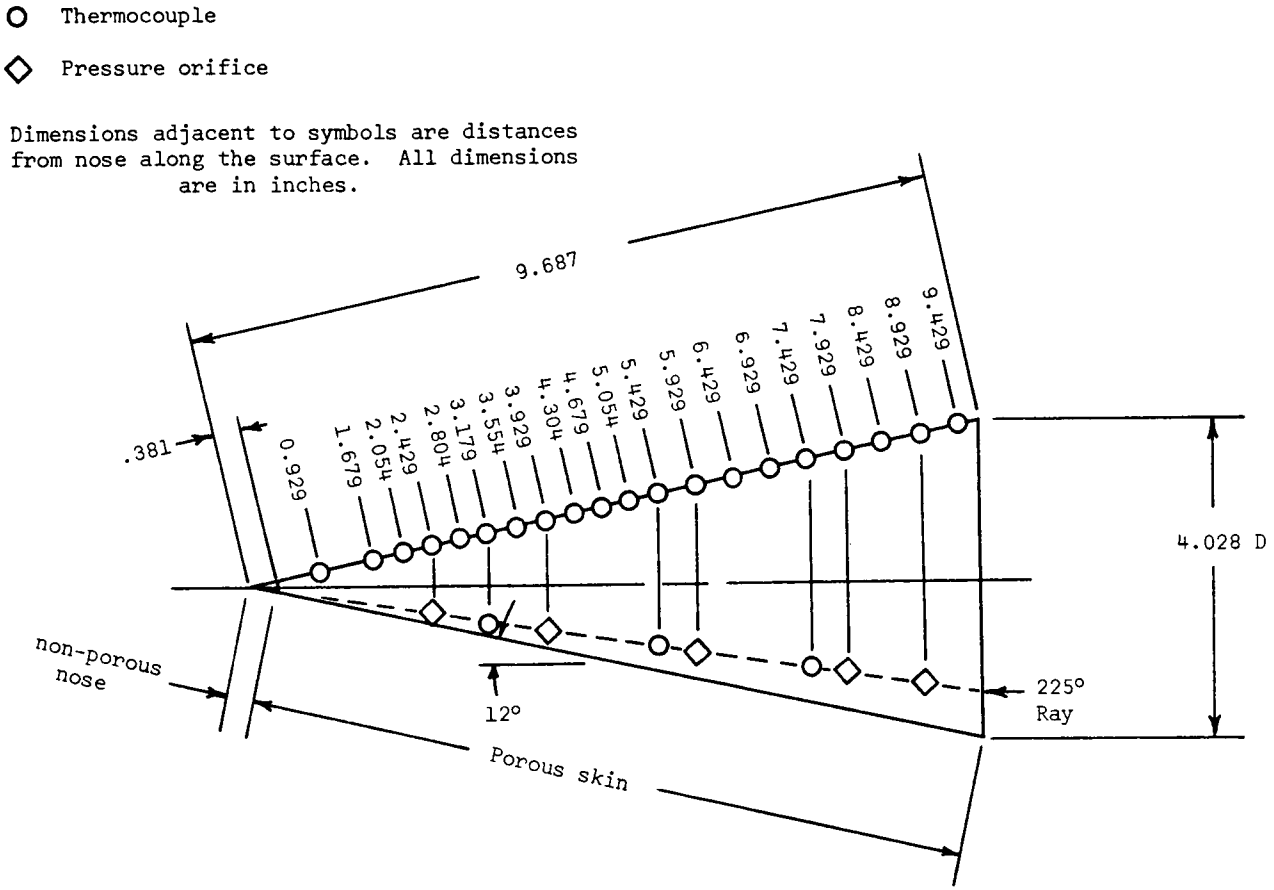

FIGURE 1 SENSOR LOCATIONS ON THE DOUBLE-SKIN MODEL

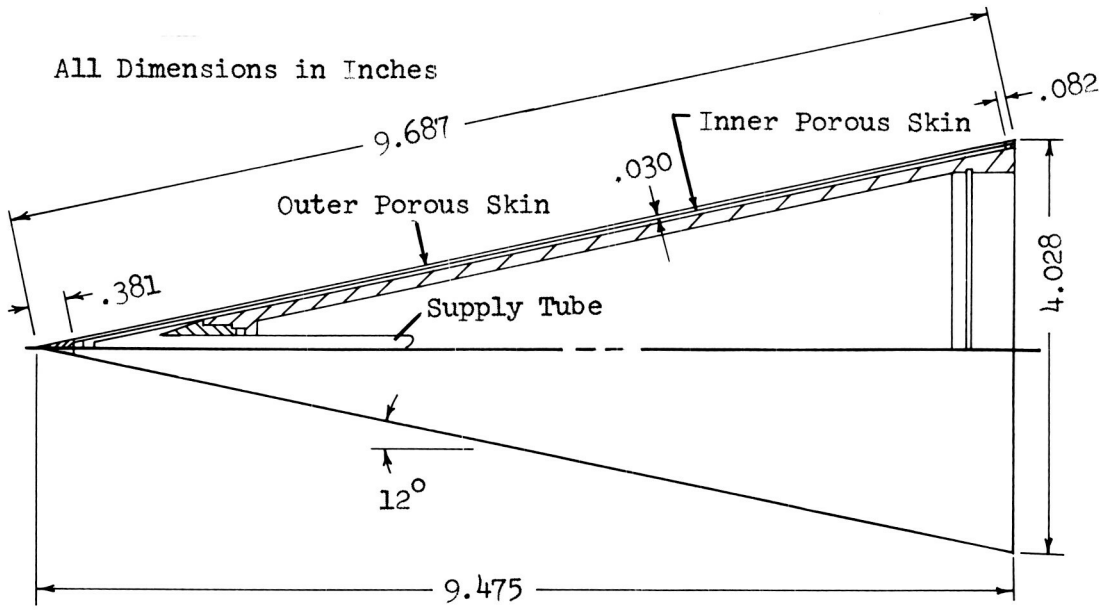

FIGURE 2a INJECTANT PASSAGEWAY IN THE DOUBLE-SKIN MODEL

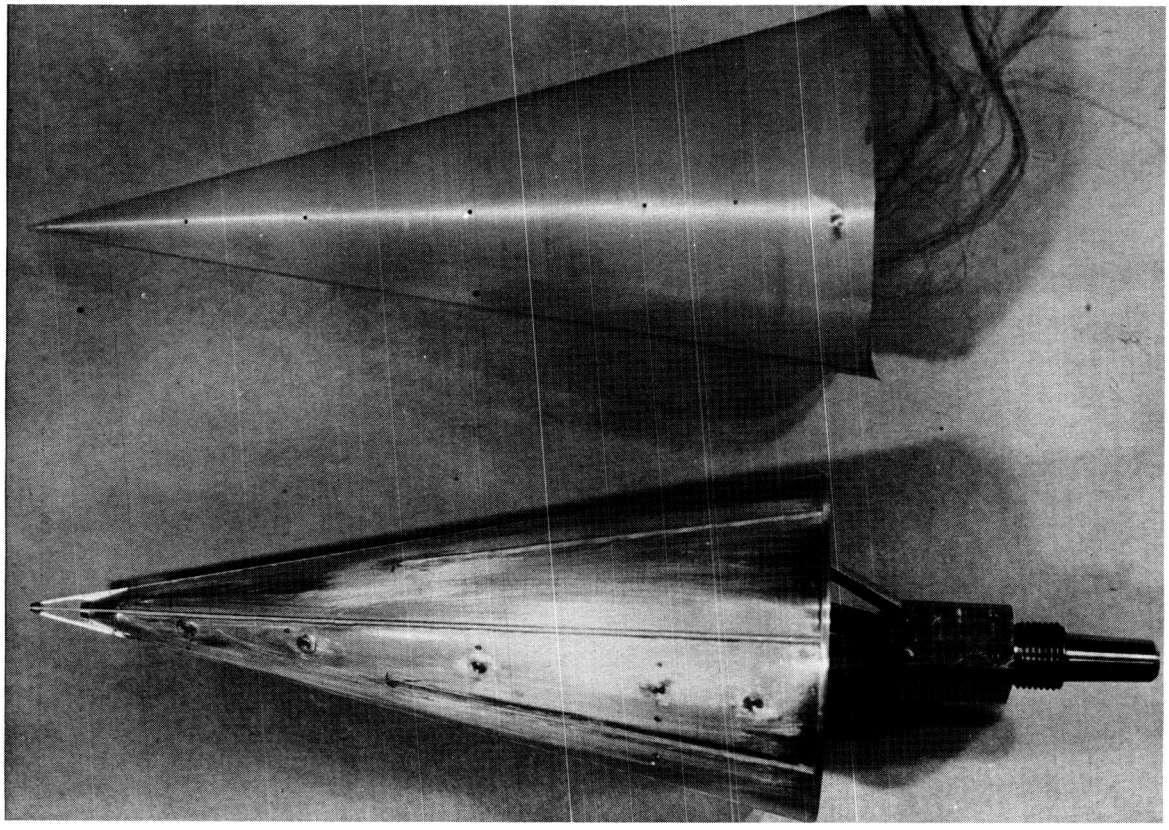

FIGURE 2b DOUBLE-SKIN MODEL PRIOR TO FINAL ASSEMBLY

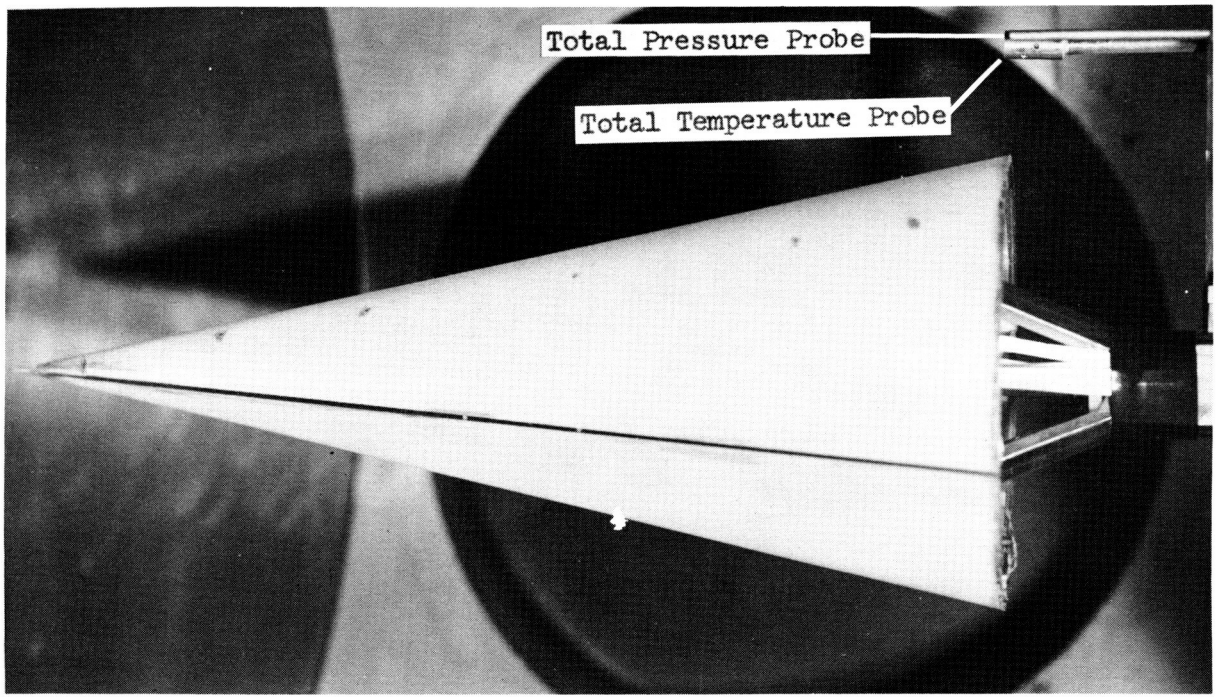

FIGURE 3a DOUBLE-SKIN MODEL IN THE TUNNEL TEST SECTION

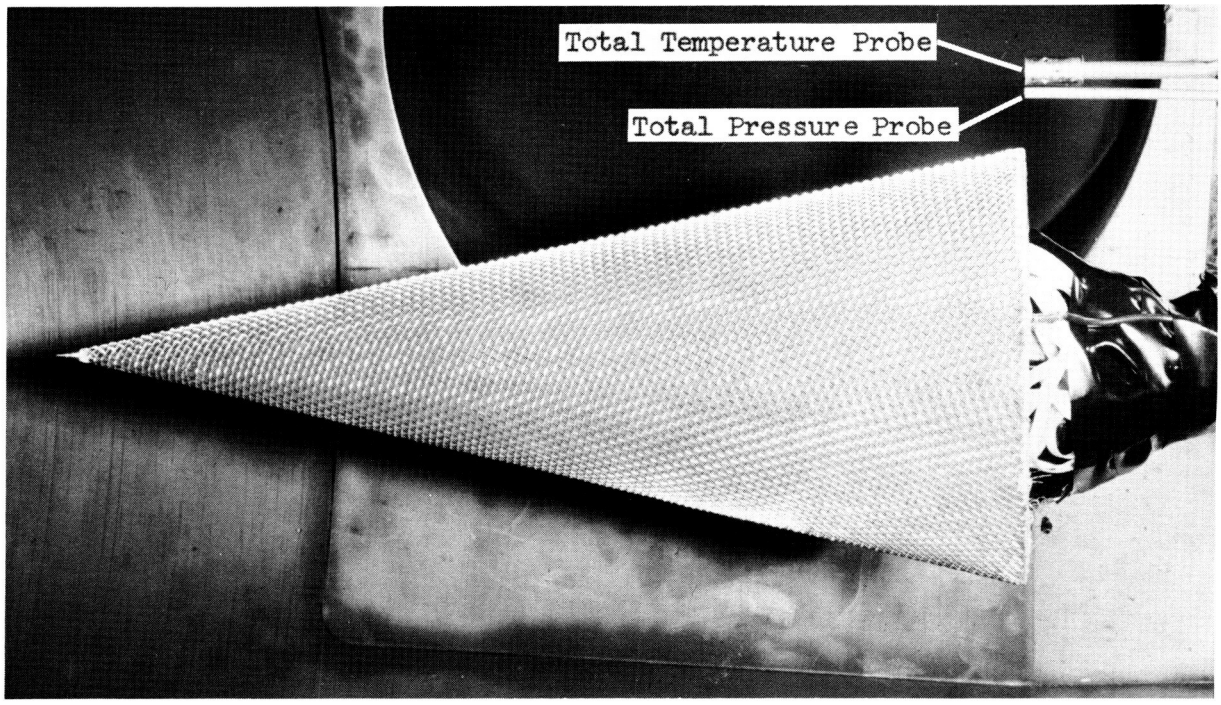

FIGURE 3b DOUBLE SKIN MODEL WITH A SCREEN OVERLAY IN THE TUNNEL TEST SECTION

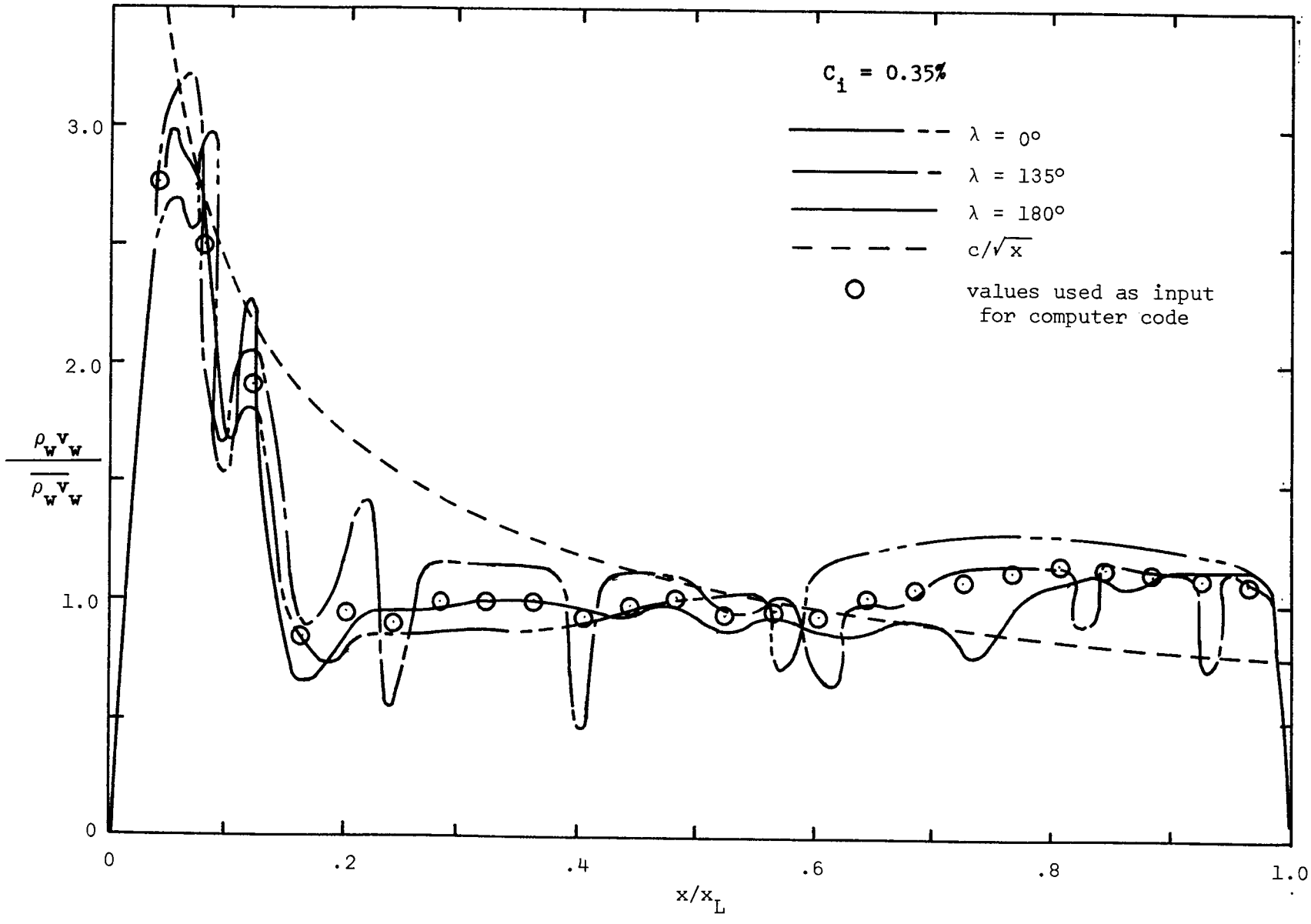

FIGURE 4a MEASURED "SIMILAR" (VARIABLE) INJECTANT DISTRIBUTION

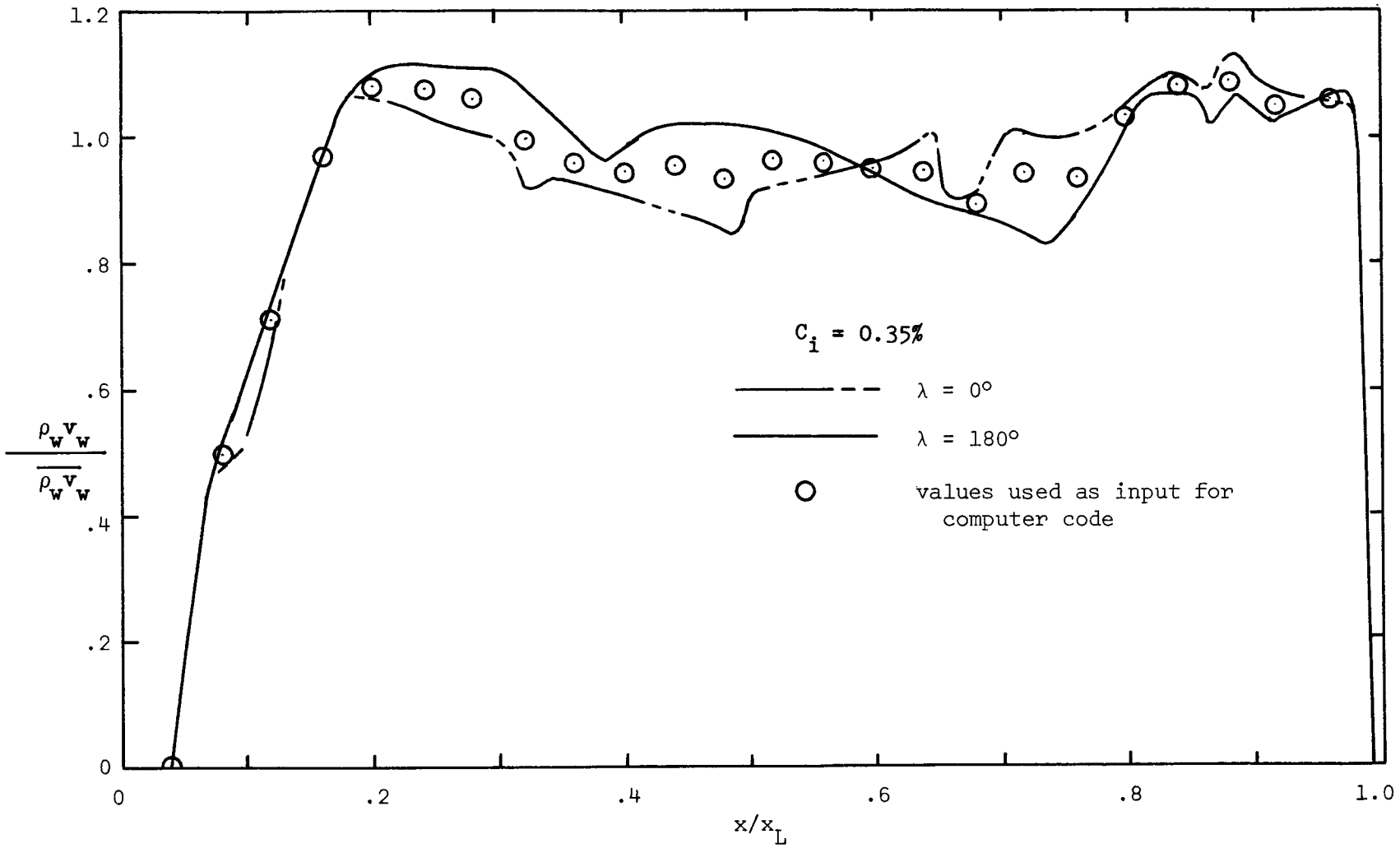

FIGURE 4b MEASURED CONSTANT (UNIFORM) INJECTANT DISTRIBUTION

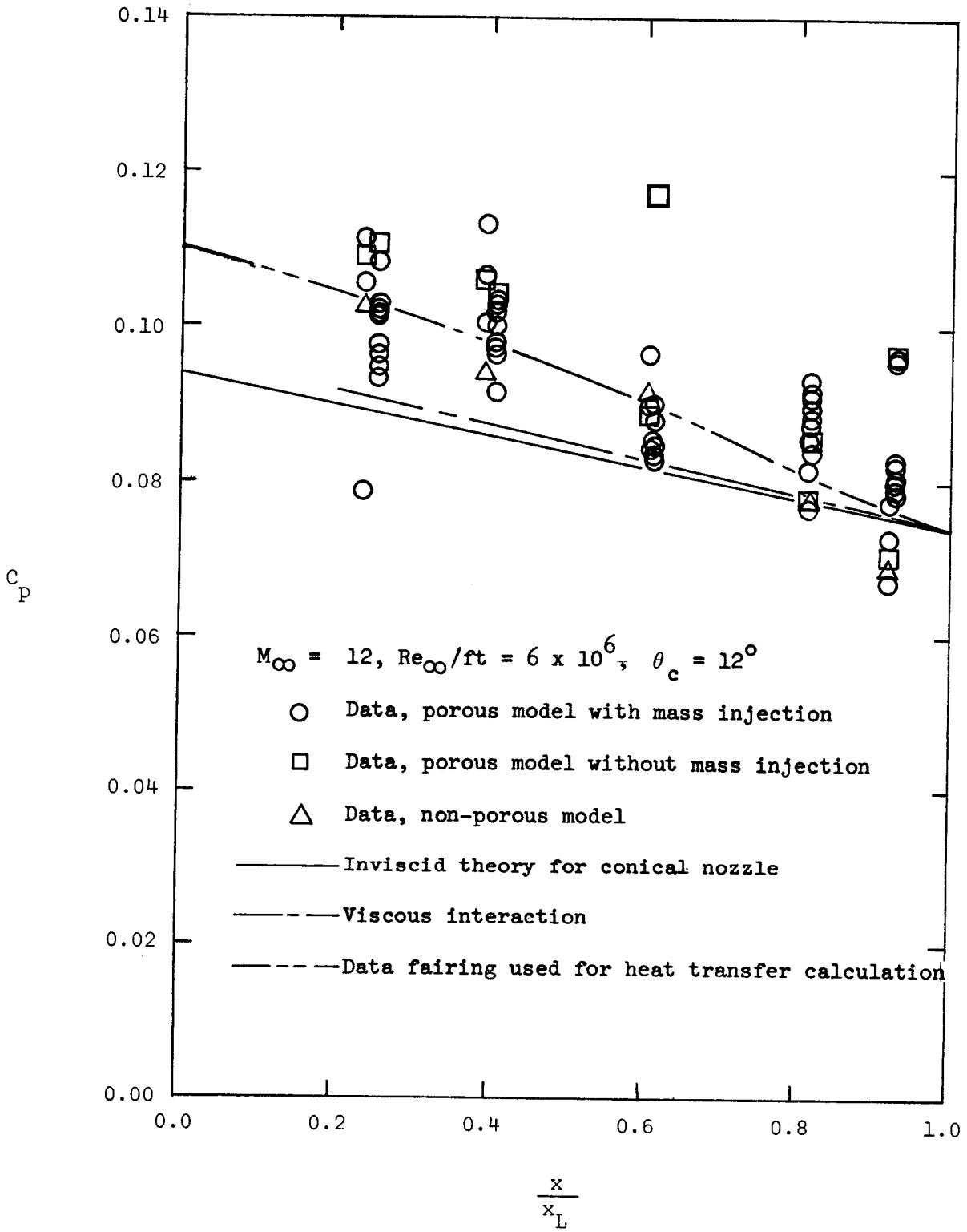

FIGURE 5 COMPARISON OF THE EXPERIMENTAL AND THE THEORETICAL SURFACE PRESSURE DISTRIBUTION

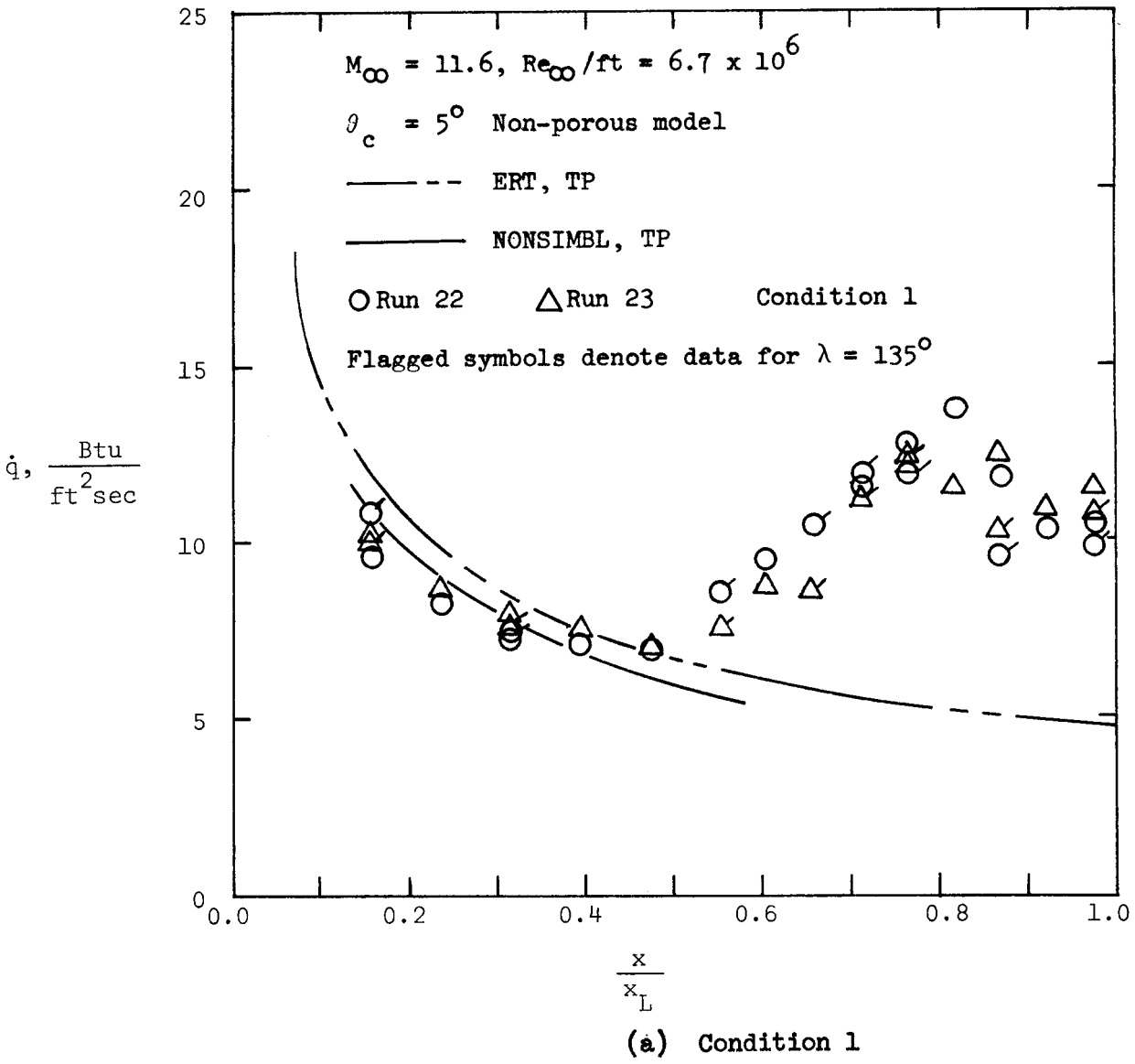

(a) Condition 1

FIGURE 6 COMPARISON OF THE EXPERIMENTAL AND THE THEORETICAL HEAT-TRANSFER RATE DISTRIBUTION FOR THE NO-INJECTION CONDITIONS

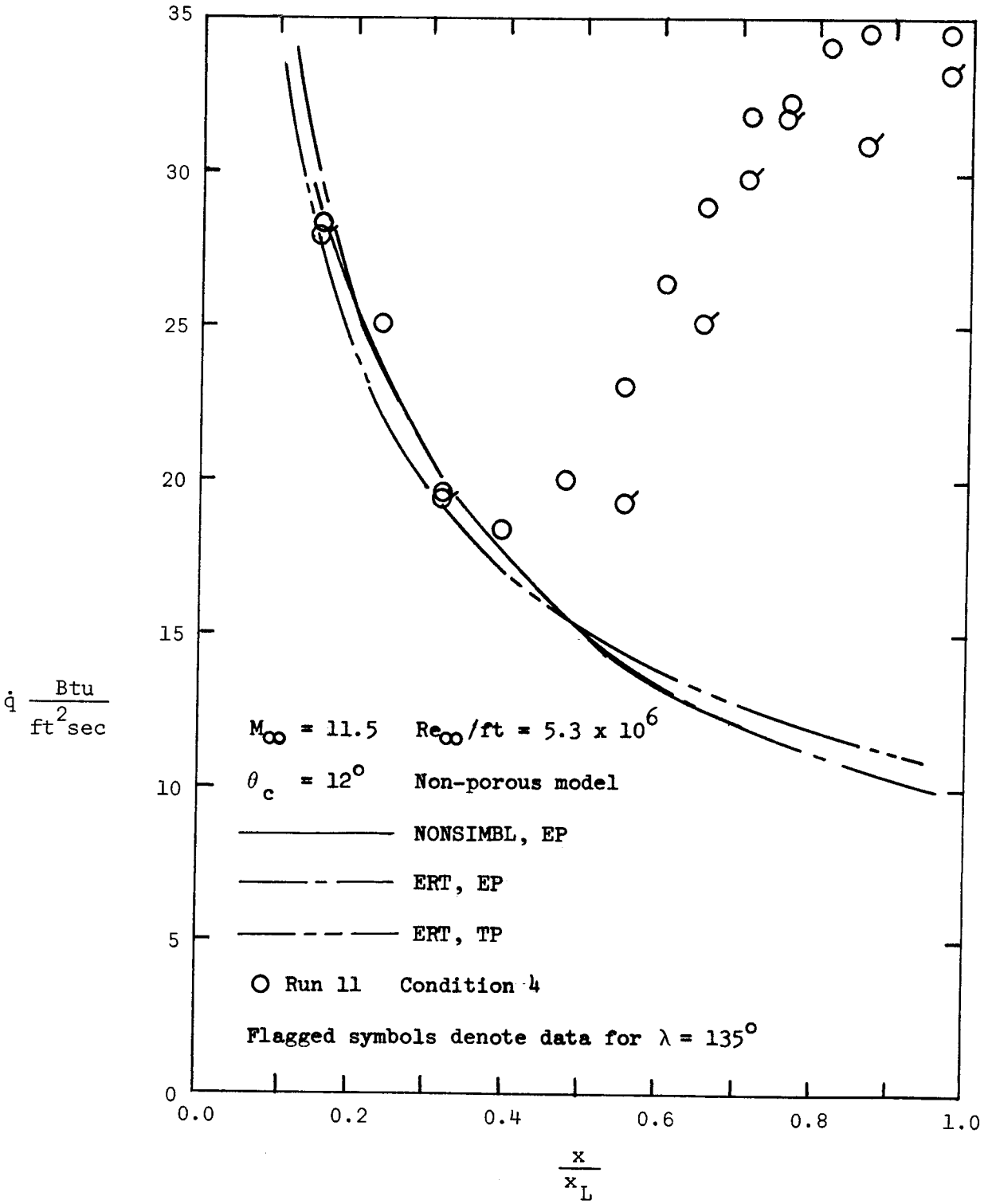

(b) Condition 4
FIGURE 6 CONTINUED

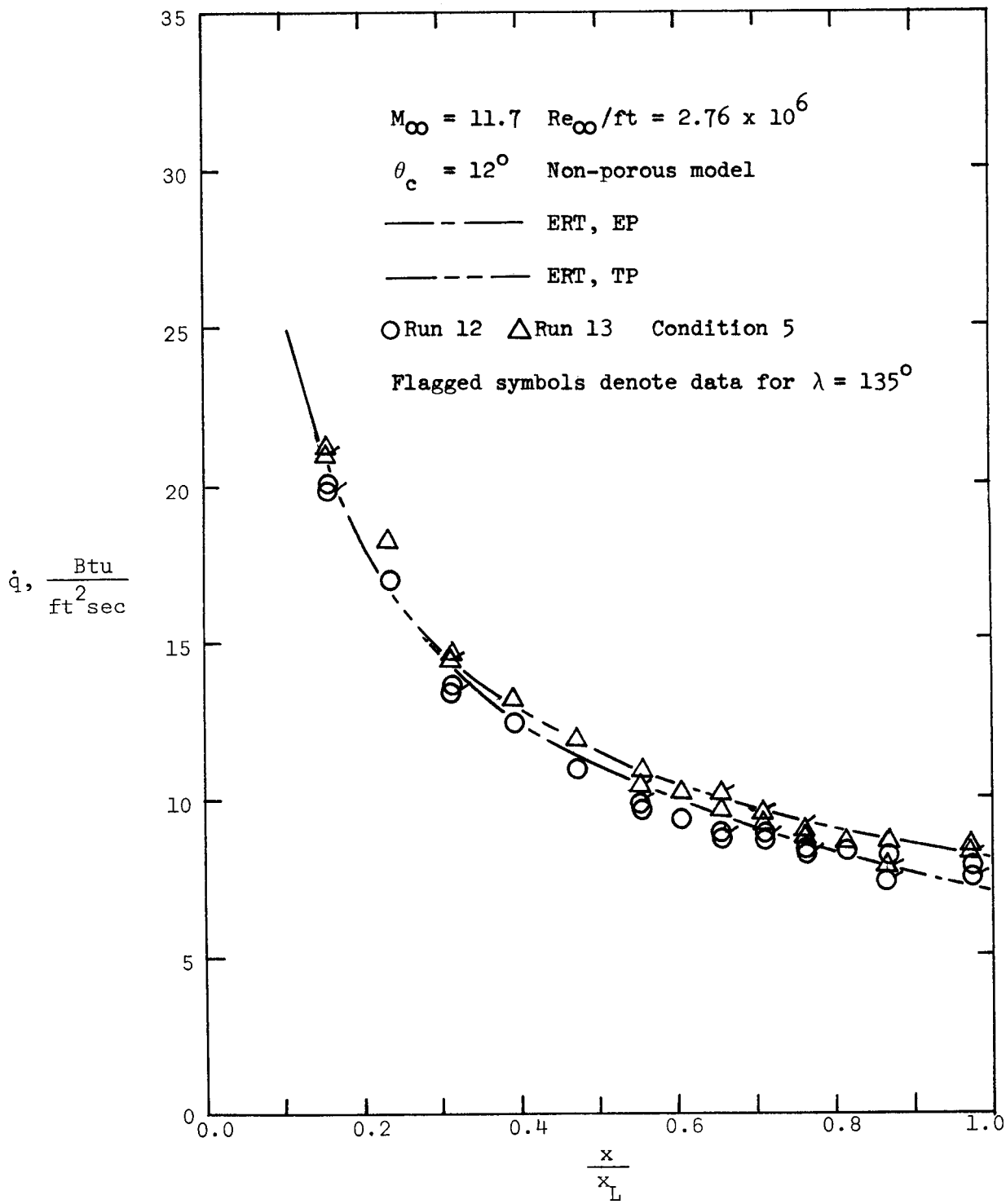

(c) Condition 5
FIGURE 6 CONTINUED

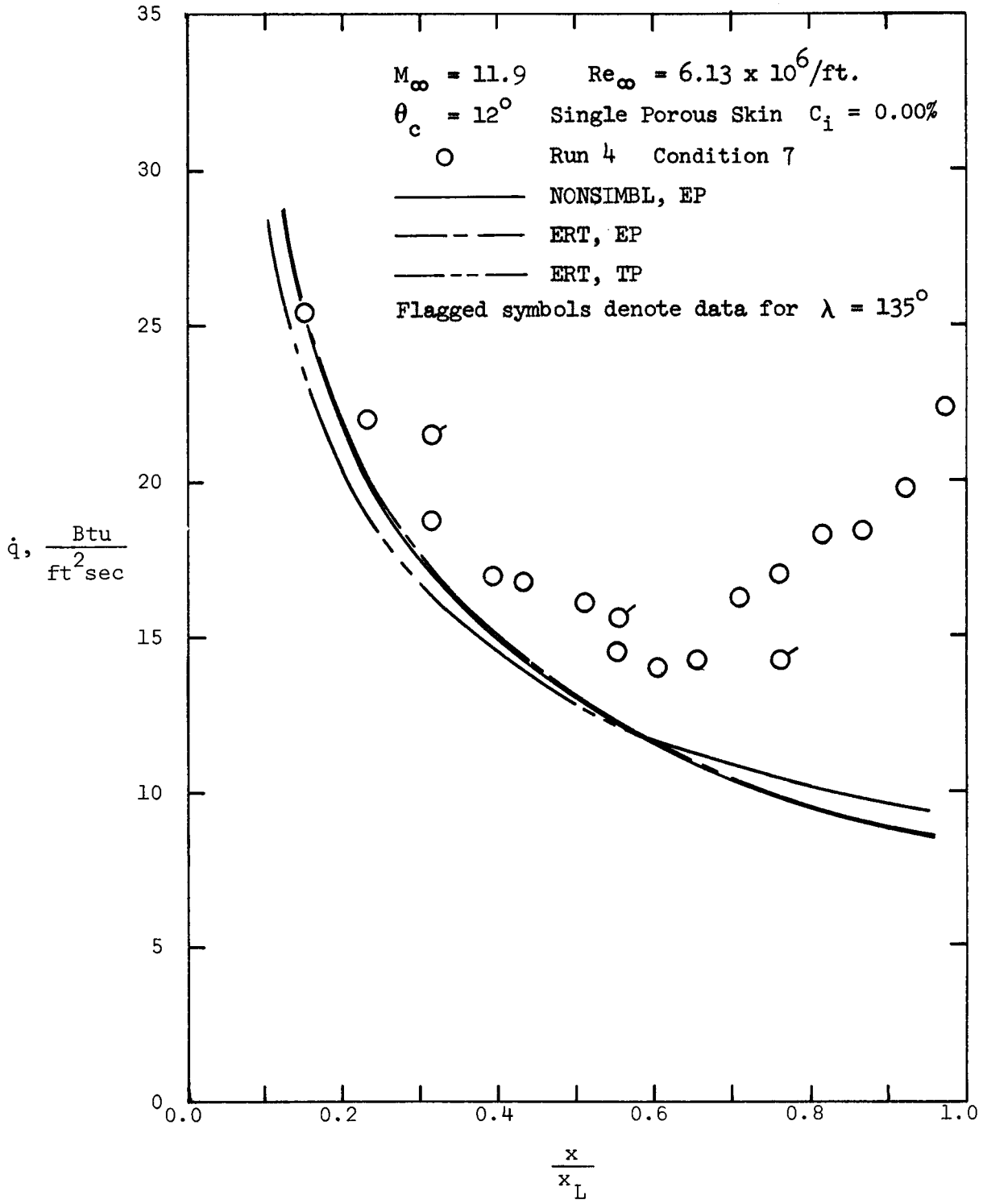

(d) Condition 7
FIGURE 6 CONTINUED

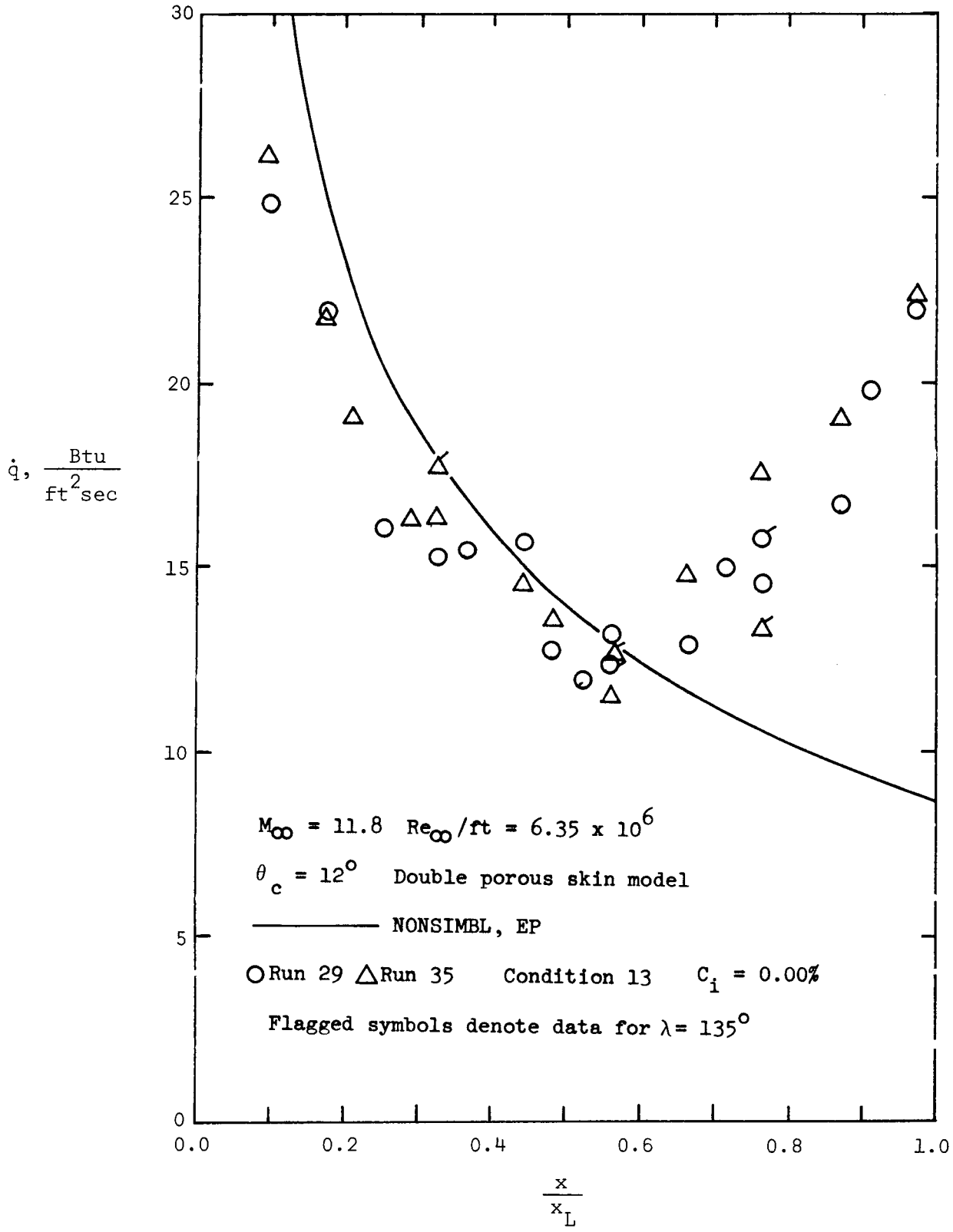

(e) Condition 13
FIGURE 6 CONTINUED

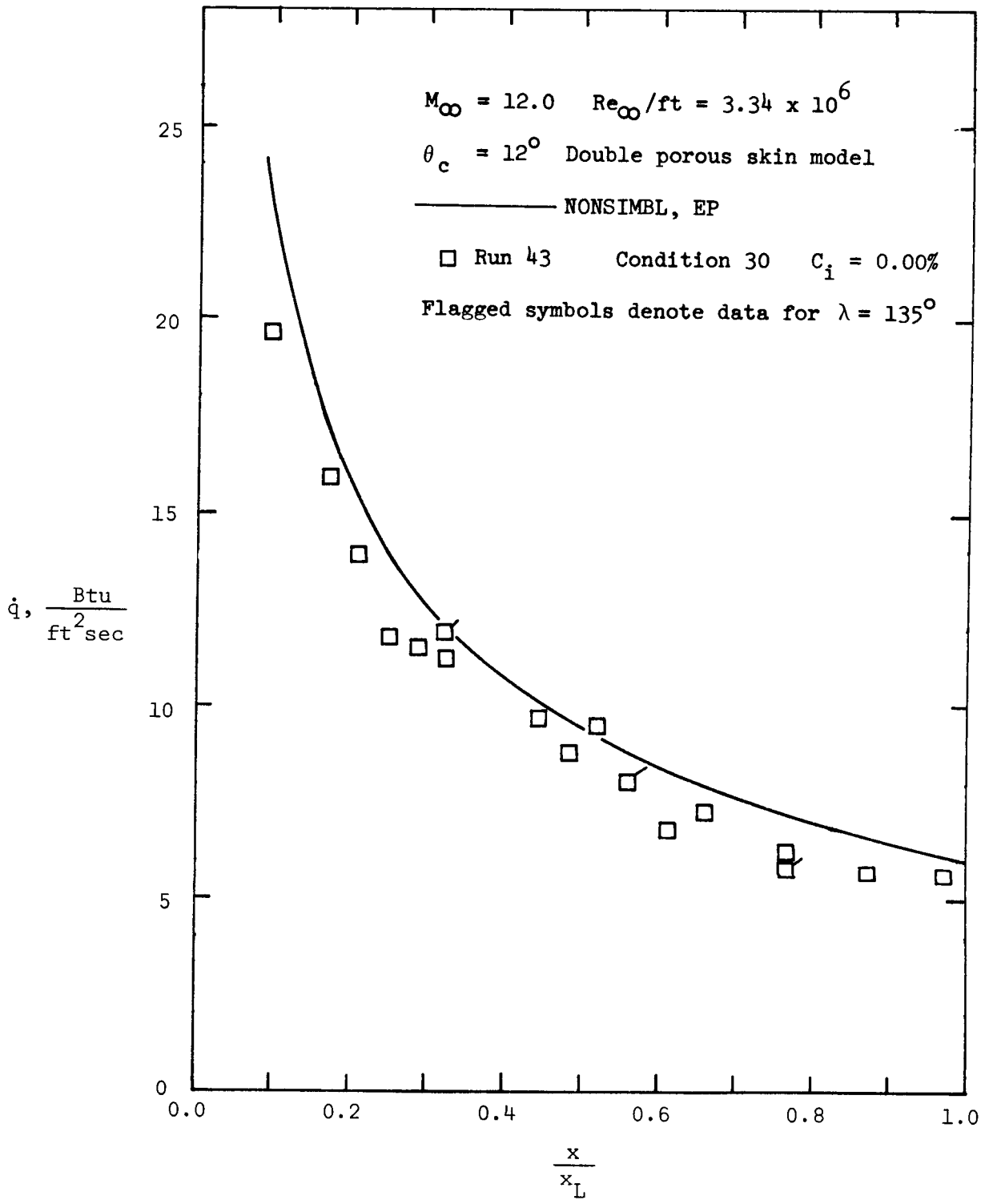

(f) Condition 30
FIGURE 6 CONCLUDED

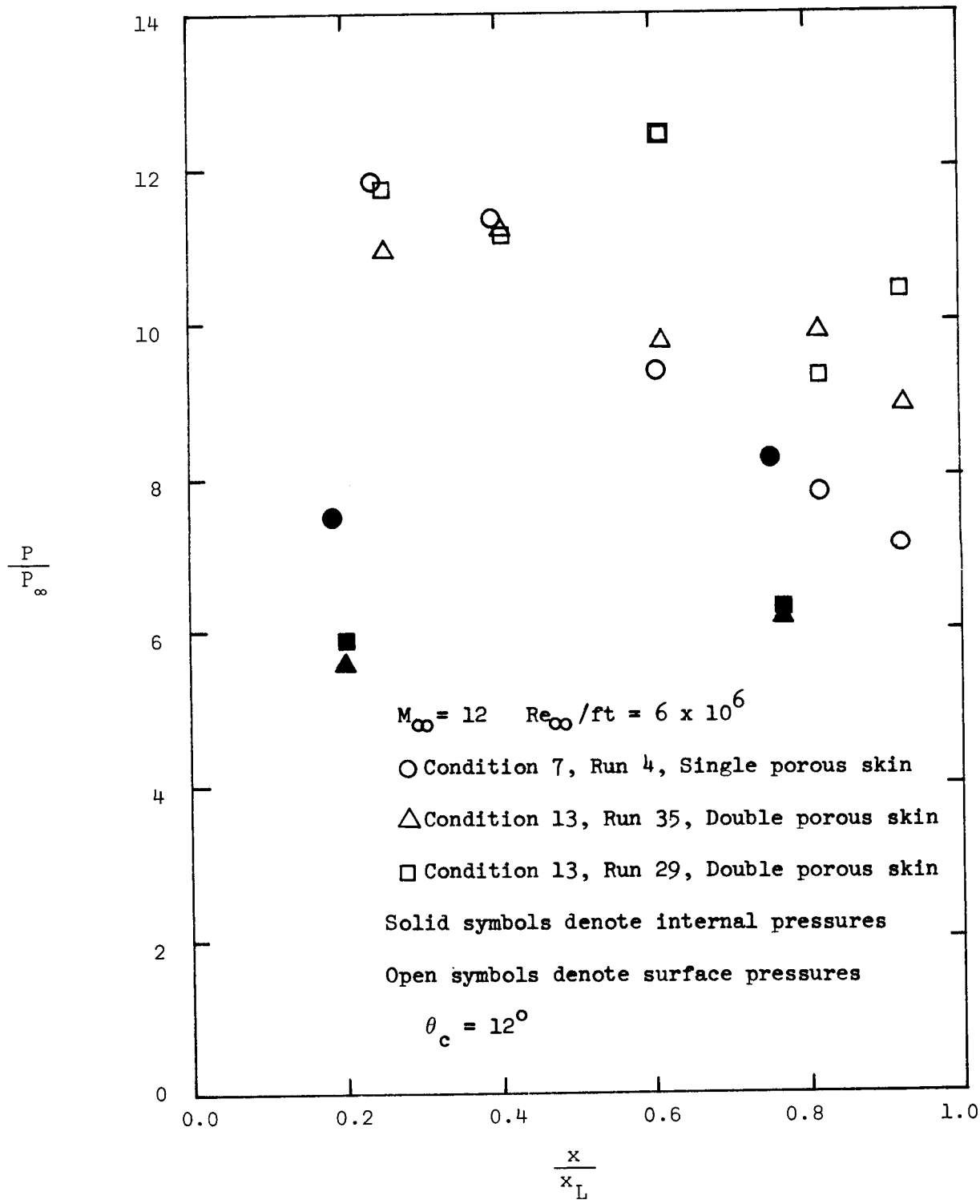

FIGURE 7 COMPARISON OF THE DISTRIBUTION FOR THE SURFACE AND THE INTERNAL PRESSURES FOR POROUS MODELS WITH NO INJECTION

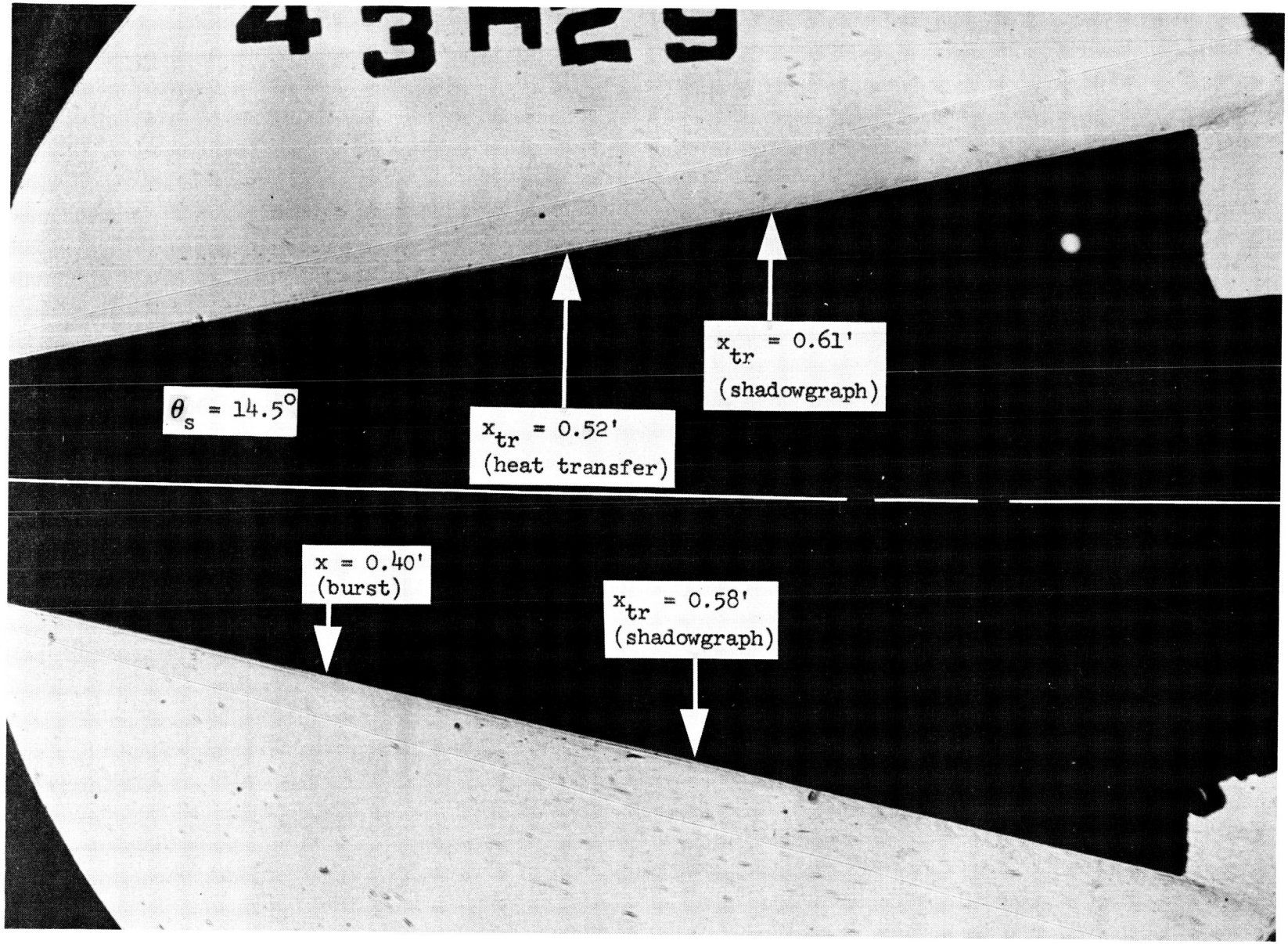

FIGURE 8 SHADOWGRAPH ILLUSTRATING THE TRANSITION "LOCATIONS" AND SHOCK-WAVE ANGLE M_∞ = 11.8, Re_∞ /ft = 6.35 x 10^6, C_i = 0.0

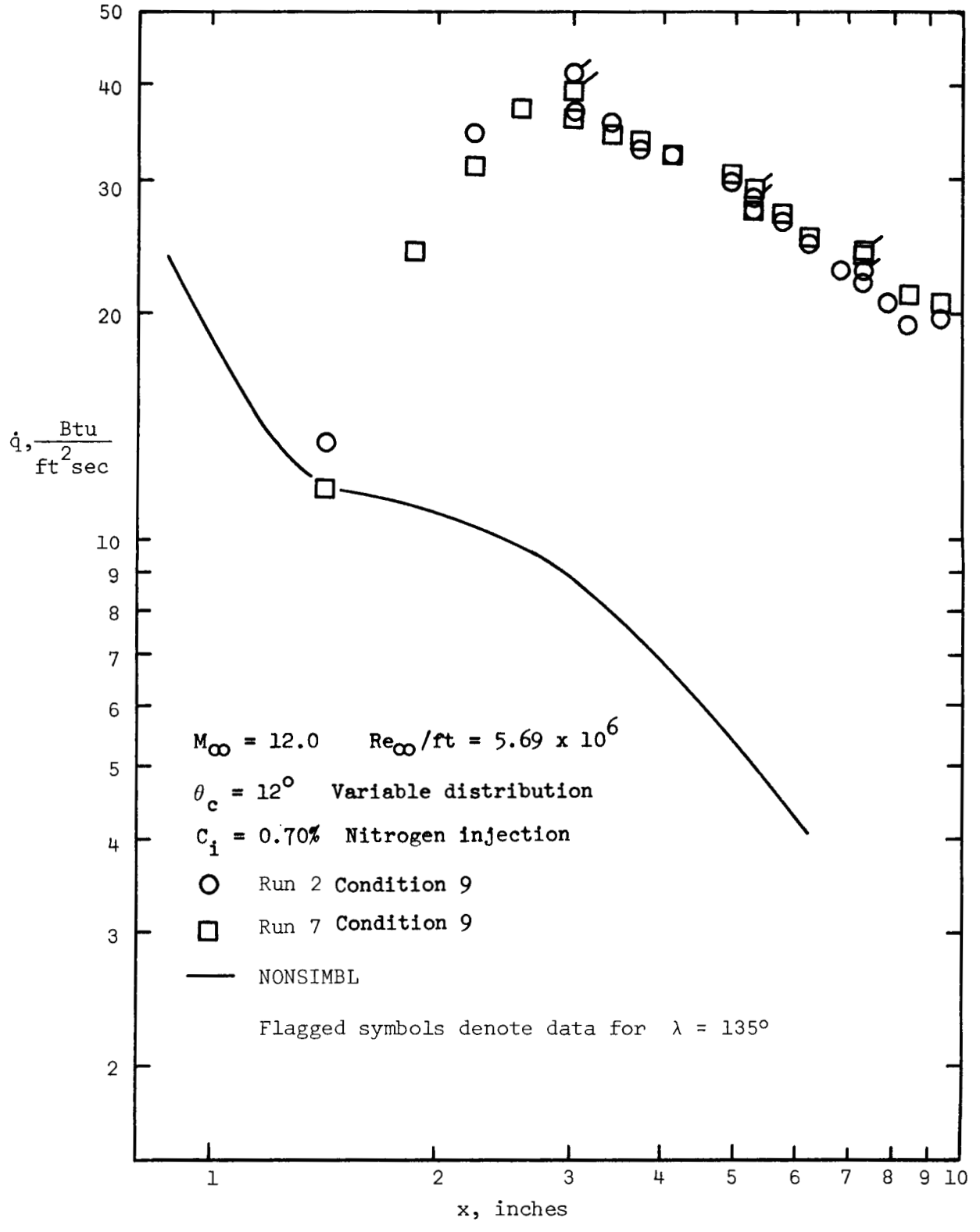

(a) Condition 9

FIGURE 9 COMPARISON OF THE EXPERIMENTAL AND THE THEORETICAL HEAT-TRANSFER-RATE DISTRIBUTION

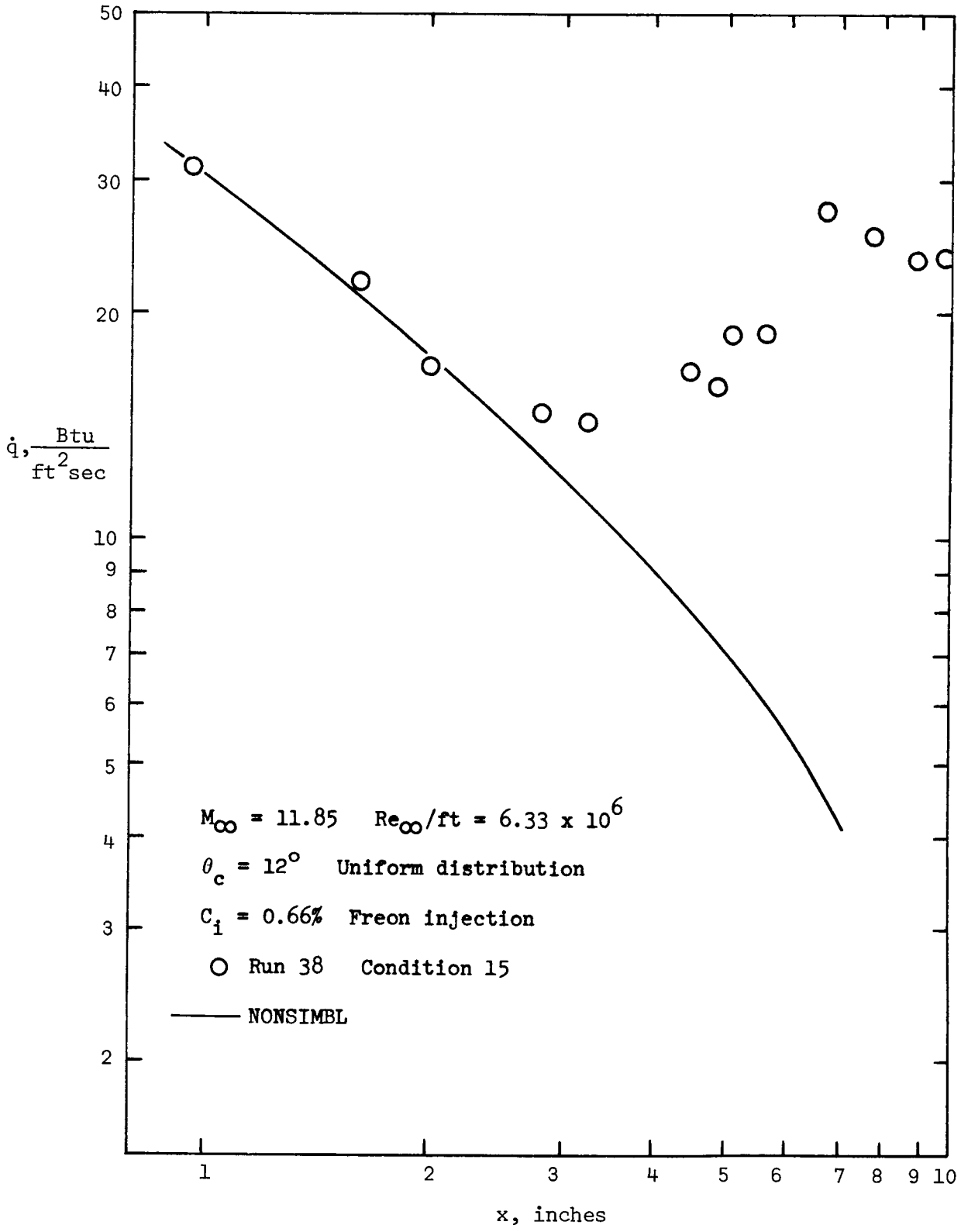

(b) Condition 15
FIGURE 9 CONTINUED

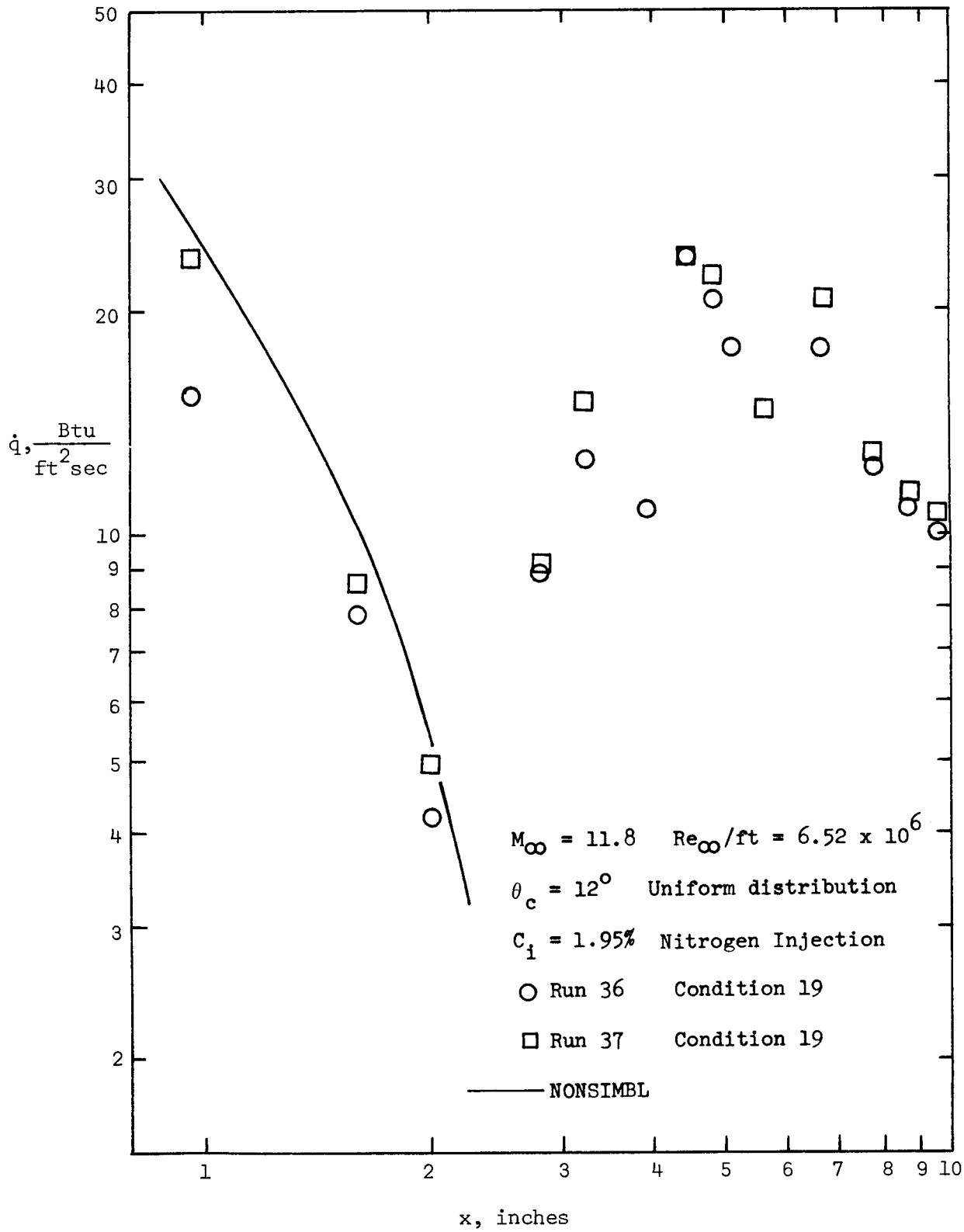

(c) Condition 19
FIGURE 9 CONTINUED

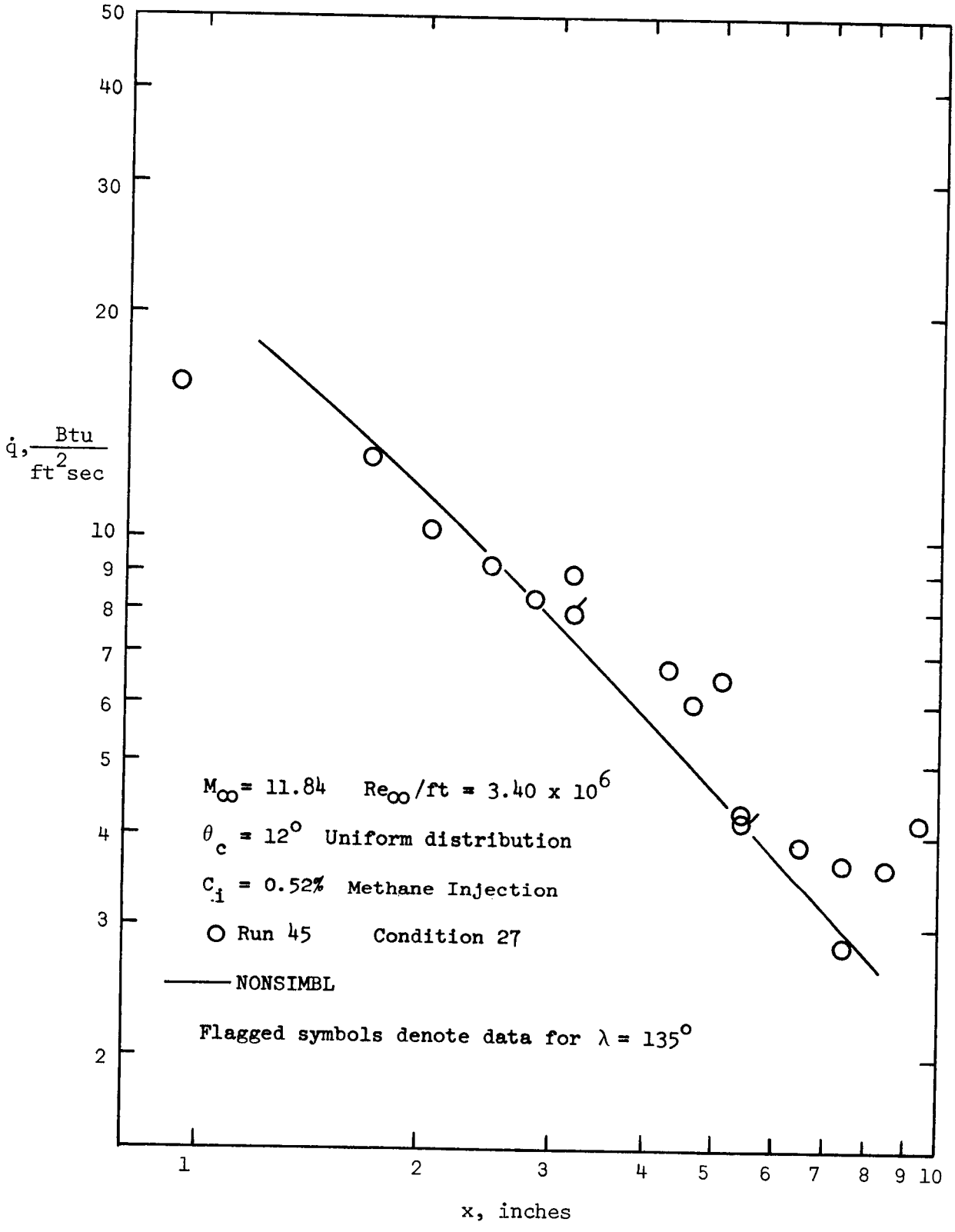

(d) Condition 27
FIGURE 9 CONTINUED

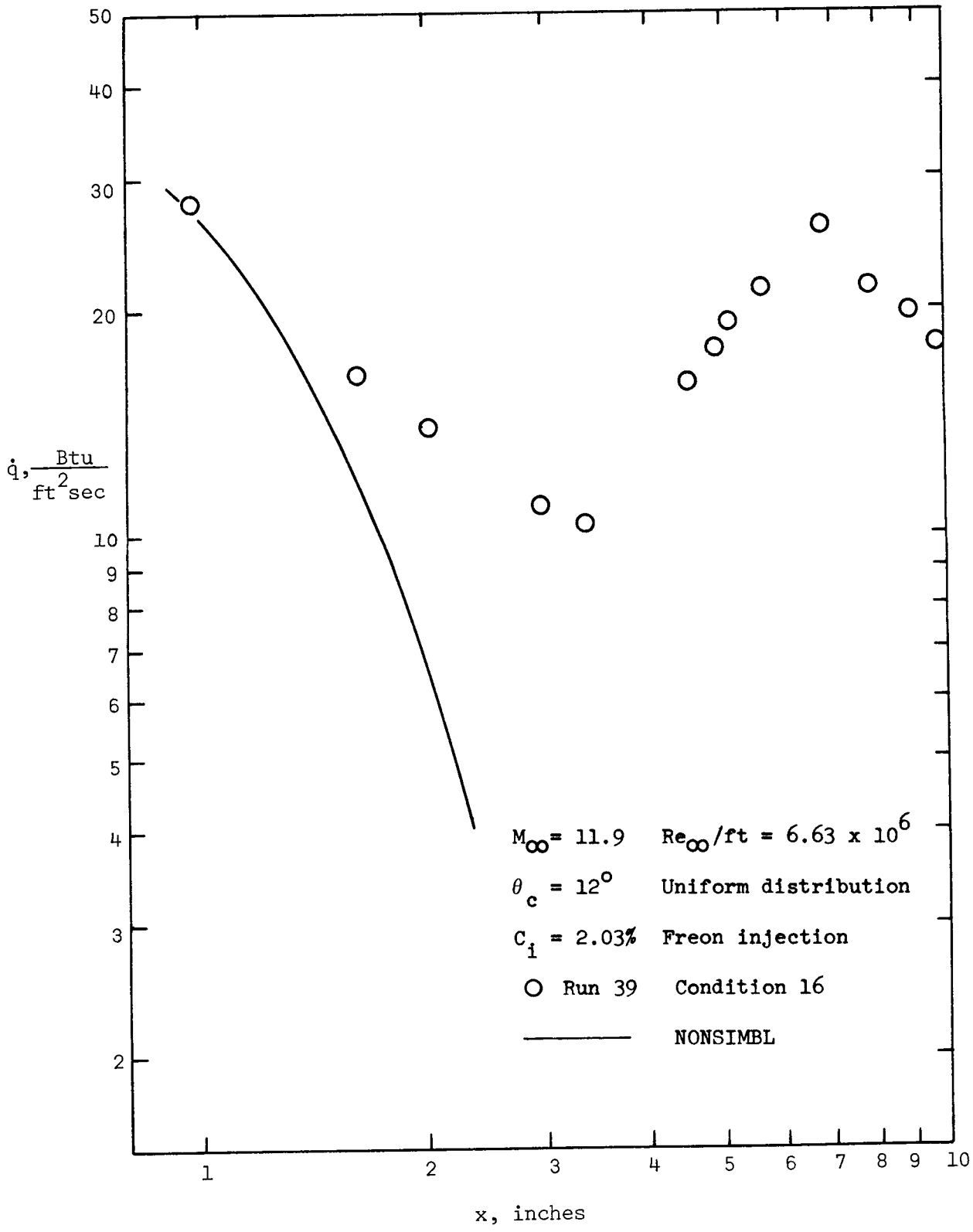

(e) Condition 16

FIGURE 9 CONCLUDED

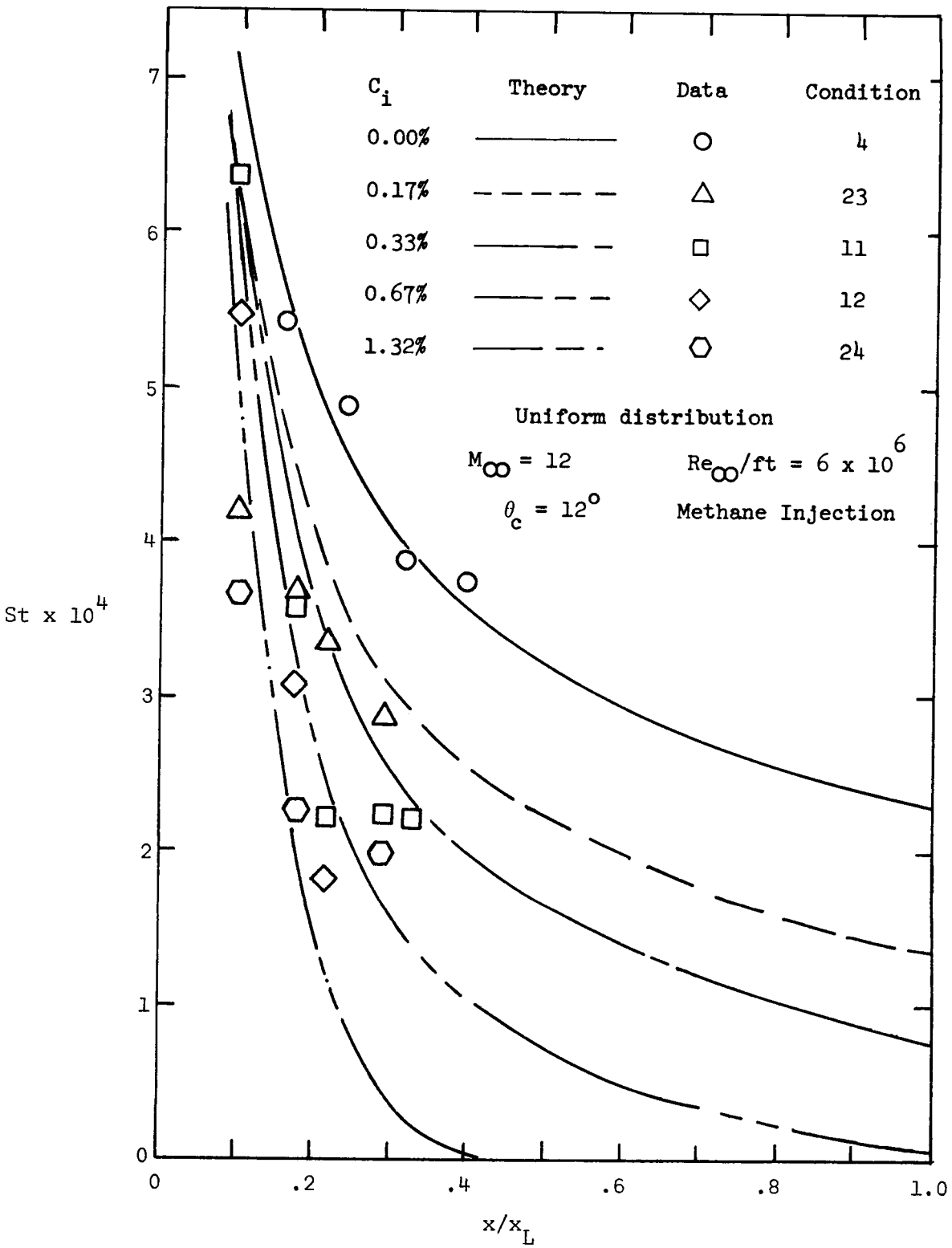

(a) Methane

FIGURE 10 COMPARISON OF THEORETICAL AND EXPERIMENTAL HEAT-TRANSFER-RATES WITH A CONSTANT MASS-INJECTION DISTRIBUTION

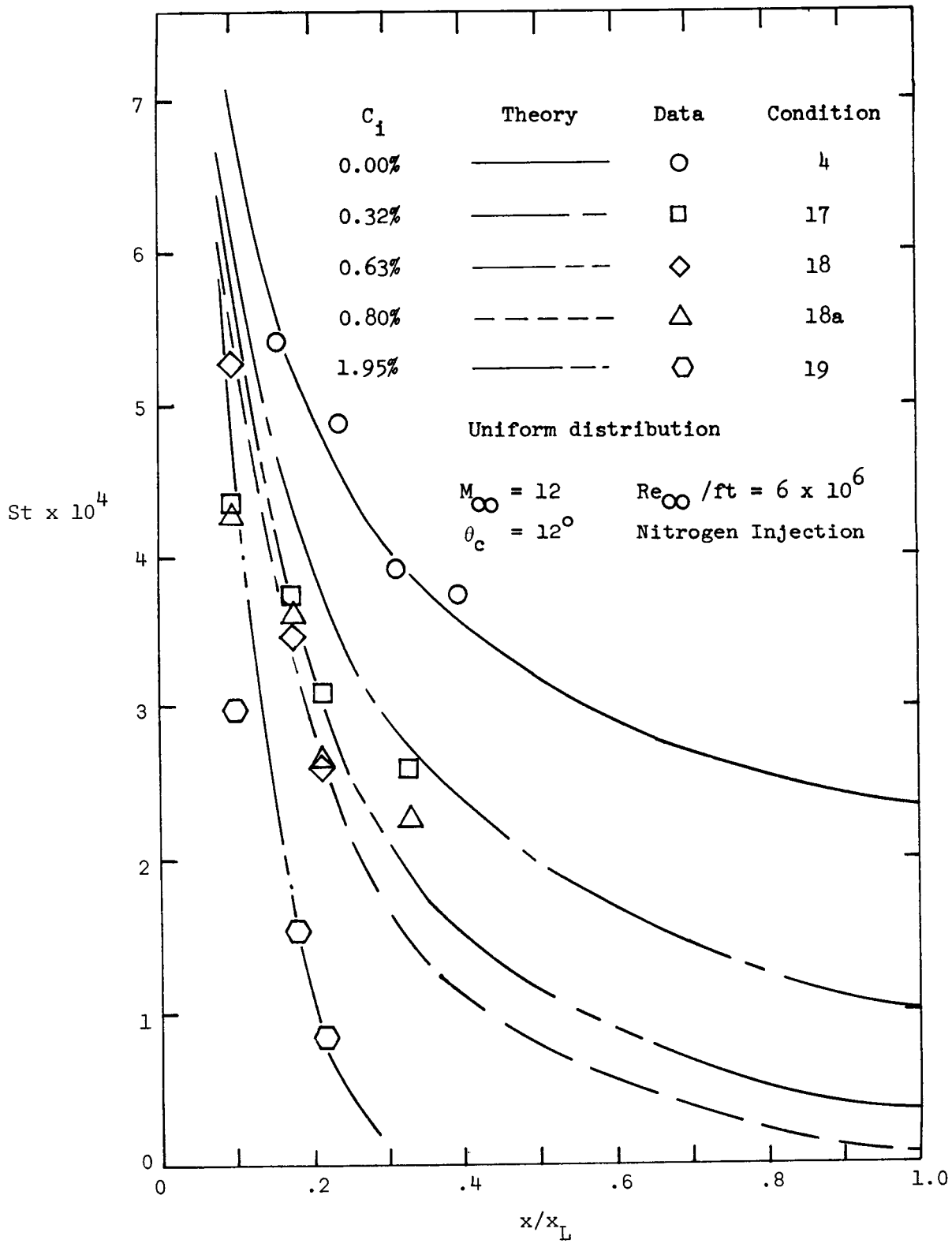

(b) Nitrogen
FIGURE 10 CONTINUED

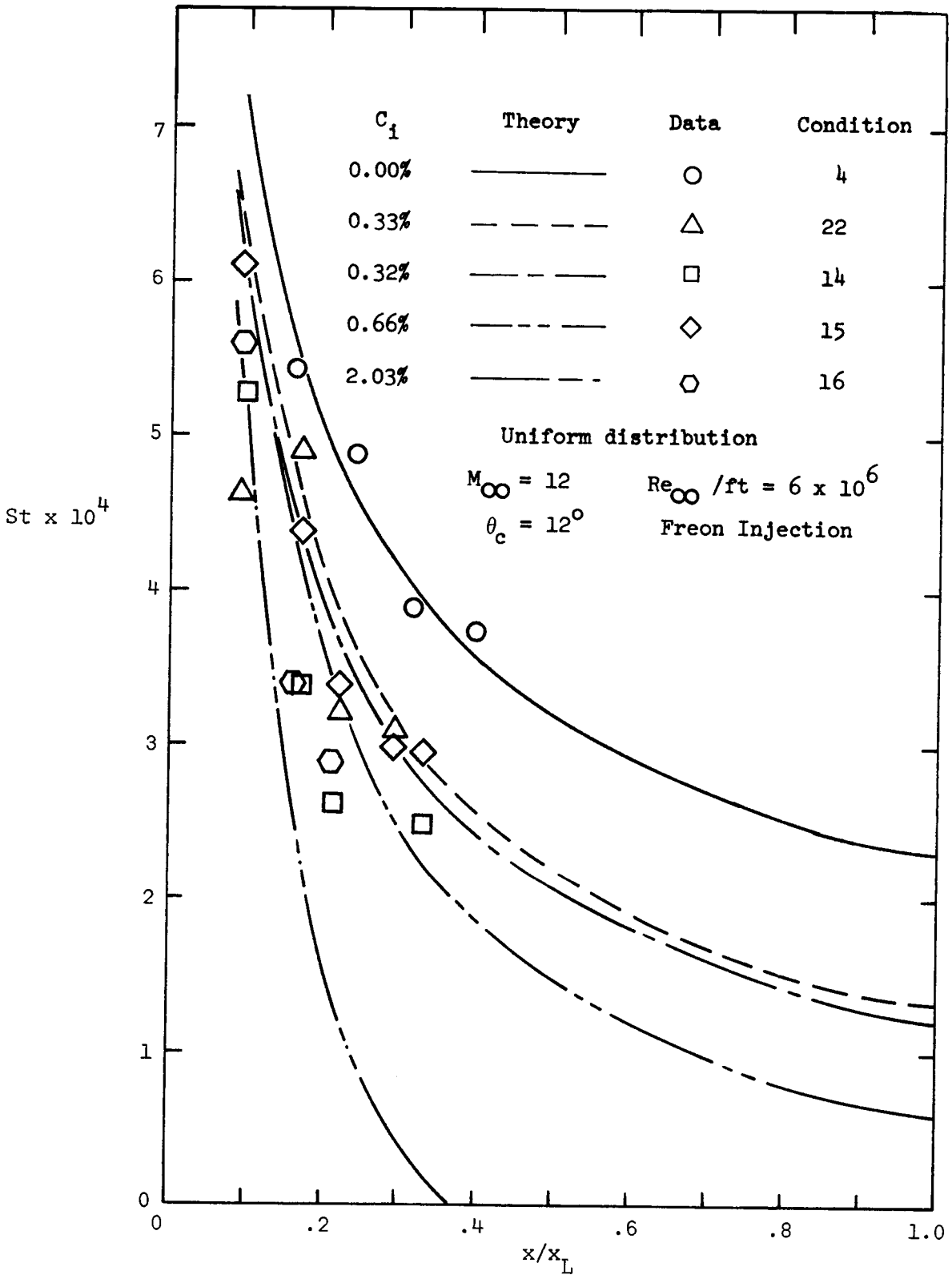

(c) Freon

FIGURE 10 CONCLUDED

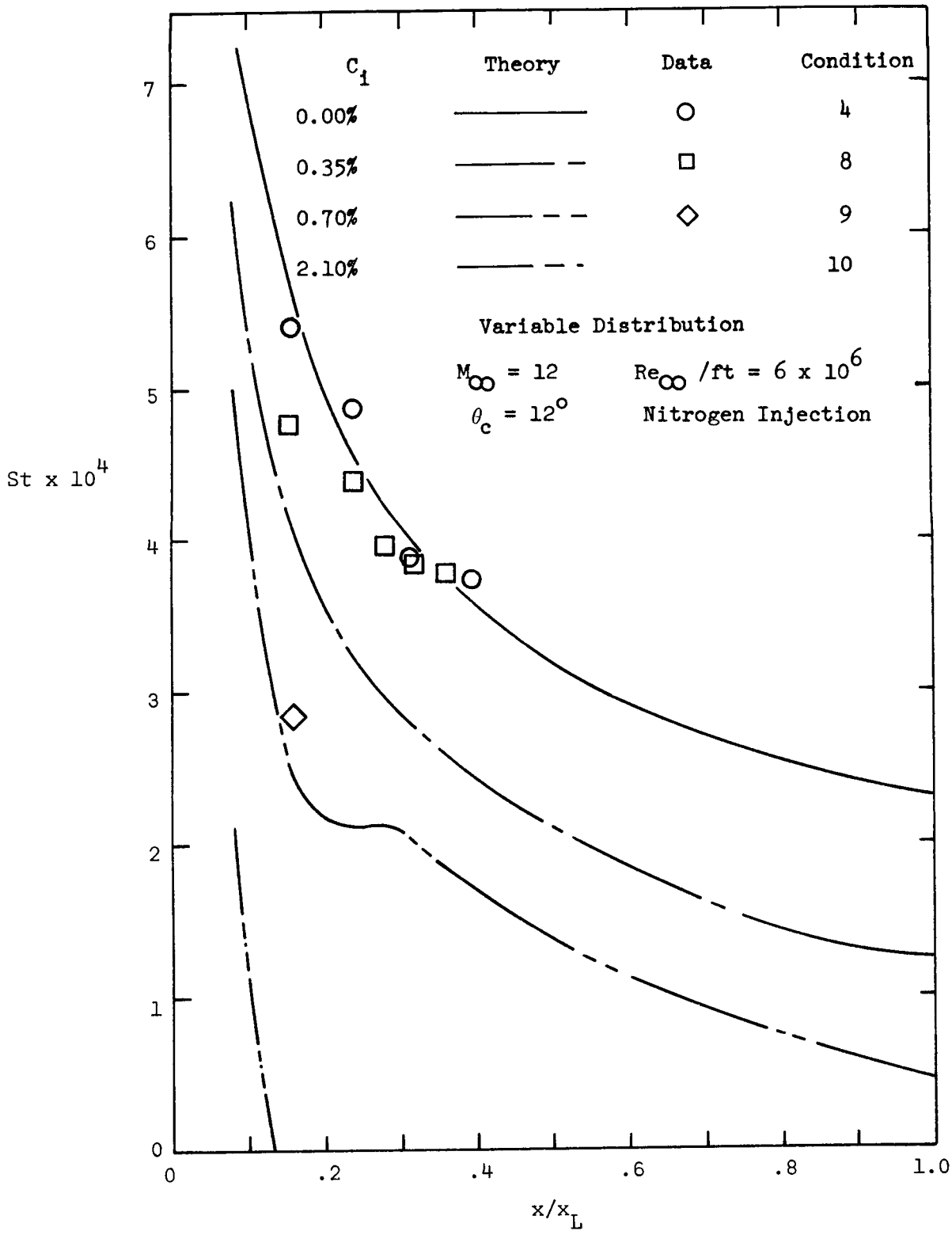

FIGURE 11 COMPARISON OF THEORETICAL AND EXPERIMENTAL HEAT-TRANSFER-RATES FOR "SIMILAR" MASS-INJECTION OF NITROGEN

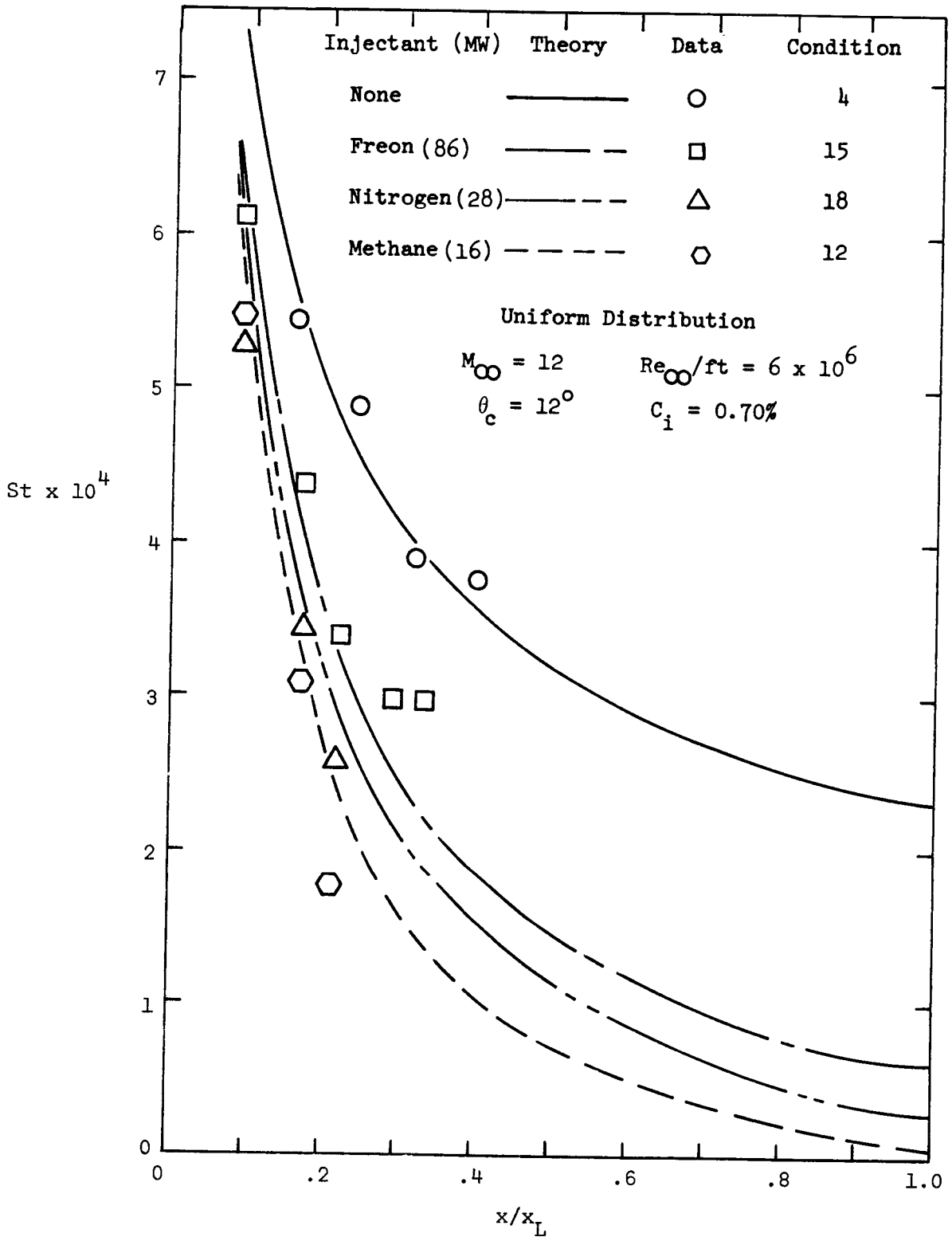

FIGURE 12 COMPARISON OF THEORETICAL AND EXPERIMENTAL HEAT-TRANSFER-RATES FOR CONSTANT MASS-INJECTION OF DIFFERENT GASES

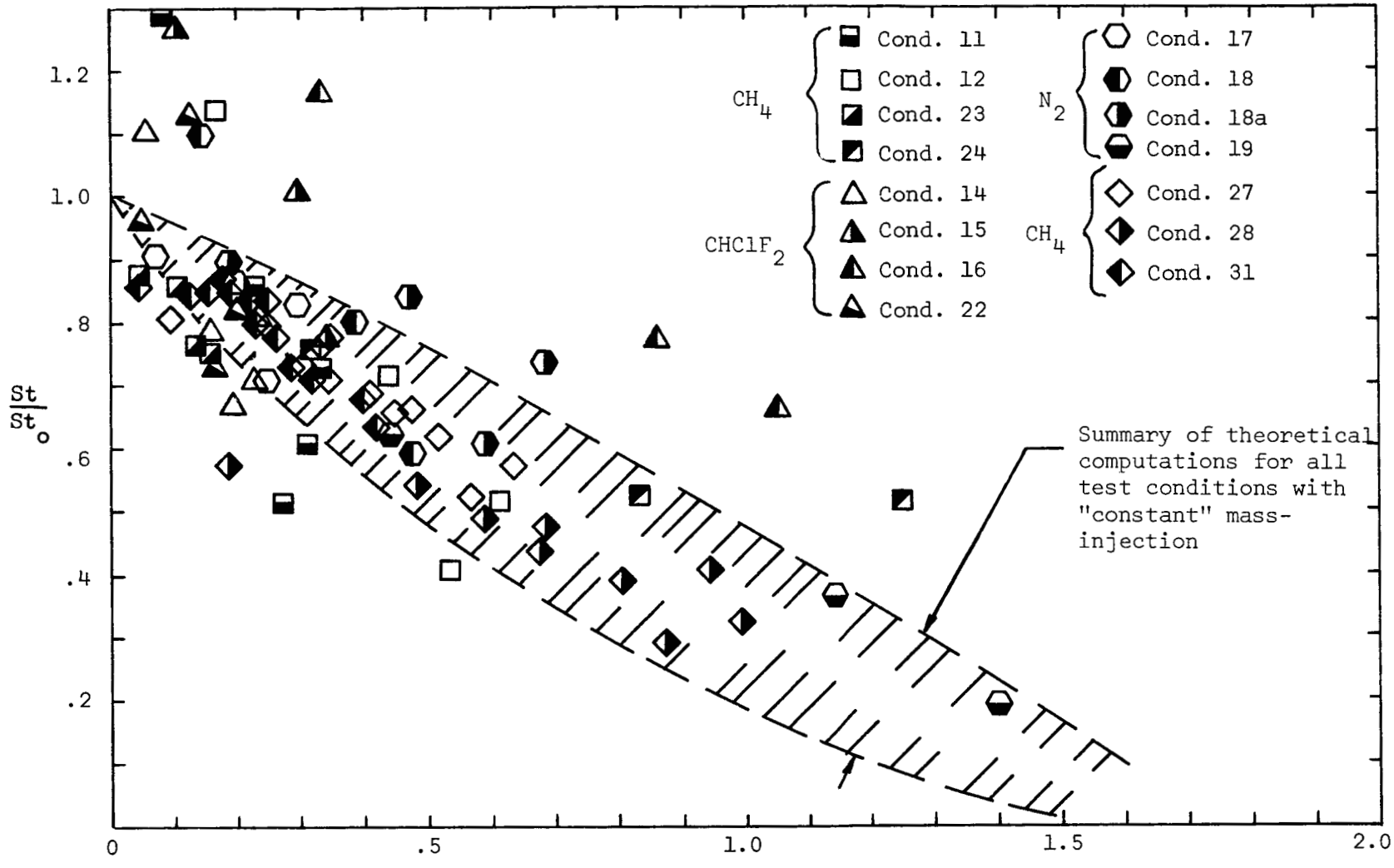

FIGURE 13 EFFECT OF GAS INJECTION ON THE LAMINAR STANTON NUMBER, CONSTANT MASS INJECTION DISTRIBUTION

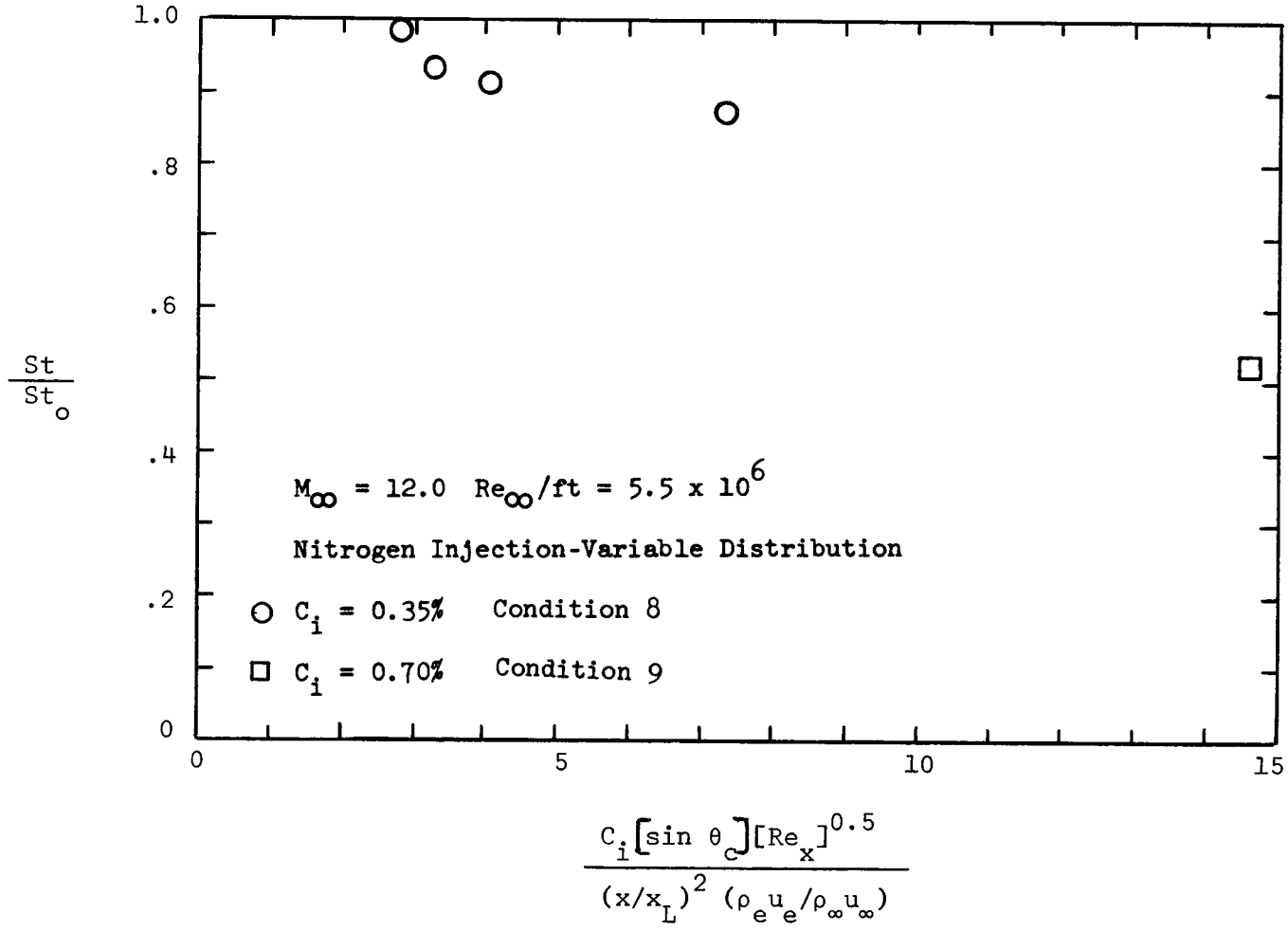

FIGURE 14 THE EFFECT OF GAS INJECTION ON THE LAMINAR STANTON NUMBER "SIMILAR" MASS INJECTION DISTRIBUTION

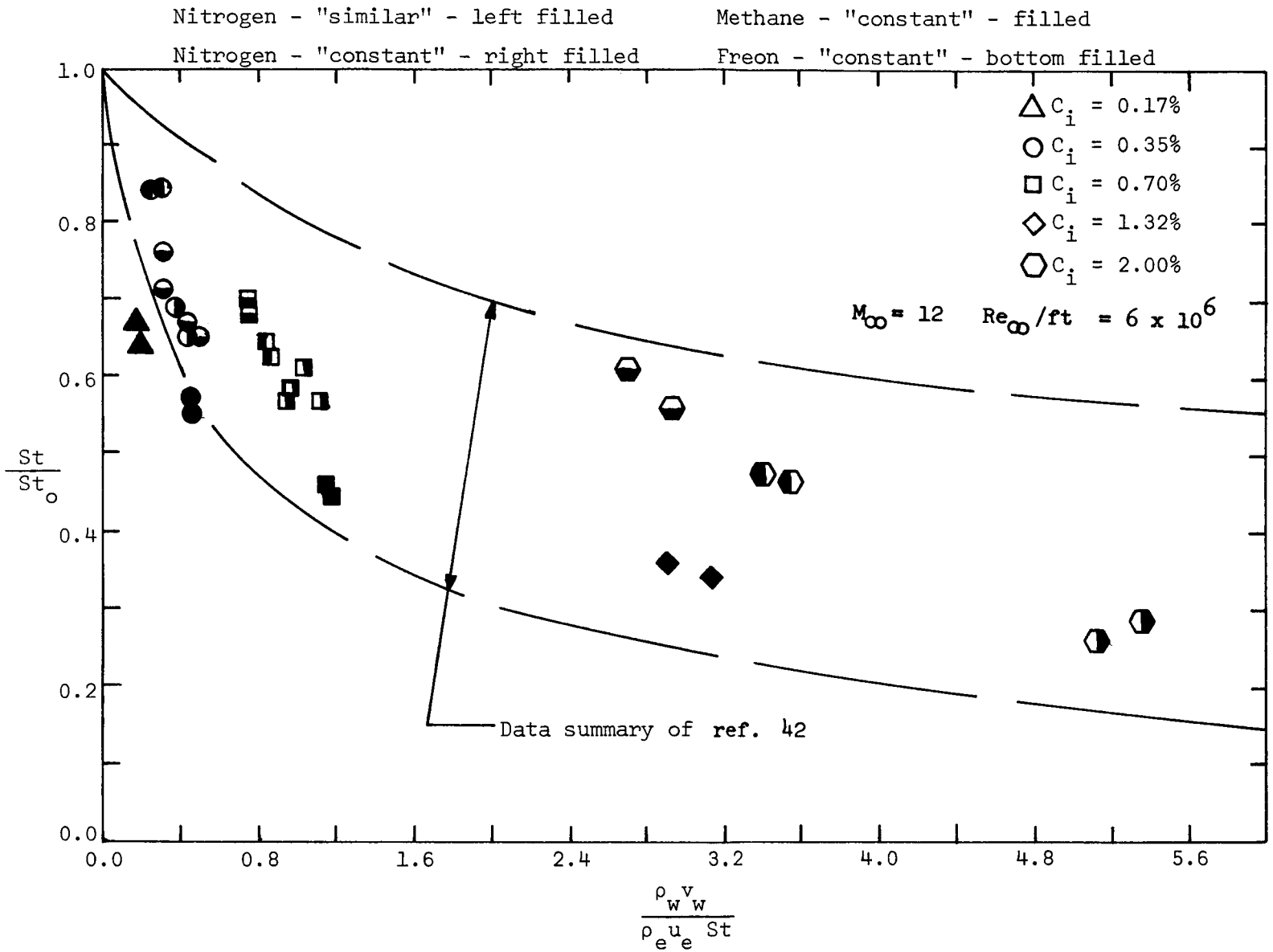

FIGURE 15 STANTON NUMBER REDUCTION DUE TO MASS-INJECTION FOR FULLY TURBULENT FLOW

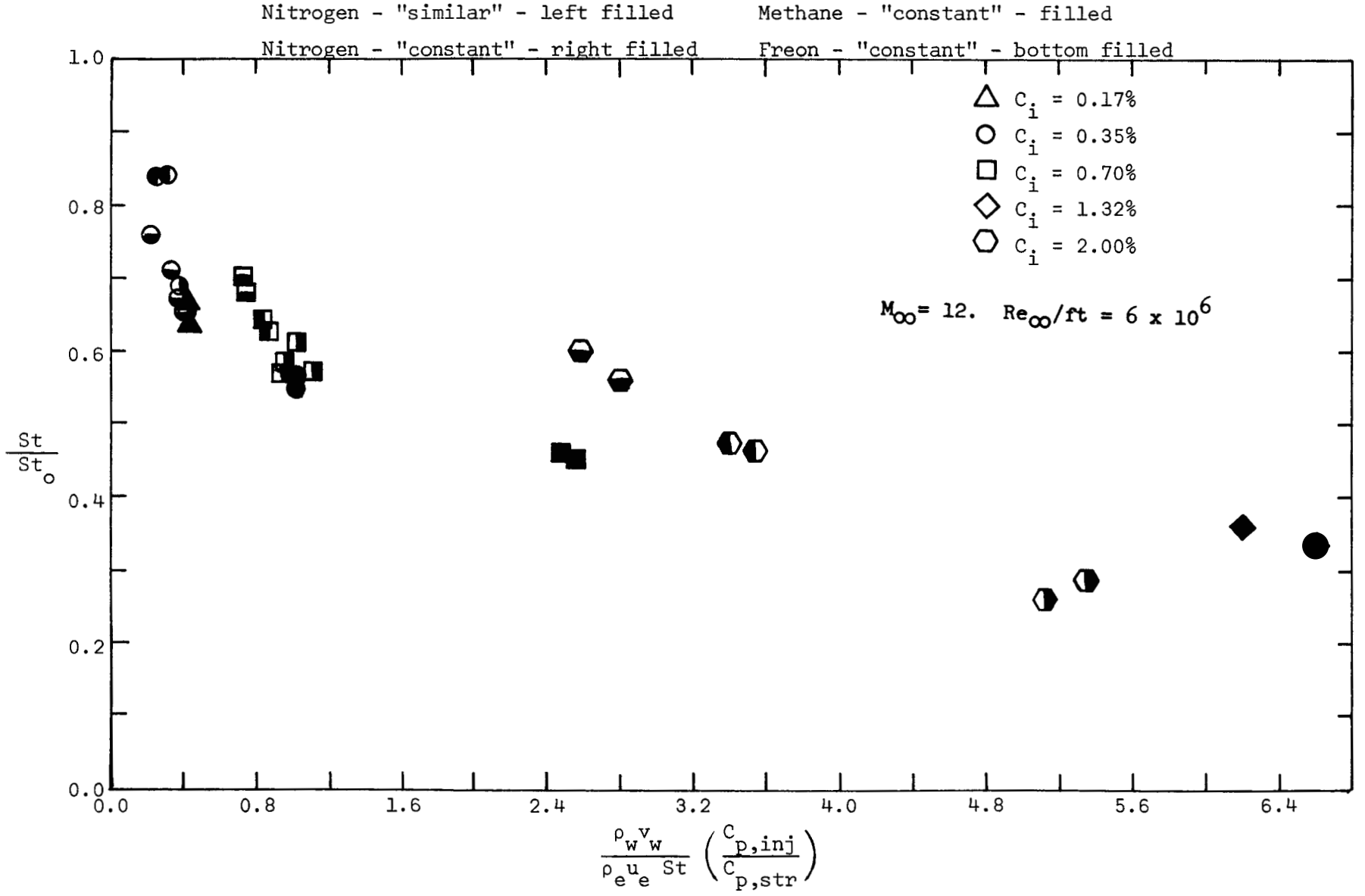

FIGURE 16 STANTON NUMBER CORRELATION OF THE EFFECT OF MASS-INJECTION ON FULLY TURBULENT FLOW

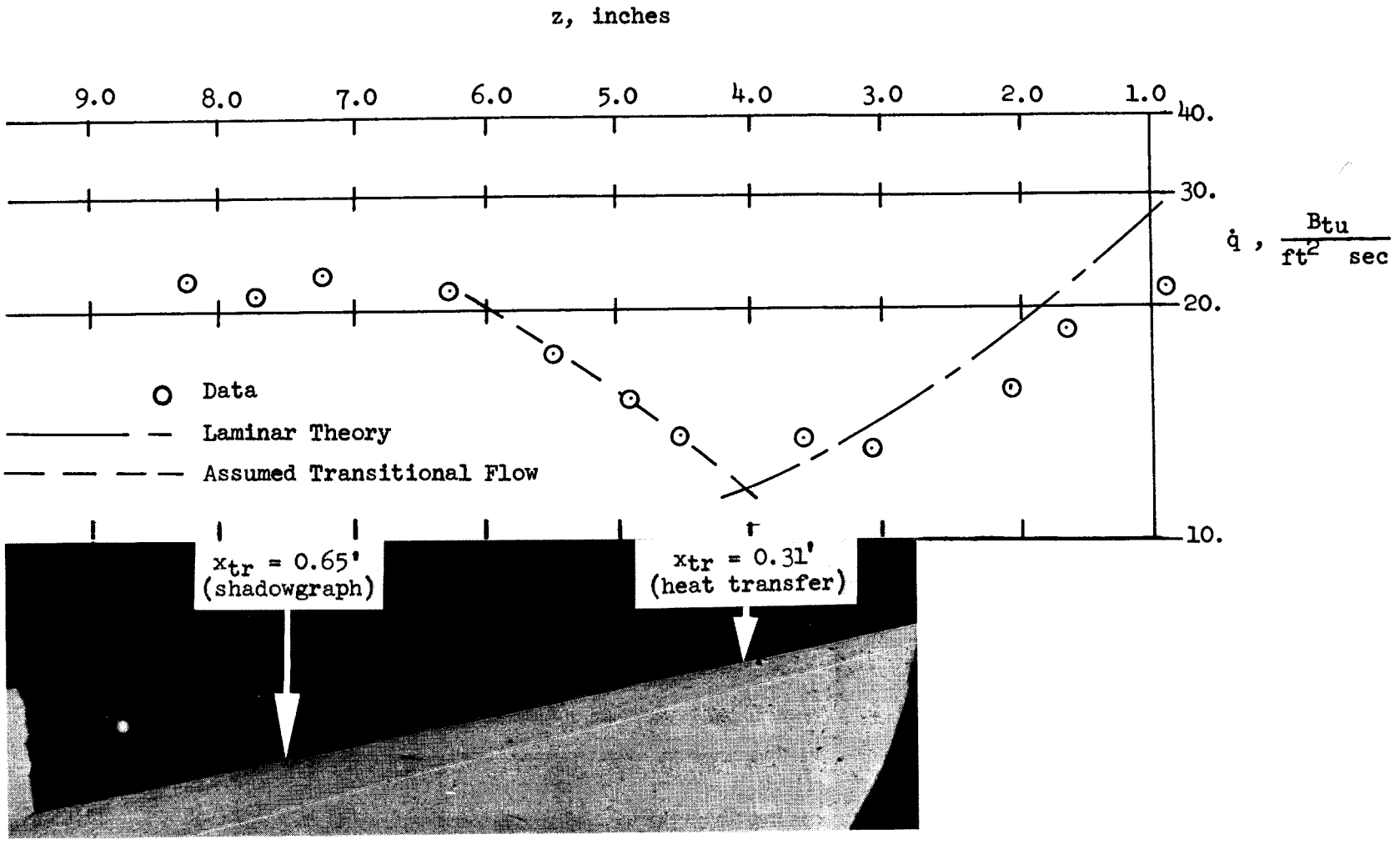

FIGURE 17 COMPARISON OF THE HEAT-TRANSFER-RATE DISTRIBUTION AND THE SHADOWGRAPH FOR CONDITION 17, $M_\infty = 11.9$, Re_∞ /ft = 6.77×10^6, $C_i = 0.32\%$, UNIFORM NITROGEN INJECTION

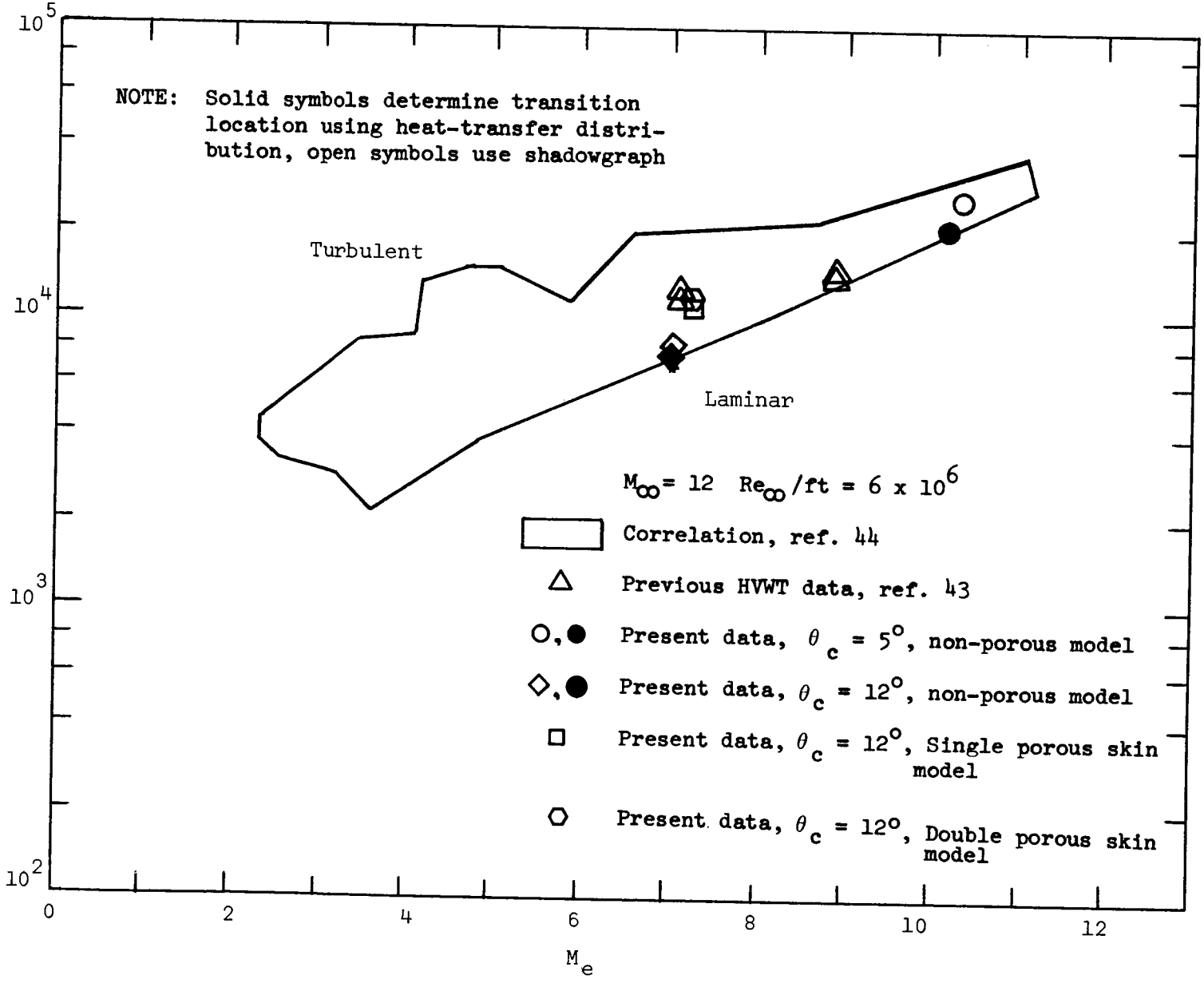

FIGURE 18 CORRELATION OF TRANSITION DATA FOR SLENDER CONES

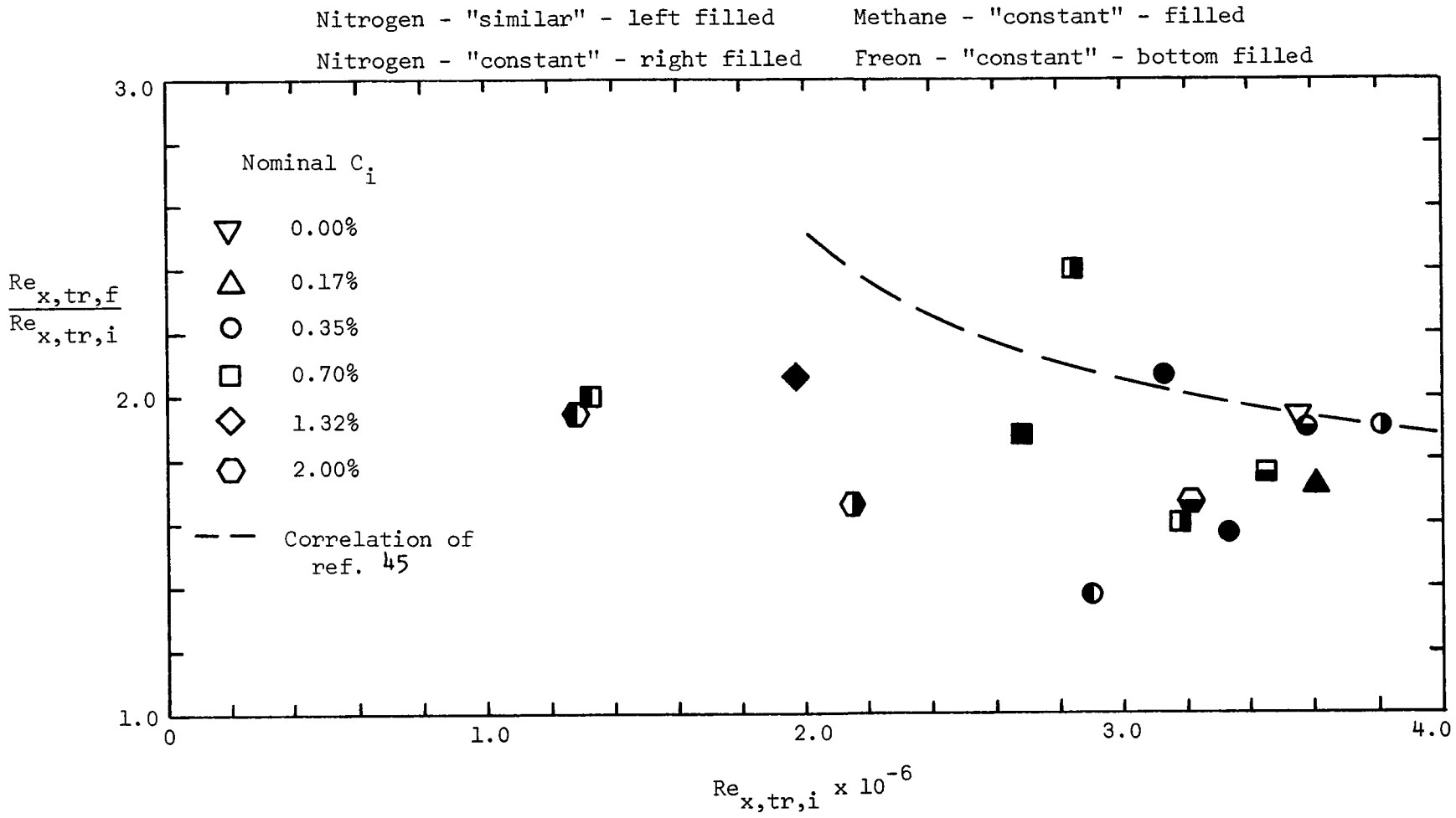

FIGURE 19 THE EFFECT OF GAS INJECTION ON THE LENGTH OF THE TRANSITIONAL ZONE

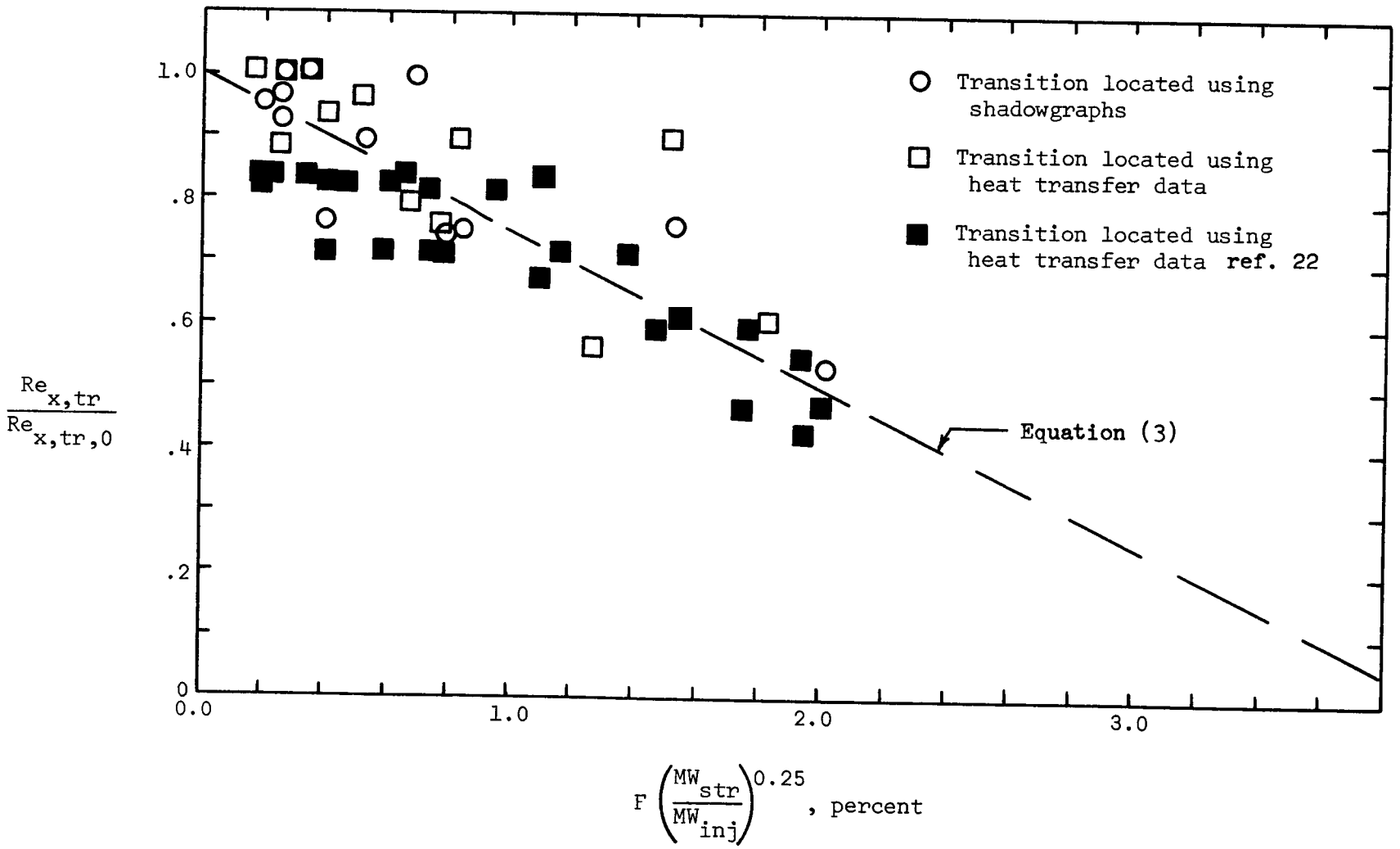

FIGURE 20 THE VARIATION OF TRANSITION REYNOLDS NUMBER WITH THE CORRELATION PARAMETER OF REF. 22, CONSTANT MASS-INJECTION DISTRIBUTION

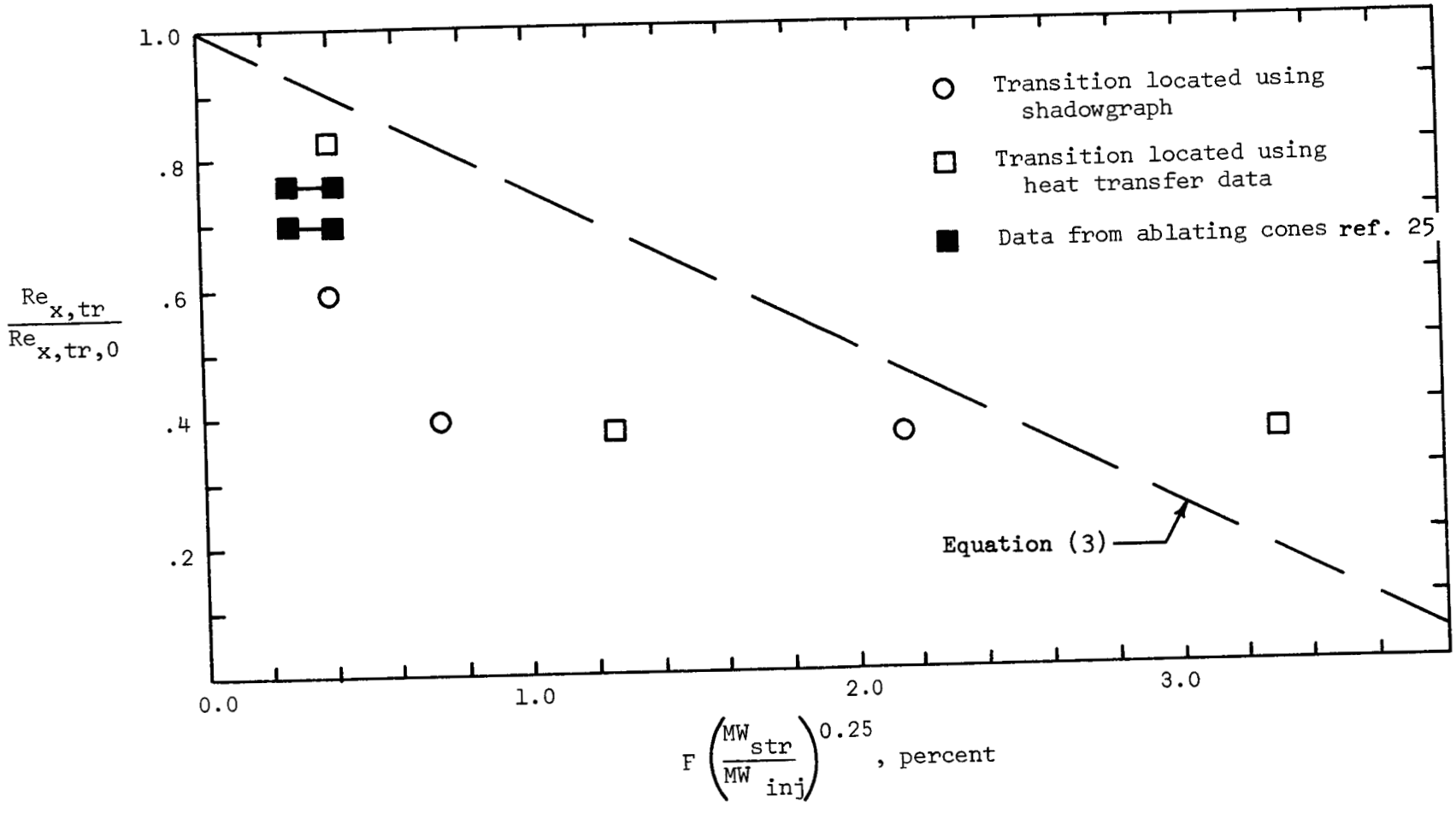

FIGURE 21 THE VARIATION OF TRANSITION REYNOLDS NUMBER WITH THE CORRELATION PARAMETER OF REF. 22, "SIMILAR" MASS-INJECTION DISTRIBUTION

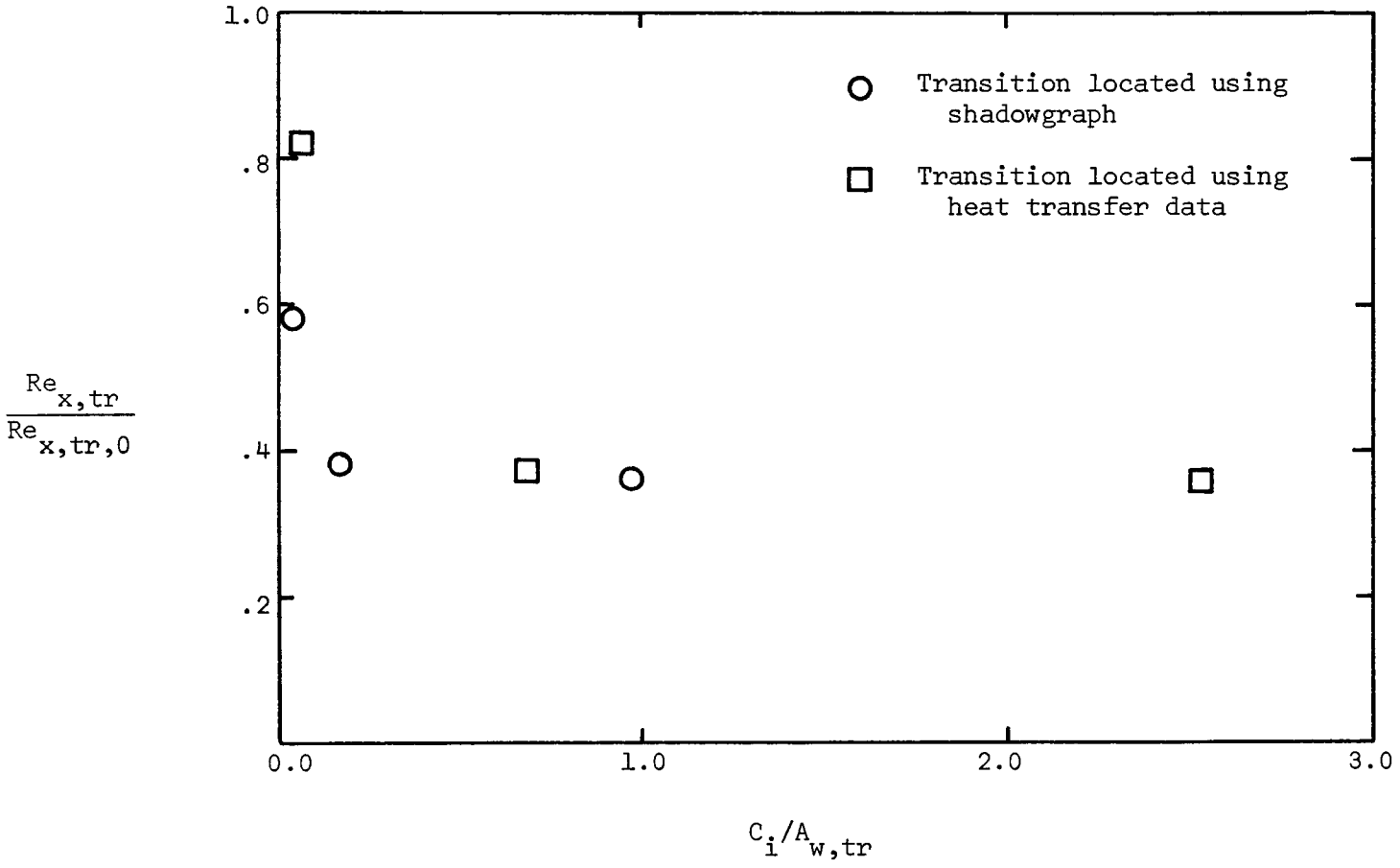

FIGURE 22 THE VARIATION OF TRANSITION REYNOLDS NUMBER AS A FUNCTION OF INJECTANT RATE AND WETTED AREA TO TRANSITION, "SIMILAR" MASS-INJECTION DISTRIBUTION

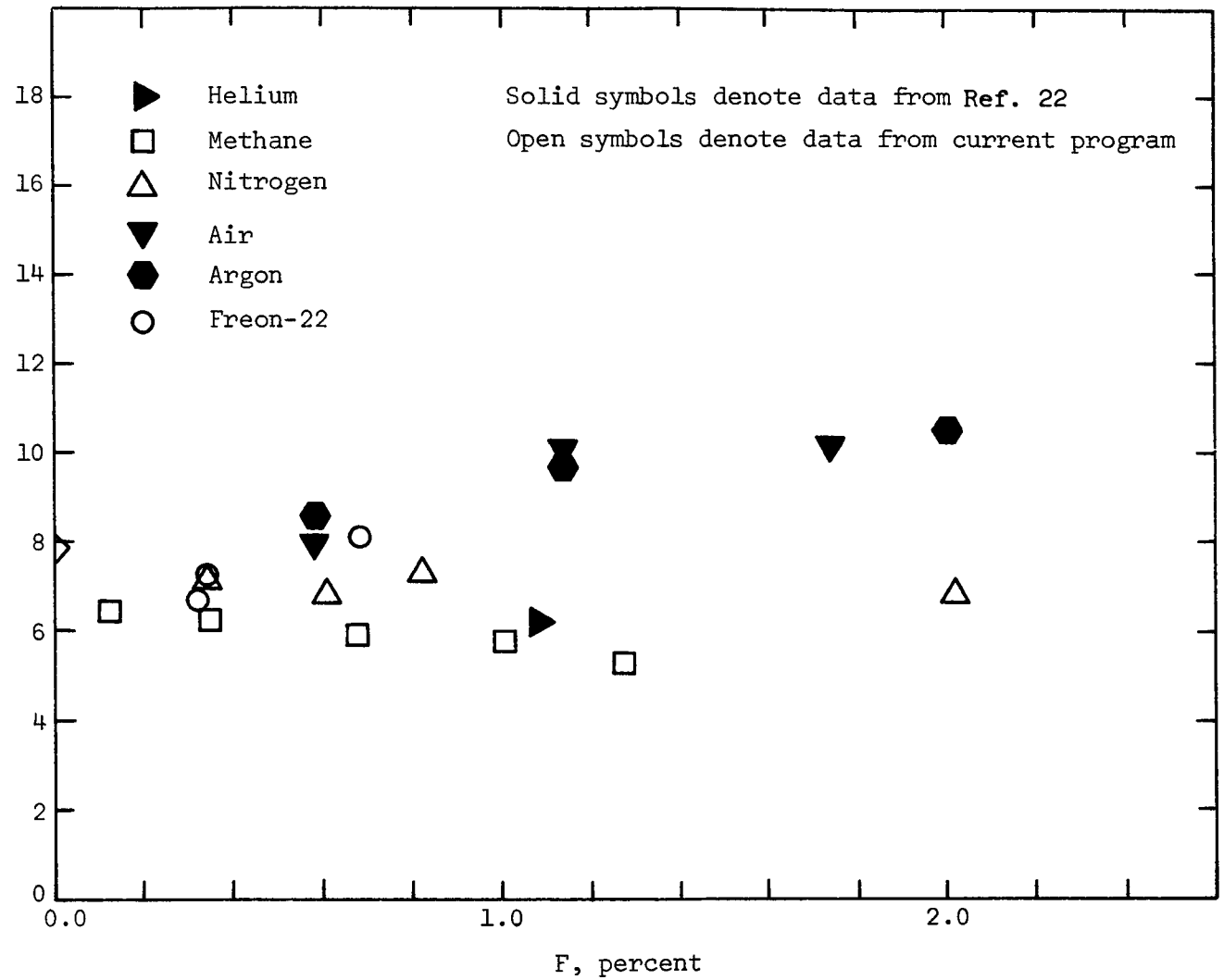

FIGURE 23 THE VARIATION OF TRANSITION REYNOLDS NUMBER WITH INJECTION PARAMETER, F

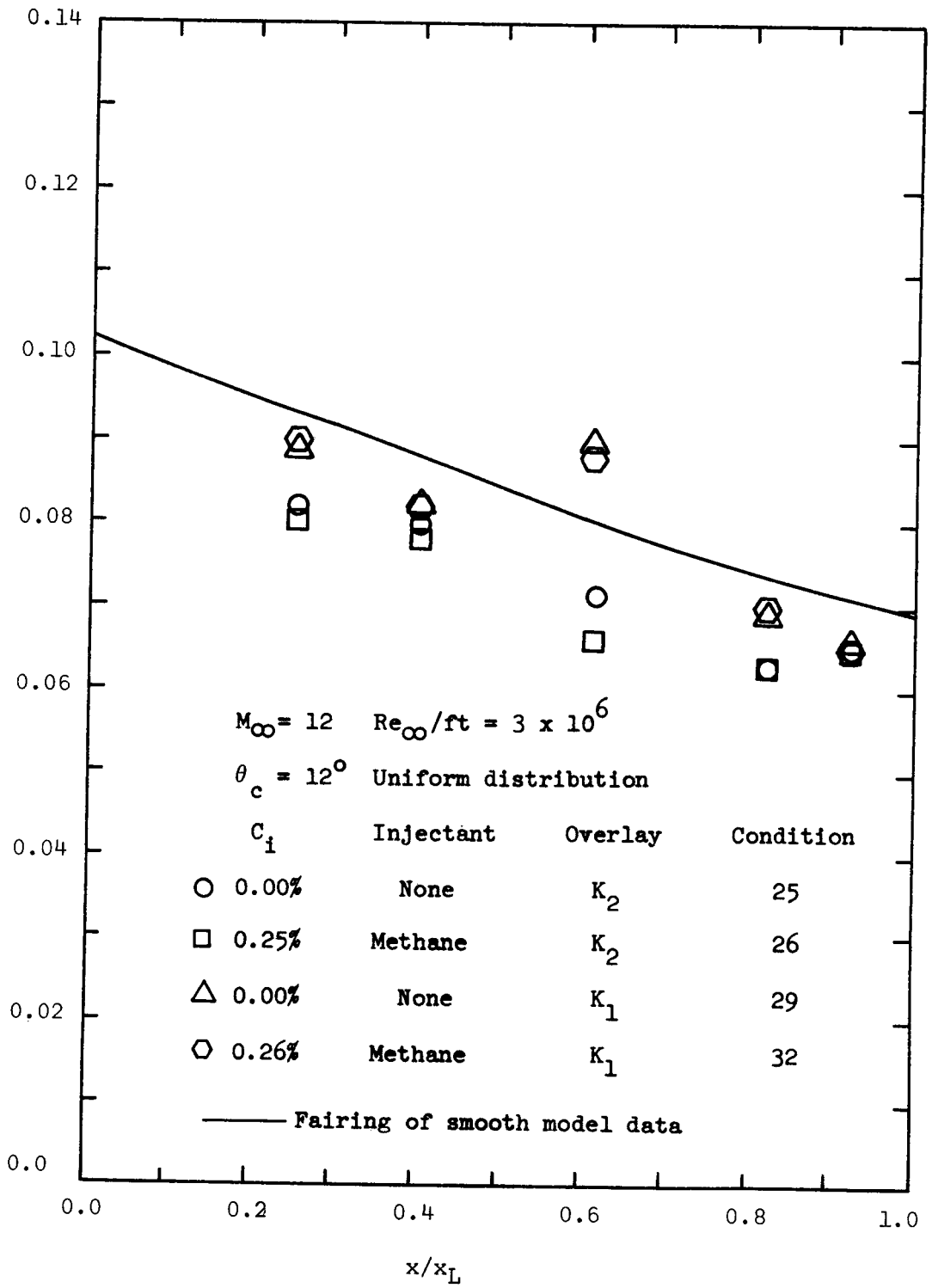

FIGURE 24 SURFACE PRESSURE DISTRIBUTION FOR MODELS WITH SURFACE ROUGHNESS

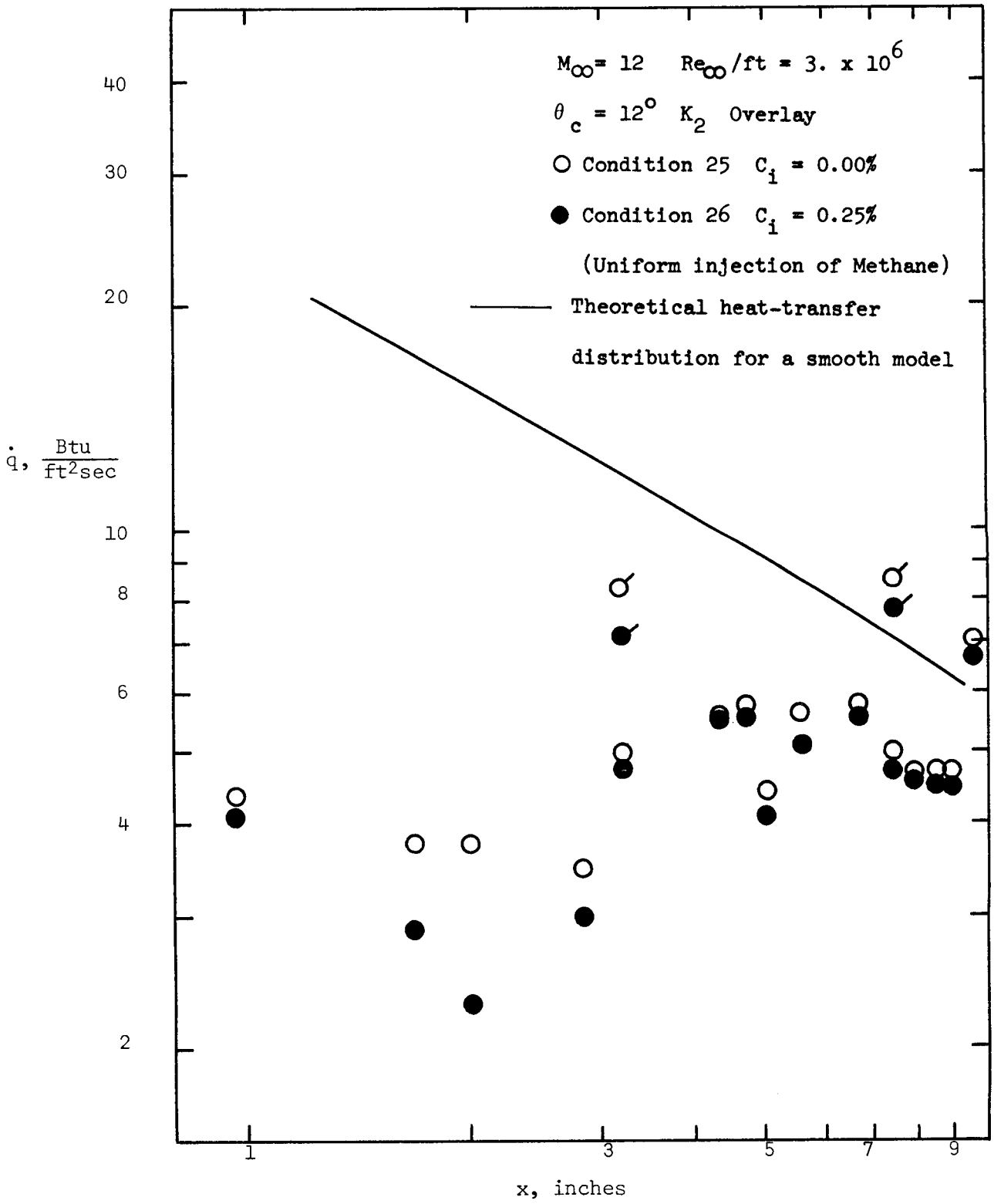

FIGURE 25 THE EFFECT OF MASS-INJECTION ON THE HEAT-TRANSFER-RATE DISTRIBUTION FOR ROUGHENED CONE

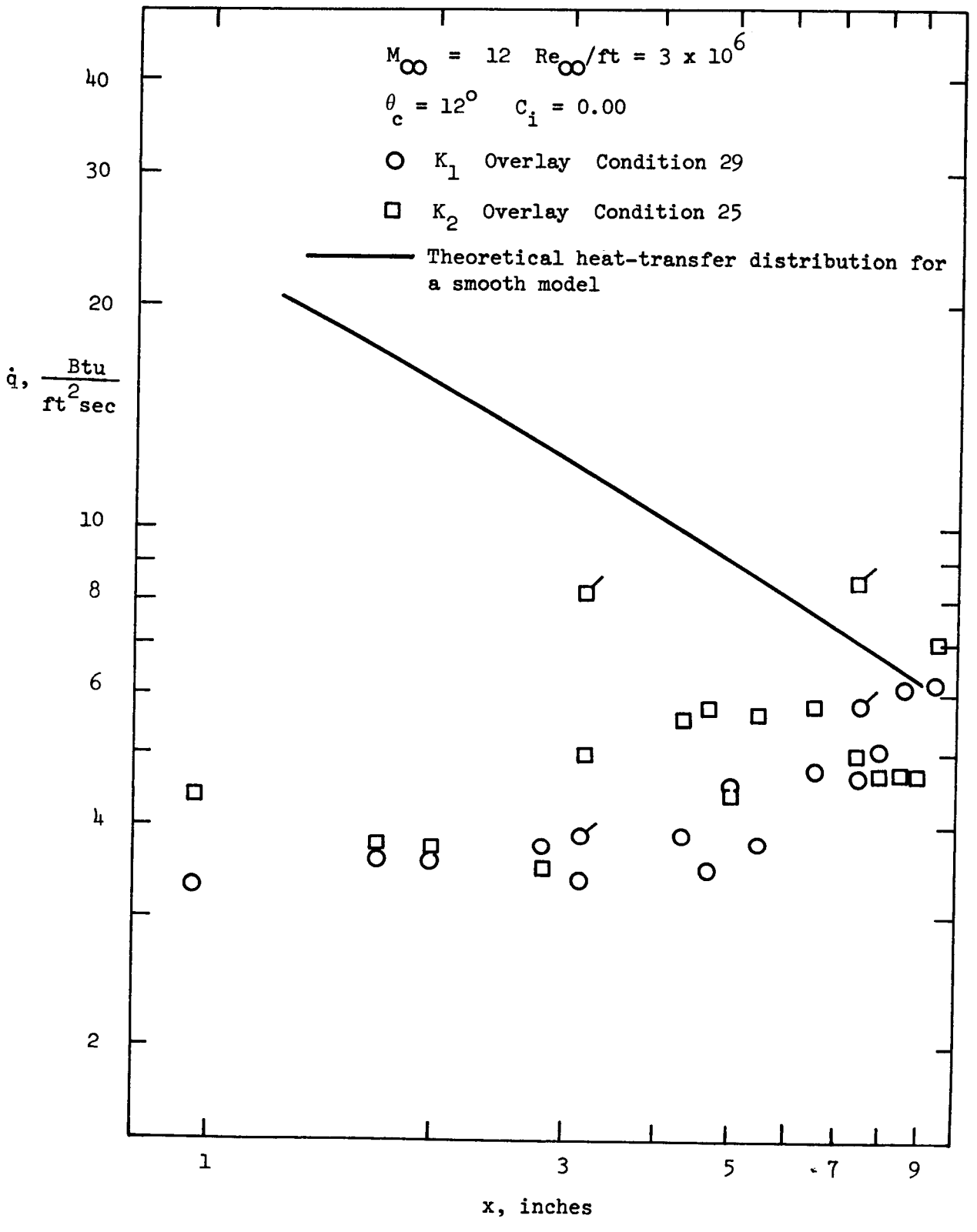

FIGURE 26 THE EFFECT OF SURFACE ROUGHNESS ON THE NON-INJECTION HEAT-TRANSFER-RATE DISTRIBUTION